地 震 研 究 所 彙 報
Bull. Earthq. Res. Inst.
Univ. Tokyo
Vol. 82 (2007) pp. 119-178

Detailed Stratigraphical and Geological Characteristics of Volcanic and Epiclastic Deposits Burying a Roman Villa on the Northern Flank of Mt. Vesuvius (Italy)

Kenji Niihori[1)*], Masashi Nagai[2)], Takayuki Kaneko[1)], Toshitsugu Fujii[1)], Setsuya Nakada[1)], Mitsuhiro Yoshimoto[3)], Atsushi Yasuda[1)] and Masanori Aoyagi[4)]

[1)] Earthquake Research Institute of Tokyo University
[2)] Institute of Natural Sciences, College of Humanities and Sciences, Nihon University
[3)] Department of Earth Sciences, Faculty of Science, Hokkaido University
[4)] National Museum of Western Art

Abstract

An archaeological excavation site at the northern foot of Mt. Vesuvius in Italy provided a three-dimensional outcrop with a height of 8 m to study its volcanic succession. Through a stratigraphical study of sediments and chemical analyses of juvenile materials, the timing and the sequence of the burial processes of the villa, which is attributed to Emperor Augustus, have been revealed. The sediments filling the villa can be divided into five stratigraphical units (Group1, Group2, Group3A, Group3B, and Group3C) by the presence of soil. The lowermost unit (Group1) directly covering the partially collapsed Roman building includes air-fall deposits, surge deposit, and epiclastic flow deposits. One of charcoals found in this unit give an age of 1500 yBP, and the juvenile scoria have the same compositional range as ejecta of the AD472 Sub-plinian eruption, and differ from ejecta of major eruptions. The next three units (Group2, Group3A, and Group3B) include thick epiclastic flow deposits interbedding air-fall deposits. The uppermost unit (Group3C) consists of alternating scoria and ash-fall layers and an overlying ash-fall layer. The petrographical features and the composition of juvenile materials coincide with those of the AD1631 Sub-plinian eruption. From these geological and geochemical features, the burial process of the Roman villa is described as follows. When the AD472 eruption started, the villa had partially collapsed. This damaged building was mantled by an air-fall deposit a few tens of centimeters thick. The remaining building was soon struck by several phases of lahars, and was buried up to a height of 5 m. The villa experienced at least five eruptions, and their ejecta and subsequent lahars buried the building further. The last eruption, which completely buried the villa, was the AD1631 eruption. This reconstructed scenario suggests lahars generated just after the eruptions were major agents in the burial of the Roman villa.

Key words: Vesuvius, volcanoes, burial process, excavation site, Roman villa

1. Introduction

A luxurious Roman villa was found under thick volcanic materials in Somma Vesuviana, at the northern foot of Mt. Somma-Vesuvius, Italy (Fig. 1) during excavation in the 1930s, and was thought to belong to the first Roman emperor Augustus. In 2002, a Japanese-Italian joint archeological team with members from various academic disciplines was organized to extensively re-excavate the site. As members of the team, we have been working to understand the burial processes and the age of the villa based on geological and geochemical methods. Preliminary results have been reported by Kaneko *et al.* (2005). They concluded that the first eruption, which buried the villa, was the AD 472 eruption, based on a combination of carbon-14 ages and chemical analyses

*e-mail: niihori@npo-cemi.com（〒160-0011 東京都新宿区若葉 1-22 ローヤル若葉 505 号）

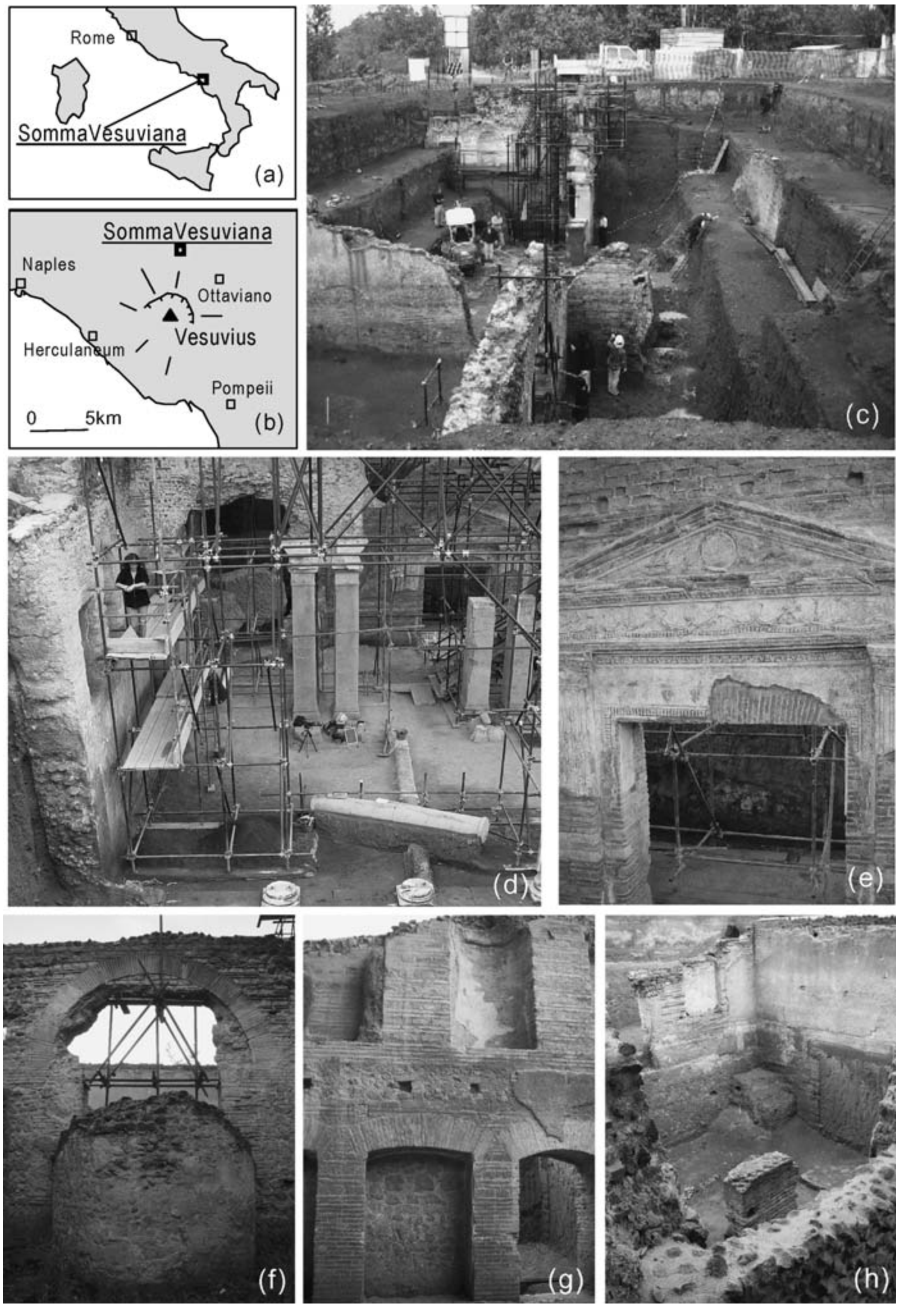

Fig. 1. (a) Location map of Mt. Somma-Vesuvius Volcano and (b) the sites of the Roman villa at Somma Vesuviana. (c) Photograph of excavation site from the west (taken in 2004). (d) Photograph of excavation site from the north (This photograph was taken in 2005). A variety of archaeological architectures at the site are shown. They are the eastern wall of this building, pillars, columns, and the south gate. Plane view with architectural structures is shown in Fig. 2. (e) Photograph of timpano (tympanum) of the south gate. (f) Photograph of apsis fixed to the south wall of a small chamber named Vano2. (g) Photograph of the eastern wall of Vano2 with a niche. (h) Photograph of Vano2 from the southeast.

of juvenile materials obtained during the 2002 and 2003 excavations. Moreover, they roughly divided the deposits covering this villa into three groups from depositional hiatus and lithological differences.

Enlargements of the excavation site in 2004 and 2005 gave us significant opportunities to investigate the detailed stratigraphy and lithofacies of the deposits. In particular, progressive excavation with contemporary geological observations allowed us to understand the spatial distributions of the deposits, as well as the relationships between their sedimentary structure and the archeological building. As a result, we recognized some air-fall deposits, which had not been reported by Kaneko *et al.* (2005). They might be a useful temporal marker to determine the burial age because of their characteristic of spreading over a wide area in a very short time. Recently, several research groups in Italy have published the results of their intensive geological and geochemical surveys on the AD 472 and post-AD 472 eruptions (Rosi and Santacroce, 1983; Arrighi *et al.,* 2001; Mastrolorenzo *et al.,* 2002; Principe *et al.,* 2004; Rolandi *et al.,* 2004; Sulpizio *et al.,* 2005; *Perrotta *et al.,* 2006a; Perrotta *et al.,* 2006b). They show the detailed stratigraphy and the distribution of each eruptive deposit around the volcanic edifice, which provide the entire eruptive history of Mt. Somma-Vesuvius since the AD 472 eruption. Comparing this information with a detailed geological and geochemical data set at the excavation site, we can reconstruct how the villa was buried corresponding to volcanic activity.

In this paper, we provide detailed stratigraphy and sedimentary structure, including relations with the building, using geological information obtained from new trenches dug during the 2004 and 2005 excavations. In addition, we report the results of a stratigraphic correlation using chemical compositions of the juvenile materials collected at the excavation site, and the reported chemical analyses of historical eruptions (Rosi and Santacroce, 1983; Rosi *et al.,* 1993; Ayuso *et al.,* 1998).

* When this manuscript was almost in the final writing we learned that two articles describing the stratigraphy of the deposits within the excavation site had been published independently. The authors of the articles include Drs Perrotta and Scarpati, who frequently visited our excavation site. We offered them opportunities to make geological observations at the excavation site, but gave no agreement to the publication of their observed results without our permission. Although they described the deposits fairly precisely, their results contain some flaws. In addition, they completely neglected the previous stratigraphic notation adopted by Kaneko *et al.* (2005), which first described the stratigraphy of the deposits at the excavation site, and clearly stated that the Roman villa was buried by volcaniclastic deposits of the AD 472 and later eruptions. Therefore, we describe here deposits extending the notation of Kaneko *et al.* (2005), and discuss the burial process of the Roman villa. To eliminate any confusion, we do not mention the descriptions of Perrotta *et al.* (2006a) and Perrotta *et al.* (2006b) in the text; however, a corresponding table of stratigraphic notations comparing our findings and those of Perrotta *et al.* (2006b) is given in an appendix.

2. Eruption history of Mt. Somma-Vesuvius

Mt. Somma-Vesuvius, situated east of Naples, is a composite volcanic system comprising the Vesuvius main cone (1281 m a.s.l.), which grew after the famous AD 79 Pompeii eruption, and the pre-existing Mt. Somma (1131 m a.s.l.) caldera (Cioni *et al.,* 1999). The Mt. Somma caldera was formed by four collapse events (Cioni *et al.,* 1999). The first collapse occurred during the Pomici di Base Plinian eruption (18,000 y.B.P.). Following this eruption, caldera collapses occurred during three Plinian eruptions named Mercato (8,000 y.B.P.), Avellino (3,400 y.B.P.), and Pompeii (AD 79). After the AD 79 event, the Mt. Somma caldera had a quasi-elliptical shape with a 5 km-long, east-west major axis (Fig. 1). The northern rim of the caldera is a well-defined steep wall, while the southern rim is indistinct because it is covered by historical lava flows.

After the AD 79 eruption, Mt. Vesuvius erupted repeatedly many times until the AD 1944 event, including two Subplinian events in AD 472 and AD 1631 (e.g., Rolandi *et al.,* 1998; Arrighi *et al.,* 2001; Principe *et al.,* 2004). During these eruptions, epiclastic flows such as debris flows occurred numerous times (Lirer *et al.,* 2001).

The AD 472 Pollena eruption was an intermediate-scale explosive event in the eruptive history of Mt. Vesuvius. The first comprehensive study of stratigraphy and petrology was reported by Rosi and Santacroce (1983). They highlighted some similarities between the AD 472 eruption and other Plinian and Subplinian eruptions of Somma-Vesuvius, all of which are generally characterized by thick, fall deposits covered by pyroclastic flow deposits. They also described compositional variations of eruptive products from phonolite to tephri-phonolite. Mastrolorenzo *et al.* (2002) studied the impact of debris flows derived from remobilization of the AD 472 fall deposits at some archaeological sites near Somma-Vesuviana. More recently, a detailed stratigraphic succession of the AD 472 eruption was reported by Rolandi *et al.* (2004) and Sulpizio *et al.* (2005). They also showed isopach maps of each deposit. According to Sulpizio *et al.* (2005), the first phase was a small magmatic explosion, which formed a well-vesiculated white pumice fall layer, followed by generation of alternating scoria and ash layers, suggesting the formation of a sustained column. The second phase was an alternation of scoria fall and pyroclastic flow. The final phase was characterized by extensive phreato-magmatic activity as observed in other explosive eruptions of Mt. Somma-Vesuvius.

The AD 1631 eruption is an intermediate-scale explosive event similar to the AD 472 eruption. This eruption is recorded as a destructive event that killed more than 4,000 persons (Barberi *et al.,* 1989). According to Rosi *et al.* (1993), this eruption began with the ejection of ash from a lateral vent on the western flank of Mt. Vesuvius, followed by scoria and lithic fallouts from the central vent. After these fallouts, nuees ardentes traveled down to the foot of the volcano. The scoria and gravel fallouts dispersed to the east and northeast of the volcano. After these activities, extensive lahars and floods struck the radial valleys of the volcano, as well as the plain to the north and northeast.

After the AD 472 eruption, minor explosive and effusive eruptions occurred intermittently for about 700 years (AD 512, 536, 685, 787, 968, 991, 999, 1006 or 1007, 1037, and 1139), and were followed by a 500-year repose until the AD 1631 eruption (Principe *et al.,* 2004). Subsequently, effusive eruptions occurred every three to four years until the AD 1944 eruption (Arrighi *et al.,* 2001).

3. Archaeological site in Somma-Vesuviana

The Roman villa in Somma-Vesuviana was built on an alluvial fan that developed at the northern flank of Mt. Somma (Fig. 1), which is located about 6 km from the summit. By 2005, this excavation site had been enlarged to about 29 m × 36 m in width and about 8 m in depth (Fig. 2). This rectangular excavation trench is surrounded by four walls consisting of layers of volcaniclastic deposits, which are named the North Wall, the South Wall, the East Wall, and the West Wall (Fig. 2). These walls are divided into three parts by two scaffolds—the lower wall: 0–3 m from the floor, the middle wall: 3–5.5 m, and the upper wall: 5.5–8 m (Fig. 2). The scaffolds at the East Wall can barely be observed due to the presence of a wall of the building (Fig. 2).

The constructions of this villa comprise the south gate with tympanum (Fig. 1e), the Vano2 (Fig. 1h), which is a small chamber located at the north-west corner, the east building wall (Fig. 1d) located along the outcrop, pillars of limestone located at the north side, a mosaic floor on the ground floor, etc. (Fig. 2). These Roman buildings are constructed with stucco-decorated bricks, and some of the ground plates are made of lavas from Mt. Somma-Vesuvius. Some parts of these buildings had already become ruins and were scattered as rubble before the AD 472 eruption (Kaneko *et al.,* 2005).

4. Stratigraphy and lithology of the deposits

Kaneko *et al.* (2005) roughly divided the deposits burying the villa into three groups—Group1, Group2, and Group3—each of which consists of subgroups. For this study, enlargement of the excavation site allowed us to divide the deposits into five groups—Group1, Group2, Group3A, Group3B, and Group3C—based on the presence of soil indicating time gaps and lithological differences. Although the names of deposits mostly follow Kaneko *et al.* (2005), we redefined some of them. Schematic stratigraphy and characters of these deposits are shown in Fig. 3 and Table 1, respectively. Complete stratigraphy on the four walls is also shown in Fig. 4. In this section, we describe the redefined units.

In this study, three types of epiclastic flow—debris flow, mudflow, and fluvial flow—are mentioned. The major differences among the three types of deposit are grain-size distributions and sedimentary structures, which are affected significantly by sediment/water ratio during flowage and emplacement (e.g., Lirer *et al.,* 2001). In this study, the definitions of the three epiclastic flow deposits are as follows. The debris flow and the mudflow deposit are considered together and named Mf. They are massive with broad distributions of grain size. The matrix is composed of fine ash particles and lithic fragments range in size from a few centimeters to

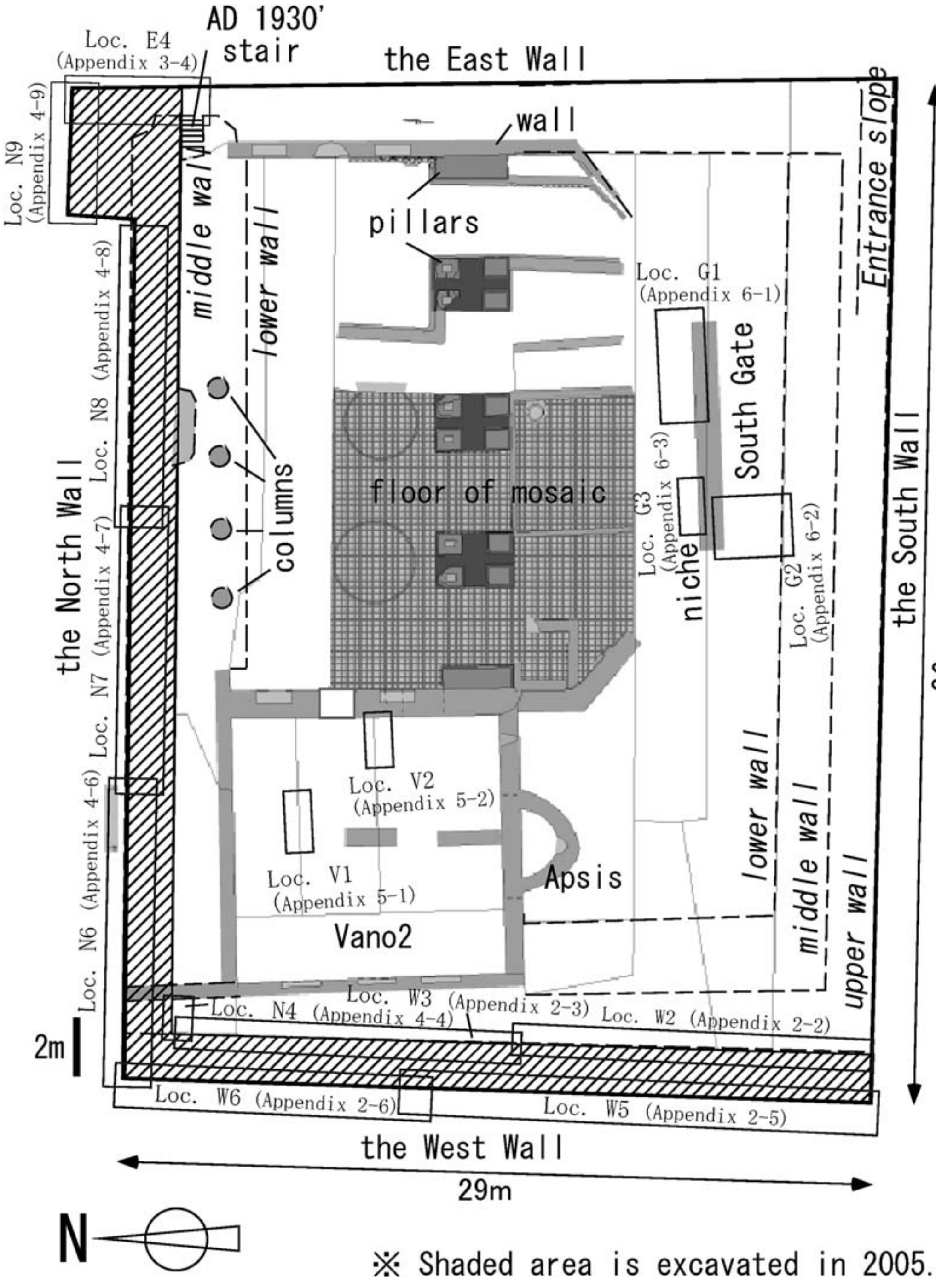

Fig. 2. Plane view of the Roman villa. The Roman architectural structures in this villa are shown in gray. Dashed lines indicate scaffolds erected for the excavation. Detailed explanations of the numbered locations are shown in Appendix 2〜6.

one meter in diameter. The fluvial deposit is named Df, which is a well-stratified bed. It is a well-sorted deposit without cobble gravel.

4. 1 Group1

Group1 consists of three subgroups: G1-Af, G1-Mf, and G1-Df in ascending order (Kaneko *et al.*, 2005). The total thickness of this group is 5 m, which is the thickest among the five groups. Group1 is significant because it was the first deposit to cover the villa, and also buried it to half of its height.

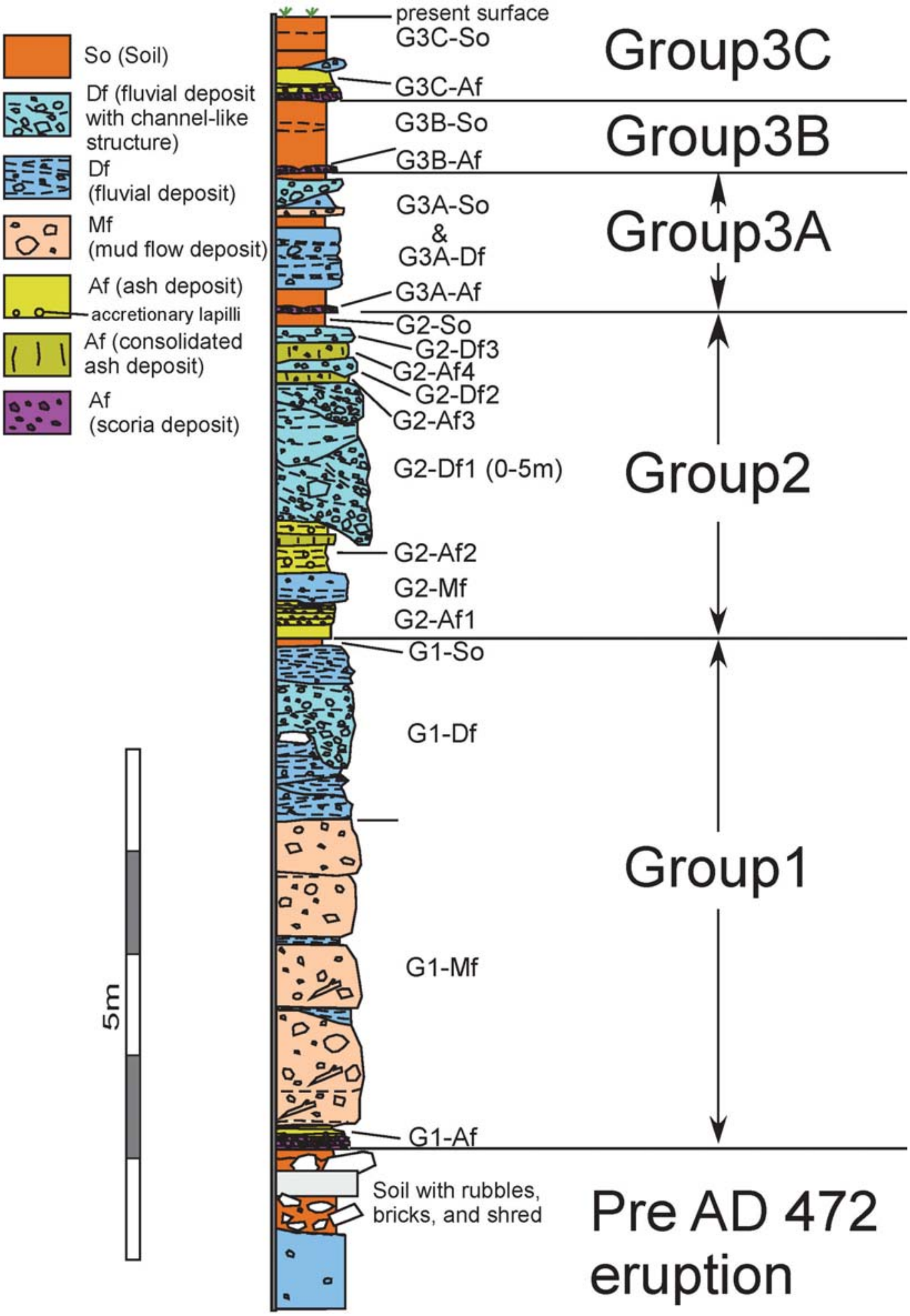

Fig. 3. Stratigraphic section at the excavation site.

Table 1-1. Characteristics of volcanic and epiclastic flow deposits of Group1.

Unit	Subunit	Bedding features and texture	Grain size and component features	Thickness	The remnant of Roman structure
G1-Df	Df2	Laminated layer with channel like structure	Silt to fine pebble size matrix. Up to 6cm rounded lithic composed of lava, scoria, pumice, and carbonate.	～80cm	Bricks (～5cm) and fragments of painted stucco.
	Df1	Laminated and massive layer with channel like structure	Silt to fine pebble size matrix. Up to 12cm rounded lithic fragments composed of lava, scoria, pumice, carbonate, and plutonic rocks.	～100cm	
G1-Mf	Mf4	Massive and firly stratified layer	Fine sized matrix. Up to 40 cm angular and subangular lithic fragments composed of lava, scoria, and carbonate.	30～60cm	Parts of Roman wall structure on the top of Mf4.
	Mf3	Massive and firly stratified layer	Fine to medium sized matrix. Up to 18 cm rounded and subangular lithic fragments composed of lava, scoria, and carbonate with high proportion of lithic fragments.	70cm	
	Mf2	Massive and consolidated layer	Fine to medium sized matrix. Up to 6 cm rounded and subangular lithic fragments composed of lava, scoria, pumice, carbonate, plutonic rock.	70cm	
	Mf1	Massive and consolidated layer	Fine to medium sized matrix. Up to 25cm rounded and subangular lithic fragments composed of lava, scoria, pumice, carbonate, plutonic rock.	80cm	Bricks (～5cm), sherd, parts of pillar, and parts of statue.
G1-Af	Af8	Mantle bedding, massive ash layer	Fine ash bed: brown ash.	5cm	
	Af7	Well stratified (planar- to dune-bedded) ash layer	Fine to medium ash beds: reddish ash.	1～30cm	Bricks (～5cm), tesserae ,and fragments of painted stucco.
	Af6	Mantle bedding ash layer with accretionary lapilli	Fine ash with accretionary lapilli (3-6mm in diameter).	1～5cm	
	Af5	Normal grading scoria layer	Scoria lapilli beds: vesiculated, greenish grey scoria.	6cm	Bricks (～5cm), tesserae ,and fragments of painted stucco.
	Af4	Mantle bedding, massive ash layer	Fine ash bed: black ash.	1cm	
	Af3	Mantle bedding scoria layer	Scoria lapilli beds: pooly vesicluated, greenish grey scoria.	2cm	
	Af2	Stratified appearance due to color variations, mantle bedding ash layer	Fine to medium ash beds: reddish or greenish grey ash.	2cm	
	Af1	Stratified appearance due to rhythmic grain size variations, mantle bedding ash layer	Granule pumice and medium scoria beds: light-green pumice and greenish grey scoria.	2cm	Bricks (～5cm).

i) G1-Af

Kaneko *et al.* (2005) defined G1-Af as one unit. We, however, divided it into eight sub-units based on lithological differences. They are named G1-Af1 to G1-Af8 in ascending order (Table 1), and the total thickness is about 20 cm. G1-Af1 is a light-colored fallout deposit composed of ash, and well-vesiculated white pumice with an average size of 1 cm (Fig. 5). G1-Af2 is a yellowish ash-fall deposit. G1-Af3 is a dark-colored fallout deposit, composed of scoria (Fig. 5) and a small amount of accidental lithic fragments. The average grain size of scoria is about 2 cm. G1-Af4 is a dark-colored ash-fall deposit. G1-Af5 is a dark-colored fallout deposit composed of scoria (Fig. 5), accidental fragments lava, plutonic rocks, and carbonate rocks. The grains are mostly about 3 cm in size, but on rare occasions reach 12 cm. G1-Af6 is an ash-fall deposit characterized by including accretionary lapilli. G1-Af7 is a planner- to dune-bedded surge deposit, which consists of fine to medium-sized ash (Appendix 5-2). G1-Af8 is a silt-sized ash-fall deposit. Small fragments of stucco and brick are included in G1-Af5, G1-Af6, and G1-Af7 (Appendix 5-2).

G1-Af usually covers the remnants and rubble of the Roman buildings directly, and it occasionally fills voids among rubble of building. Around the corner

Table 1-2. Characteristics of volcanic and epiclastic flow deposits of Group2.

Unit	Bedding features and texture	Grain size and component features	Thickness
G2-Af3-4	Massive layer	Fine to medium ash beds: brown ash including white lithic fragments.	～20cm
G2-Df2-3	Laminated and massive layer with channel like structure	Fine size matrix. Up to 5cm rounded lithic fragments composed of lava, scoria, pumice, and carbonate.	～20cm
G2-Df1	Laminated and massive layer with channel like structure	Silt to fine pebble size matrix. Up to 30cm rounded lithic fragments composed of lava, scoria, pumice, carbonate, and plutonic rocks.	～5m
G2-Af2	Two accretionary lapilli layers interbedded consolidated ash layer	Fine to medium ash beds: reddish or greenish grey ash.	55cm
G2-Mf	Massive layer with weakly stratified (planar- to dune-bedded) layer	Silt to fine sized matrix. Up to 3 cm rounded and subangular lithic fragments composed of lava, scoria, and carbonate.	20～40cm
G2-Af1	Alternance of ash and scoria layer	Fine ash beds: brown ash including highly vesiculated scoria (5～10mm). Scoria lapilli beds: highly vesiculated scoria including lithic fragments composed of lava and carbonate.	35cm

Table 1-3. Characteristics of volcanic and epiclastic flow deposits of Group3A～Group3C.

Unit	Bedding features and texture	Grain size and component features	Thickness
G3C-Af	Alternance of ash and scoria layers overlying accretionary lapilli ash layer	Fine ash beds: brown ash including highly vesiculated scoria (5～10mm). Scoria lapilli beds: highly vesiculated scoria including lithic fragments composed of lava and carbonate.	30～40cm
G3B-Af	Lenticular scoria layer	Scoria lapilli beds: highly vesicluated, black scoria (～1.5cm in size).	～3cm
G3A-Df	Alternance of laminated and massive layers with channel like structure	Laminated bed: silt to fine pebble size, black matrix. Up to 10cm rounded lithic fragments composed of lava, scoria, and pumice. Massive beds: fine size, dark brown matrix, enclosing sparse black	～100cm
G3A-Af	Mantle bedding scoria layer showing contrasting grain size	Scoria lapilli beds: highly vesicluated, black scoria. Lowermost bed fine size scoria (～3cm in size).	10cm

of the East and South Walls, rubble from the demolished building lies to a maximum height of 2.9 m (Loc. E1, Appendix 3-1). G1-Af1, G1-Af3, and G1-Af5, mainly composed of scoria, fill voids among the rubble. The building of Vano2 (Fig. 2) seems to have had no roof at the time of the AD 472 eruption because the G1-Af fall deposits uniformly cover all of the architectural waste such as bricks, plasters, mosaics, and shreds, which had buried the original floor of the villa (Appendix 5-1). The bricks, stucco, and charcoal are interbedded or included in G1-Af5, G1-Af6, and G1-Af7 (Appendix 5-1 and Appendix 5-2).

One of the important characteristics of G1-Af is that its thickness increases near the building wall. Although the average thickness of G1-Af is 20 cm, it reaches up to 65 cm near the wall of Vano2 at Loc. N2 (Appendix 4-2). In particular, G1-Af4, Af5, and Af7 become thick approaching the wall. We can observe similar characteristics around the Apses and the South Gate. The South Gate is decorated with stucco and two niches on the northern side (Fig. 2). We recognized G1-Af deposits at both sides of the gate.

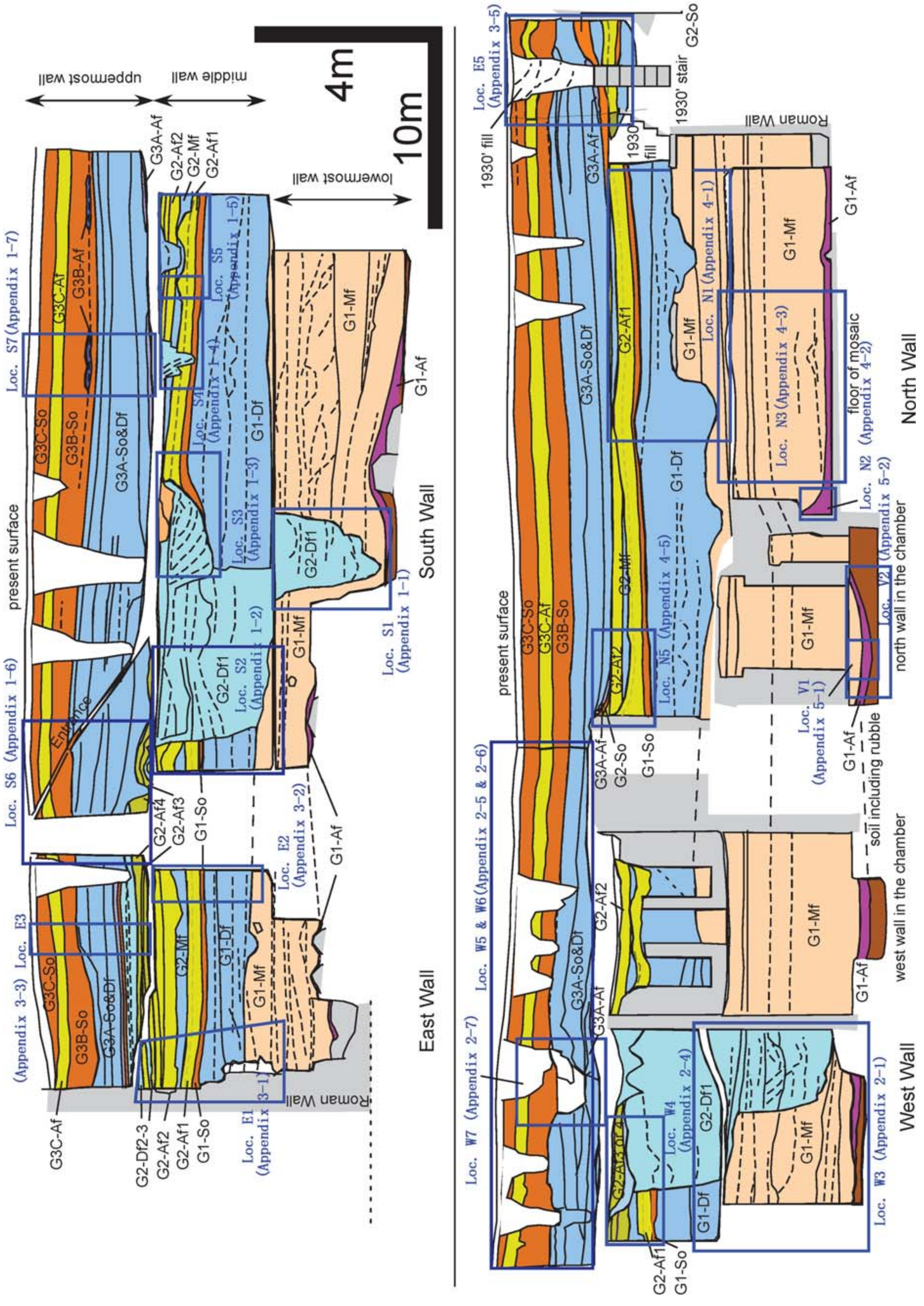

Fig. 4. Complete stratigraphy at the Roman villa on the South Wall, East Wall, West Wall, and North Wall of the 2004 excavation. Detailed explanations of the numbered locations are shown in Appendix 1~6.

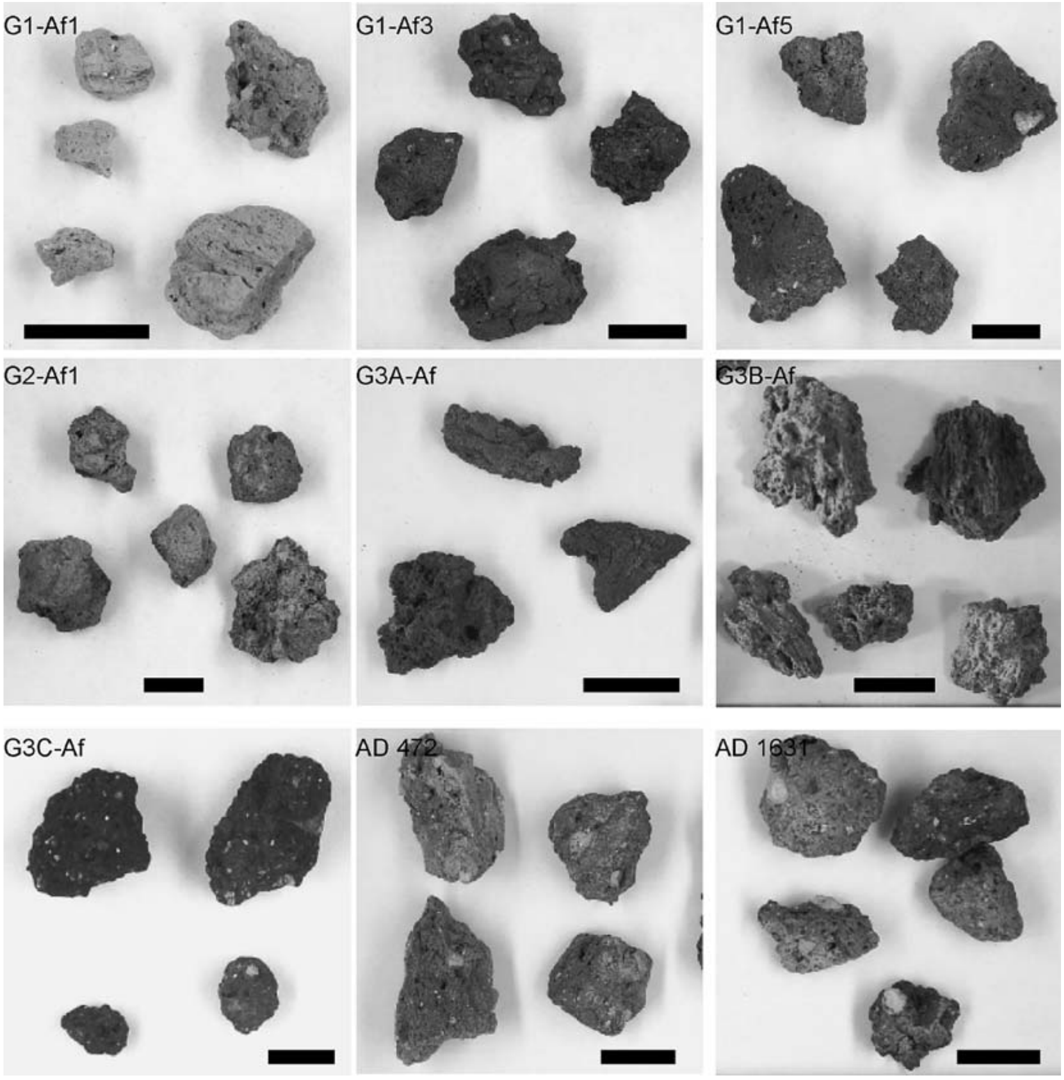

Fig. 5. Photographs of juvenile fragments collected from the excavation site (a∼g) and type locality, Ottaviano (h, i). Black scale bar is 1 cm.

Around its south side, the thickness of G1-Af7 increases toward the gate to 30 cm (Appendix 6-1). Around its north side, G1-Af overlies the floor with average thickness as well as the floors of two niches, which are semicircular recesses covered by a hemispherical vault (Appendix 6-2). Although the niches face away from Mt. Somma-Vesuvius, the thickness of G1-Af7 increases towards the interiors of the niches. These features imply that G1-Af7 is a pyroclastic surge deposit.

ii) G1-Mf

G1-Mf is characterized by a consolidated massive mudflow deposit with a fine matrix. The components are fragments of lavas, scoria including AD 472 juveniles, pumices, plutonic rocks, and carbonate rocks. Roman remnants such as statue, brick, and mosaic are also included. The maximum grain size of the lithic fragments is about 40 cm. This deposit can be divided into four flow-units (G1-Mf1, G1-Mf2, G1-Mf3, and G1-Mf4, e.g., Appendix 4-1) based on flow boundaries and lithological differences (Kaneko *et al.,* 2005). The flow boundaries are defined by well-sorted stratified deposits (Appendix 2-1). All boundaries are almost horizontal without erosional surfaces, even near the walls of buildings (the Roman wall; Appendix 3-1, the wall of Vano2; Appendix 4-3).

This flow deposit buried most of the buildings, including pillars and rubble, without causing a collapse, and most of the buildings are not damaged, as indicated by an overview of the North Wall at Loc.

N1 (Appendix 4-1). It is noteworthy that the pillars had been partially destroyed and striated by the mudflows, with the exception of one pillar and a large fragment of the demolished building lying near the original position. On the other hand, several large areas of rubble are scattered in the northern area of the South Gate. Although this rubble seems to be surrounded by G1-Mf deposits, the G1-Af deposit covers it directly (Appendix 6-3). This indicates that G1-Mf filled voids among pieces of rubble.

The characteristics of each flow-unit are shown in Table 1. G1-Mf1 includes a small amount of lithic fragments, which range from about 5 to 15 cm in diameter. These lithic fragments mainly consist of lavas, although small amounts of scoria, pumices, carbonate rocks, and plutonic rocks are also included. The matrix is composed of medium to fine-sized ash particles. G1-Mf2 is characterized by a massive deposit with faint lamina. This deposit consists of a very small volume of lithic fragments such as lavas, scoria, carbonate rocks, and pumices with diameters of about 5 cm. The matrix is composed of fine to medium-sized ash particles. G1-Mf3 is characterized by a massive deposit with a high proportion of lithic fragments (about 25 vol.%). The lithic fragments are composed of lavas, scoria, and carbonate rocks with a maximum diameter of 27 cm. Weak lamination is also recognized. The matrix is composed of fine-sized ash particles. G1-Mf4 is a massive deposit with the largest lithic fragments (maximum size is 40 cm) among the G1-Mf flow-units, which are composed of lavas and a small portion of scoria and carbonate rocks. The matrix is composed of fine-sized ash particles.

Well-sorted stratified deposits interbedded between each flow-unit of G1-Mfs are composed of medium to coarse-sized sand. These deposits are rich in AD 472 juveniles and pumices from other Plinian eruptions. They are characterized by low-angle cross-bedded structures, indicating fluvial flow deposits (Appendix 2-1). In particular, the deposit between G1-Mf1 and G1-Mf2 is the thickest (up to 80 cm), which is observed at the South Wall and the West Wall at Loc. W1 (Appendix 2-1) continuously. At the North Wall at Loc. N3 (Appendix 4-3), thin fluvial deposits are recognized among these G1-Mfs.

iii) G1-Df

G1-Df is characterized by well-sorted and well-stratified layers. Although G1-Df has distinctive erosive structures itself, this deposit did not destroy structures such as the wall of Vano2 (Loc. N4, Appendix 4-4) and pillars (Loc. N1, Appendix 4-1), as well as G1-Mf. G1-Df includes rounded lapilli-sized juveniles of AD 472 and pumices from other Plinian eruptions. G1-Df is capped by a thin soil layer about 5 cm thick (G1-So).

In this study, G1-Df can be divided into two flow-units (G1-Df1 and G1-Df2) based on lithological differences (Appendix 3-1), which Kaneko *et al.* (2005) defined as one debris (fluvial) flow deposit. G1-Df1, the lower deposit, is characterized by a lithic-rich deposit with a layered structure. The components are fragments of lavas, scoria, carbonate rocks, pumices, and plutonic rocks, which range from 3 to 22 cm in diameter. The matrix is composed of medium to fine pebble-sized lithic particles. This deposit is faintly eroded by overlying G1-Df2, which is a lenticular-shaped and conspicuous low-angle laminated deposit. The components are well-sorted medium to lapilli-sized particles, which are fragments of lavas, scoria, carbonate rocks, and pumices. Grain-size ranges up to 6 cm in diameter. The matrix is composed of silt to fine pebble-sized particles.

4. 2 Group2

Group2 consists of four ash-fall and scoria-fall deposits (G2-Af1, G2-Af2, G2-Af3, and G2-Af4), interbedding one mudflow (G2-Mf) and three fluvial flow deposits (G2-Df1, G2-Df2, and G2-Df3) without soil (Fig. 3). Although Kaneko *et al.* (2005) had already identified G2-Af1, G2-Mf, G2-Af2, and G2-Df, we newly identified G2-Af3, G2-Df2, G2-Af4, and G2-Df3 above G2-Df. G2-Df is re-named G2-Df1 in this study. The total thickness of Group2 deposits is generally about one meter.

i) Fall units (G2-Af1, G2-Af2, G2-Af3, and G2-Af4)

G2-Af1 is characterized by an alternation of ash- and scoria-fall deposits with a thickness of about 35 cm (Appendix 3-2). The lower part is a stratified ash layer, and the upper part is an alternation of ash and lapilli layers. The upper part is often eroded by the mudflow associated with the overlying G2-Mf deposit at Loc. S5 (Appendix 1-5). Juvenile fragments are poor-vesiculated aphyric scoria (Fig. 5). At Loc. N5 near the eastern wall of Vano2 (Appendix 4-5), G2-Af1 and G2-Af2 are thicker than observed at the other sites. This is the same feature as G1-Af near the wall of Vano2 (Appendix 4-2).

G2-Af2 consists of three layers with a total thickness of about 55 cm (Appendix 3-2). The lower and upper parts include accretionary lapilli layers (25 cm and 15 cm thick respectively), and the middle part is a consolidated ash-fall layer (15 cm thick). Kaneko *et al.* (2005) did not recognize the upper layer because it was often eroded by fluvial flows associated with overlying G2-Dfs deposits (Appendix 1-4).

G2-Af3 and G2-Af4 are characterized by semi-consolidated thin ash-fall deposits, each with a thickness of about 10 cm (Appendix 1-6). They are indiscernible except at Loc. S-6 (Appendix 1-6) on the South Wall and Loc. E-1 (Appendix 3-1) on the East Wall, where interbedding flow deposits are observed between the two ash-fall deposits.

ii) Flow units (G2-Mf, G2-Df1, G2-Df2, and G2-Df3)

G2-Mf is a consolidated mudflow deposit (Appendix 1-5). This deposit is a clast-supported conglomerate. It is composed of rounded or subangular lava and scoria fragments of coarse to lapilli size. At Loc. N5, G2-Af1 becomes thicker towards the wall of Vano 2 (Appendix 4-5), and G2-Mf buried the topographic concave formed by G2-Af1.

G2-Df1, G2-Df2, and G2-Df3 are fluvial flow deposits characterized by planner- to dune-bedded structures. The thicknesses of G2-Dfs vary because they sometimes form channel structures due to erosion. In particular, the fluvial flow of G2-Df1 erodes the underlying Group1 deposits locally with a maximum thickness of 5 m.

G2-Df1 is a semi-consolidated deposit, whose matrix is mainly composed of small pebbles and coarse sand. The lithic fragments are subangular boulders, cobbles, and coarse pebbles, which are composed of lavas, scoria, carbonate rocks, pumices, and plutonic rocks. G2-Df1 fills channel-like erosion surfaces, and includes fragments of underlying deposits; G1-Mf to G2-Af2 at the South Wall as shown at Loc. S1〜S3 (Appendix 1-1〜Appendix 1-3) and the West Wall as shown at Loc. W-1〜W-2 (Appendix 2-1〜Appendix 2-2). G2-Df1 flows down from the central part of the South Wall to the West Wall, passing the southern margin of the building. This deposit shows weak lamination and an imbrication structure at Loc. W-1 and Loc. W-2 (Appendix 2-1 and Appendix 2-2).

G2-Df2 and G2-Df3 have similar lithological characteristics. Both are characterized by a lithic-rich deposit, whose matrix is composed of medium to fine pebble-sized particles (Appendix 3-1). The lithic fragments are composed of lavas, scoria, carbonate rocks, pumices, and plutonic rocks up to 3 cm in size. G2-Df2 and G2-Df3 are sometimes indiscernible because of their lithological similarity. When we cannot distinguish these deposits, we describe them as G2-Df2-3. At the central part of the South Wall shown at Loc. S3〜S5 (Appendix 1-3〜Appendix 1-5), the underlying Group2 deposits are eroded by the flow of G2-Df2-3 with a channel-like structure.

4. 3 Group3A

Group3A consists of a scoria-fall deposit (G3A-Af, Fig. 5), a fluvial flow deposit (G3A-Df), and a soil deposit (G3A-So) with a total thickness of about 110 cm. G3A-Af occurs as a lenticular-shape deposit with a maximum thickness of 10 cm, and is composed of vesiculated black scoria (Appendix 4-6). This deposit sometimes has a thickness of more than 10 cm, and the spaces among scoria grains are filled with fine particles. G3A-Af on the upper wall of the West Wall is, on the other hand, not disturbed. The complete sequence of this wall is shown at Loc. W5 and Loc. W6 (Appendix 2-5 and Appendix 2-6).

G3A-Df is divided into three layers, brown fine-sand layer, black sand layer with distinctive lamina, and light-brown fine sand layer in ascending order (Appendix 1-7). All three layers of G3A-Df are characterized by the presence of white pumice. Both fine-sand layers are unconsolidated and massive. They sometimes grade into G3A-So without a clear boundary. On the other hand, the black sand layer has a lenticular form, which is characterized by low-angle sigmoidal structures, including subangular to sub-rounded lithic fragments. The lithic fragments are composed of lavas and a small volume of scoria. The largest lithic fragment in the black sand layer is 27 cm in diameter, and is observed at Loc. W6 (Appendix 2-6). The matrix is composed of fine to medium-sized particles.

4. 4 Group3B

Group3B consists of G3B-Af and G3B-So in ascending order. G3B-Af is a lenticular-shaped deposit composed of vesiculated black scoria (Fig. 5) with a maximum thickness of 2 cm (Appendix 1-7). At Loc. W5, this fall deposit had been remobilized locally, and sometimes has lamina with a purplish fine-sized matrix (Appendix 2-5). G3B-So is characterized by both an orange-colored matrix and the presence of well-vesiculated scoria (Appendix 1-7).

4. 5 Group3C

G3C-Af consists of alternating scoria-fall and ash-fall layers, and an overlying ash-fall layer with a total thickness of about 40 cm (Appendix 4-6). The lower layers are only about 5 cm thick. These deposits are observed well at the North Wall at Loc. N6〜Loc. N9 (Appendix 4-6〜Appendix 4-9), but are eroded by overlying mudflows or plowed furrows artificially shown at Loc. W6 and Loc. W7 (Appendix 2-6 and Appendix 2-7). The scoria layer of G3C-Af includes poor-vesiculated juveniles, lavas, carbonate rocks, and plutonic rocks. The juvenile fragments are rich in crystals and clinopyroxene microlites in hand specimens (Fig. 5).

5. Petrography and chemical composition of juvenile materials

Juvenile materials of air-fall deposits (G1-Af, G2-Af1, G2-Af2, G3A-Af, G3B-Af, and G3C-Af, Fig. 5) were selected for chemical analyses. Air-fall scoria of Subplinian eruptions (AD 472 and AD 1631) from type locality (Ottaviano, Fig. 1) were also analyzed for comparison to estimate the eruption ages of air-fall deposits at the excavation site.

5. 1 Petrography

Photographs of typical juvenile fragments collected from the excavation site and the Ottaviano are shown in Fig. 5. Microphotographs of their thin-sections are presented in Fig. 6.

G1-Af scoria shows a porphyritic texture over the entire stratigraphic sequence. G1-Af1 scoria contains greenish clinopyroxene, coarse leucite, biotite and minor garnet, K-feldspar, and davyne phenocrysts. In G1-Af3 scoria, colorless clinopyroxene phenocrysts appear in addition to the mineral assemblage of G1-Af1 scoria, although there are fewer greenish clinopyroxene phenocrysts. In G1-Af5 scoria, greenish clinopyroxene phenocrysts almost disappear and olivine phenocrysts are rarely recognized.

G2-Af1 scoria contains colorless and greenish clinopyroxene and opaque minerals as phenocrysts, and biotite and leucite as microphenocrysts.

G3A-Af scoria contains coarse zoned clinopyroxene phenocrysts with a glomeroporphyritic texture. Rims of the clinopyroxene phenocrysts are composed of zoned greenish clinopyroxene. G3B-Af scoria contains coarse colorless clinopyroxene, fine greenish pyroxene, biotite, and leucite phenocrysts. Leucite also occurs as microlites. G3C-Af scoria contains colorless and greenish clinopyroxene, biotite, leucite, plagioclase, and K-feldspar phenocrysts. They are characterized by greenish clinopyroxene microlites with distinctive oscillatory zoning.

Samples of AD 472 fall deposits in Ottaviano, which consist of one scoria-fall unit and overlying ash-fall units including a surge-like layer, were collected from lower, middle, and upper layers of the scoria-fall unit. Scoria from the lower layer is composed of light-colored grains with the same mineral assemblage as G1-Af1 scoria. The petrographical features of the scoria from the middle and upper layers are also similar to those of G1-Af3 and G1-Af5 deposits.

AD 1631 scoria were collected from lower and upper parts of a thin scoria-fall layer at Ottaviano. These juveniles are characterized by a porphyritic texture and greenish clinopyroxene microphenocrysts with oscillatory zoning. Phenocrysts are colorless and greenish clinopyroxene, biotite, leucite, plagioclase, and K-feldspar. These petrographic features are almost the same as those of G3C-Af.

5. 2 Whole-rock compositions

Whole-rock chemical compositions were measured using a Philips 2400 XRF instrument of the Earthquake Research Institute, University of Tokyo (Appendix 7). Analytical methods are described in Kaneko *et al.* (2005). Variation diagrams are shown in Fig. 7.

G1-Af scoria ranges from phonolite (G1-Af1) to phono-tephrite (G1-Af3 and G1-Af5) in the alkali/silica diagram. Whole-rock compositions of G1-Af scoria overlap almost completely with those of the AD 472 deposits at Ottaviano in every chemical component. Moreover, these chemical data form almost the same compositional trend as those reported for the AD 472 eruption (Rosi and Santacroce, 1983; Ayuso *et al.,* 1998). Compared to reported data, our data sets of Ottaviano show a wide compositional range (SiO_2=49.3〜52.5 wt.%) having a more SiO_2-rich composition than that reported. This SiO_2-rich end corresponds to the sample from the basal layer at Ottaviano. This is probably because our data sets covering almost all stratigraphic units are more ex-

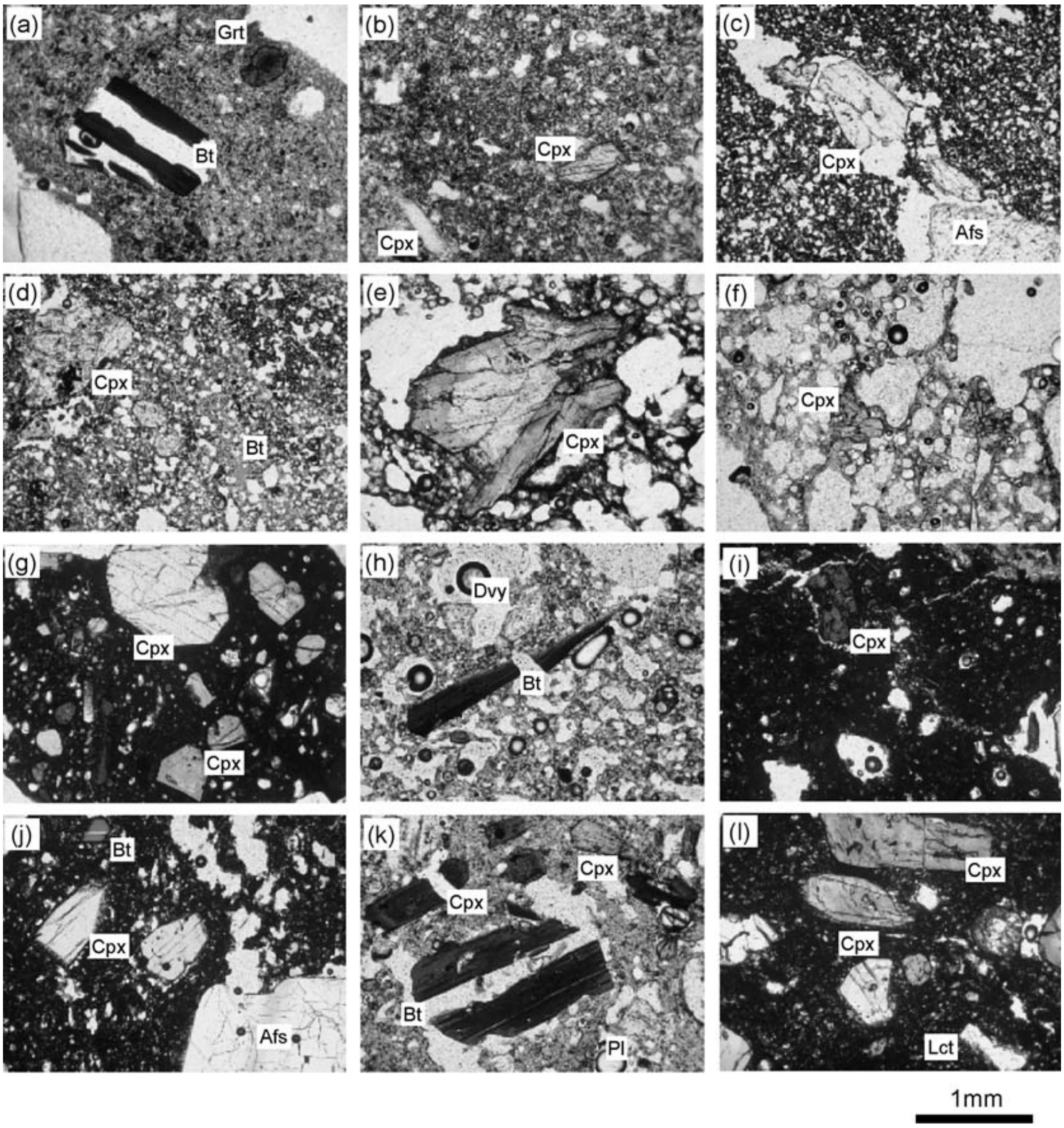

Fig. 6. Microphotographs (open nicol) of juvenile materials from excavation site (a)〜(g) and Ottaviano (h)〜(l). (a) Light-colored pumice of G1-Af1 with biotite and garnet phenocrysts. (b) Greenish grey scoria of G1-Af3 with colorless clinopyroxene phenocryst. (c) Dark-colored scoria of G1-Af5 with colorless clinopyroxene and alkali-feldspar phenocrysts. (d) Light-colored scoria of G2-Af1 with colorless clinopyroxene phenocrysts and biotite microphenocrysts. (e) Well-vesiculated black scoria of G3A-Af containing clinopyroxene phenocryst with a glomeroporphyritic texture, (f) Well-vesiculated brown scoria of G3B-Af with clinopyroxene phenocrysts and cross-shaped leucite microlite. (g) Dark-colored scoria of G3C-Af with greenish and colorless clinopyroxene phenocrysts. Greenish pyroxene phenocrysts show oscillatory zoning. Samples of AD 472 scoria were collected from (h) lower layer, (i) middle layer, and (j) upper layer. (h) Well-vesiculated light-colored pumice with biotite and davyne phenocrysts. (i) Greenish grey scoria with greenish clinopyroxene phenocryst. (j) Dark-colored scoria with colorless clinopyroxene, alkali-feldspar, and biotite phenocrysts. Samples of AD 1631 scoria were collected from (k) lower layer and (l) upper layer. (k) Well-vesiculated light-colored scoria with biotite, plagioclase, and greenish and colorless clinopyroxene phenocrysts. (l) Dark-colored scoria with leucite and colorless and greenish clinopyroxene phenocrysts. Greenish pyroxene phenocrysts show oscillatory zoning. Abbreviation: Bt, biotite; Grt, garnet; Cpx, clinopyroxene; Afs, alkali-feldspar; Kfs, K-feldspar; Pl, plagioclase; Dvy, davyne; Lct, leucite.

haustive than those of previous studies.

Juvenile scoria of G3C-Af range from tephritic basanite to tephri-phonolite in alkali/silica diagram. They almost completely coincide with AD 1631 deposits collected from Ottaviano in every chemical component. Moreover, they are also identical to

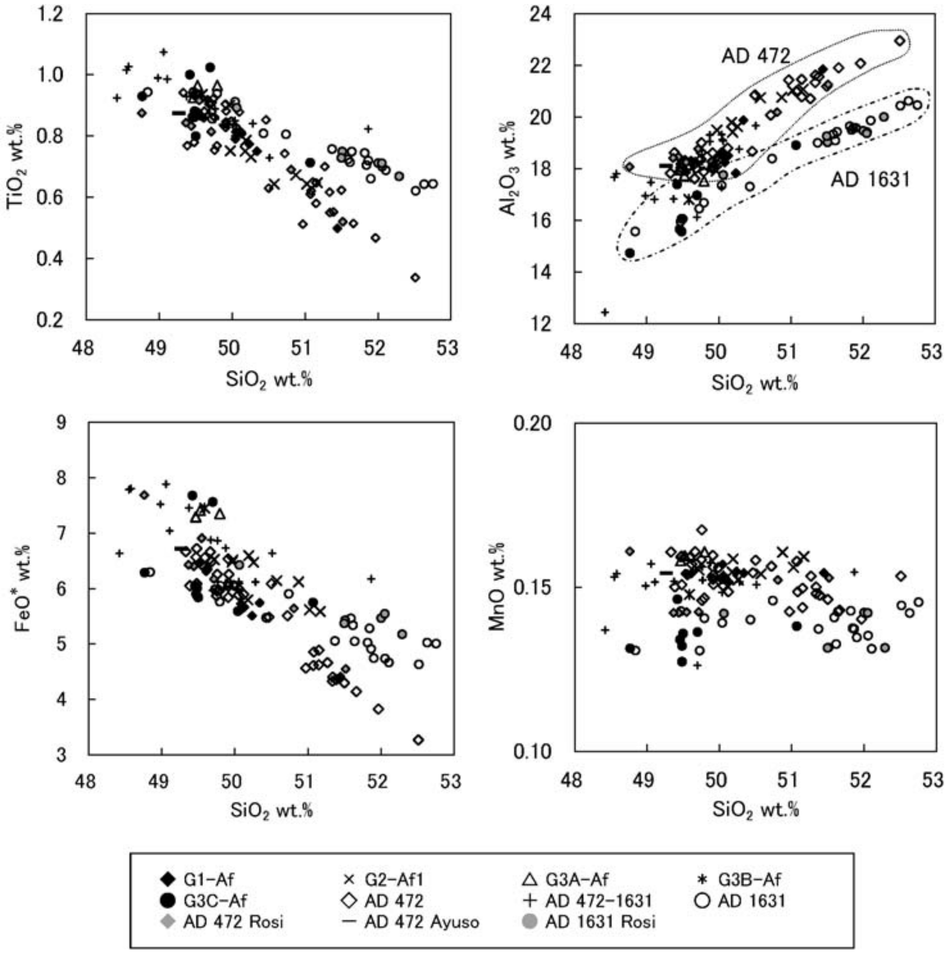

Fig. 7. Harker variation diagrams of juvenile materials of Mt. Somma-Vesuvius. G1-Af = Closed diamond, G2-Af1 = crisscross, G3A-Af = open triangle, G3B-Af = asterisk, G3C-Af = closed circle, AD 472 scoria collected from Ottaviano = open diamond, AD 472〜1631 scoria collected from Ottaviano = cross, AD 1631 scoria collected from Ottaviano = open circle, AD 472 data reported by Rosi and Santacroce *et al.* (1983) = grey diamond, AD 472 data reported by Ayuso *et al.* (1998), AD 1631 data reported by Rosi *et al.* (1993) = grey circle.

those of the AD 1631 deposit reported by Rosi *et al.* (1993), although our data sets for the 1631 eruption show a slightly wider range (SiO_2 = 48.8〜52.8 wt.%) than the reported data.

Juveniles of G2-Af1, G3A-Af, and G3B-Af are classified as phono-tephrite. They are plotted in the region between the G1-Af and G3C-Af trends in the alkali/silica diagram. Juveniles of G2-Af1 show a narrow compositional range that is clearly distinguishable from the G1-Af and G3C-Af trends. It is not so convincing that juveniles of G3A-Af and G3B-Af have distinctive compositions because of the small number analyzed.

6. Eruption ages of fall deposits at the villa

The compositional and petrographical similarities discussed above led to the conclusion that the first volcanic products that covered the villa were air-fall deposits of the AD 472 eruption. In addition, G1-Af7, which is a pyroclastic surge deposit generated during the final phase of the AD 472, is consistent with the stratigraphy and isopach maps of the AD 472 deposits by Sulpizio *et al.* (2005). This conclusion is consistent with Kaneko *et al.* (2005).

Lithological and petrological similarities between the AD 1631 deposit reported by Rosi *et al.* (1993) and the scoria of G3C-Af imply the same origin. Our chemical analyses of these samples also reinforce this view. We conclude, therefore, that G3C-Af,

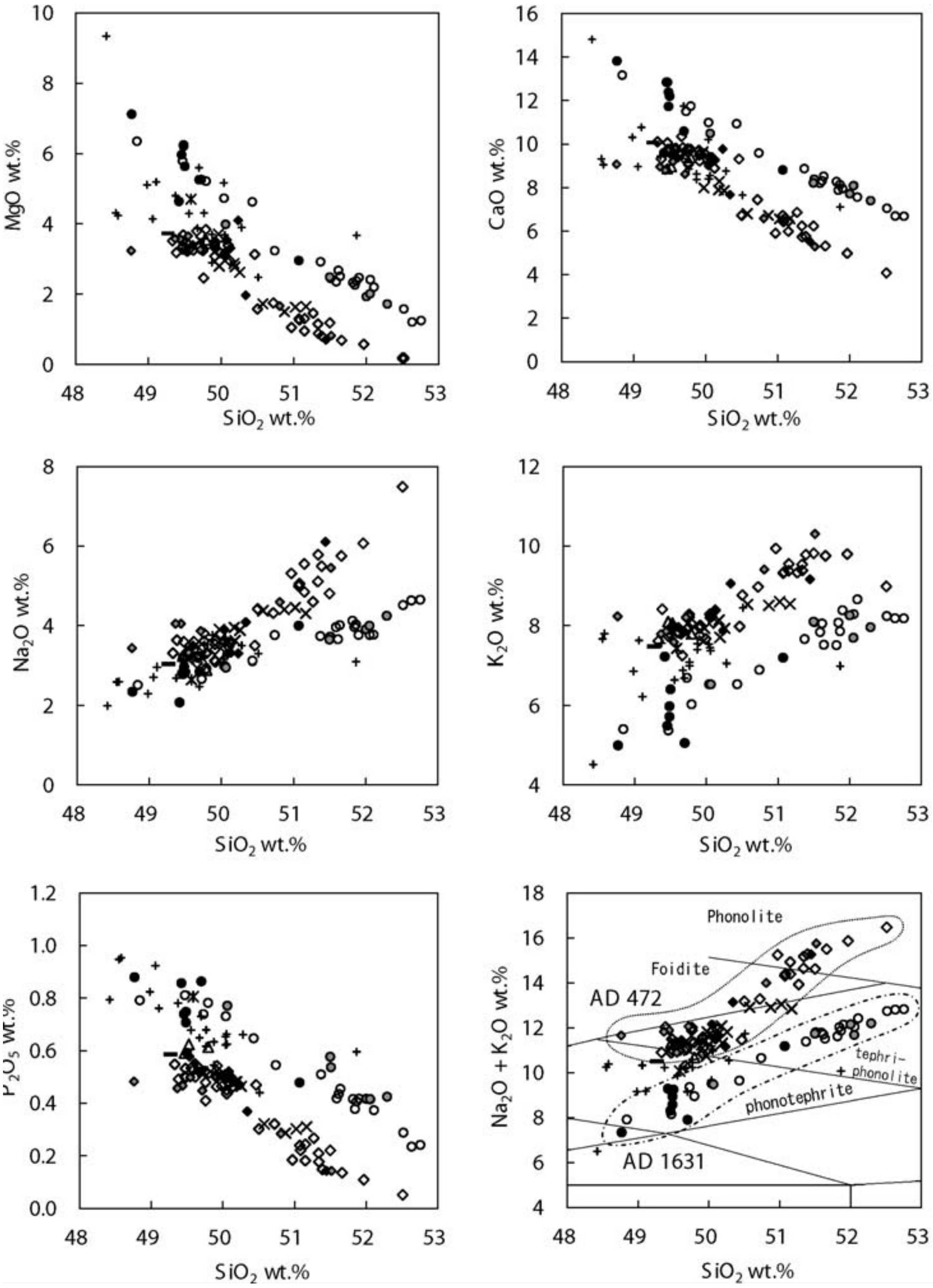

Fig. 7. (Continue)

the topmost deposit in the villa, is a product of the AD 1631 eruption.

Wide and distinctive compositional ranges of juveniles of the AD 472 and AD 1631 deposits allow us to identify each deposit at the villa. On the other hand, scoria of other groups are clustered around the phono-tephrite field (Fig. 7, Ayuso *et al.,* 1998). Therefore, it is difficult to distinguish them compositionally. Moreover, frequent eruptions after AD 472 (Principe *et al.,* 2004) prevent us from identifying the eruption ages of these groups. According to the chronology of Vesuvius summarized by Principe *et al.* (2004), the most proximal moderate-scale eruption after AD 472, which seems to have struck the villa, was the AD 536 eruption. Therefore, the deposit of Group2 could be a product of the AD 536 event.

7. Burial process of the Roman villa at Somma Vesuviana

The results presented in the previous sections

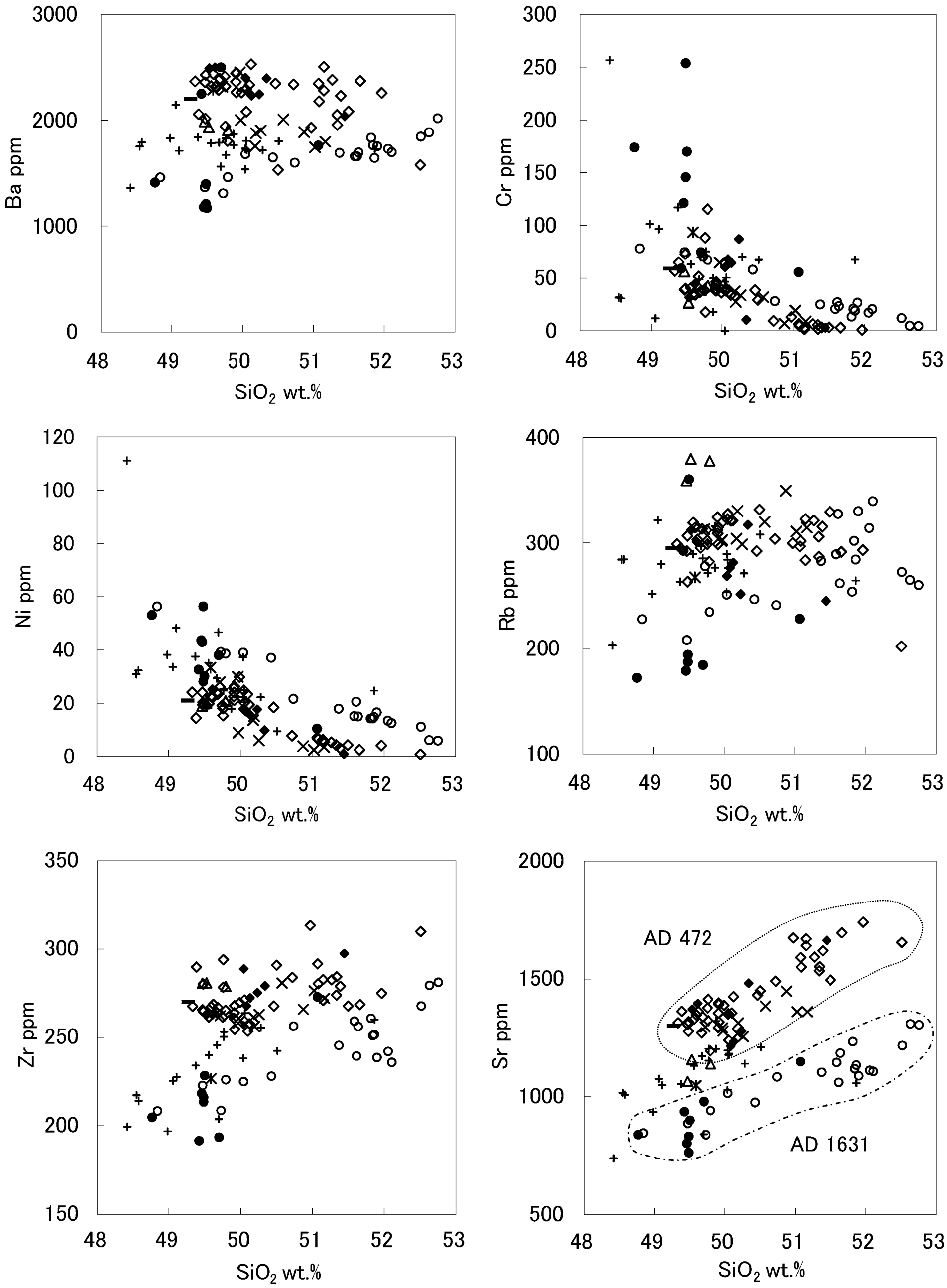

Fig. 7. (Continue)

allow us to reconstruct how the villa was buried by volcanic activities and incidental events. Effects on the buildings of the emplacement of fall and flow deposits are also discussed. Models of burial processes are summarized in several graphics (Fig. 8).

Deposition of Group1 (AD 472)

The villa had been ruined to some extent before AD 472 because the first deposit of the AD 472 eruption (G1-Af) covered the demolished Roman buildings directly (Fig. 8 (1)∼(3)). This presumption is consistent with the previous study by Mastrolorenzo *et al.* (2002), in which the presence of many ruined Roman buildings at some other excavation sites in Somma Vesuviana overlain by the AD 472 deposit were interpreted to be as a consequence of a steep decline of the Roman Empire in this area.

At the beginning of the AD 472 eruption, air-fall deposits of G1-Af covered the villa, and then a surge struck it. Following emplacement of G1-Af, continuous epiclastic flows occurred (G1-Mf and G1-Df, Fig.

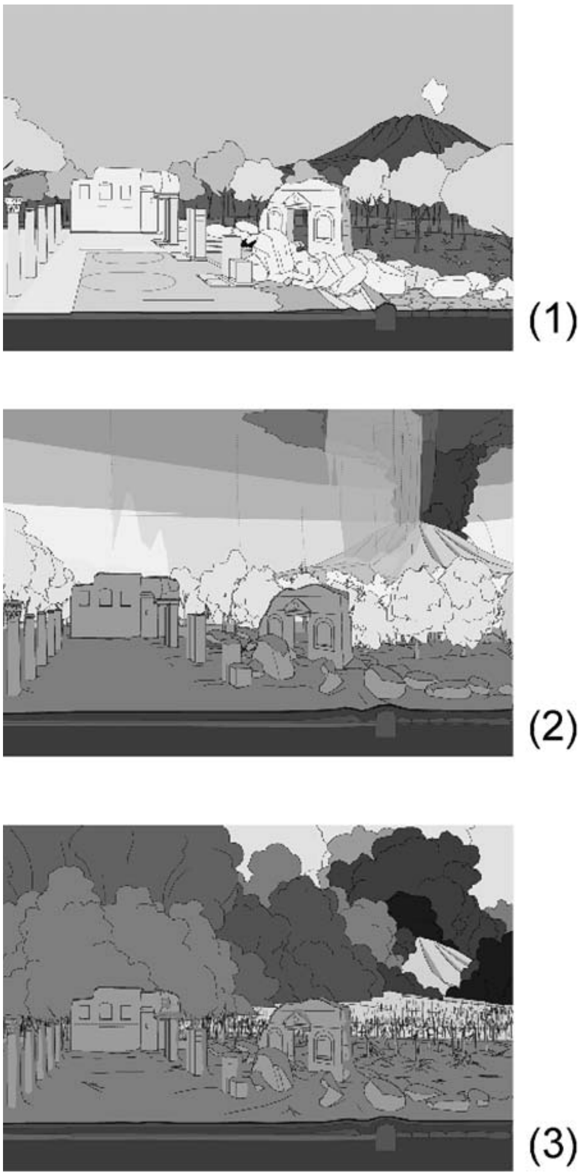

Fig. 8. Burial processes of the Roman villa. (1) Before the AD 472 eruption the Roman villa in Somma Vesuviana was already in ruins. (2) The AD 472 eruption began and the ruins of the Roman villa were covered with scoria and ash falls. (3) Pyroclastic surge occurred at the final stage of the AD 472 eruption, and covered the villa. (4) After the AD 472 eruption, mudflows struck the villa. (5) Following their deposition, the area was washed by a fluvial flow. Finally, epiclastic flows covered more than half of the Roman villa to a thickness of about 5 m. (6) During a quiet period after the AD 472 eruption, about 5 cm of soil formed. (7) The next eruption began and ash-fall covered the villa. After its deposition, epiclastic flows and eruptions occurred alternately. The epiclastic flows covered or eroded the underlying deposits. (8) After the depositions of Group2, three eruptions occurred and covered the villa. Finally, the Roman villa was completely covered by deposits (Group1〜Group3C). Their total thickness is about 8 m.

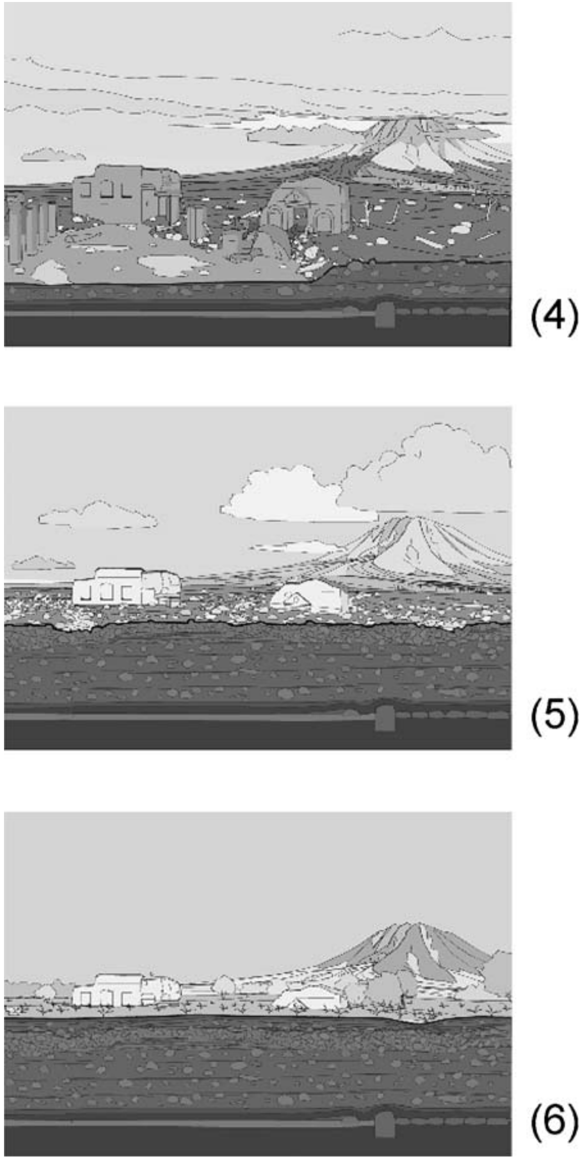

Fig. 8. (Continue)

8 (4)〜(6)), and buried half of the Roman villa to a thickness of about 5 meters.

The air-fall deposits generally cover the villa to a thickness of about 20 cm, but near the walls of buildings and voids among pieces of rubble, the air-fall deposits become thicker than at other sites (Appendix 4-2). The thickness of the air-fall deposits beside walls is probably caused by slip down along the ruined wall of building, with accumulations as reported for Pompeii (Luongo *et al.,* 2003). The air-fall deposits in voids among pieces of rubble are composed only of scoria grains of G1-Af, indicating that they have rolled down the rubble and filled the voids. Contrary to the other G1-Af fall deposits, the G1-Af7

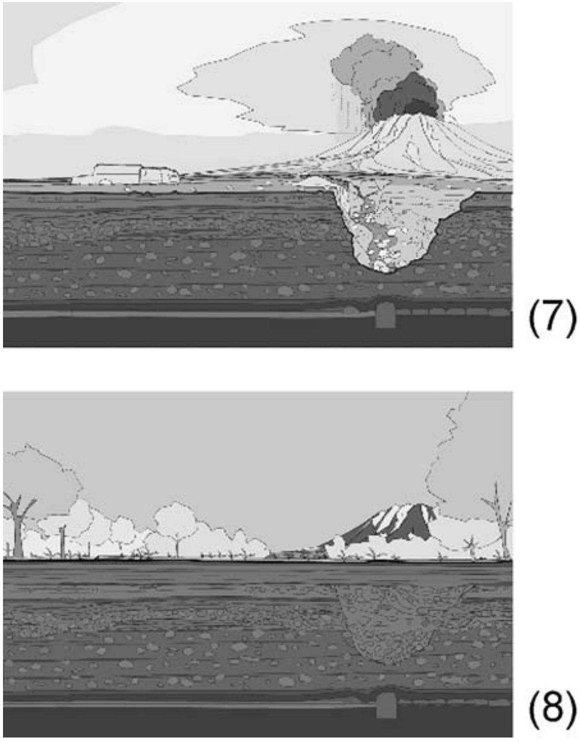

Fig. 8. (Continue)

surge covered the villa unevenly with a dune-like structure having low-angle lamina. It had settled to a remarkable thickness at the corners of the Roman buildings (Appendix 4-2, Appendix 6-1). It is considered that the surge was a highly turbulent flow having some horizontal velocity because it could enter the roofed niches facing away from Mt. Vesuvius (Appendix 6-2). As at Pompeii, inhomogeneous emplacement could reflect a temporary reduction of kinetic energy within the depositional system due to local losses of mass and velocity after a series of repeated impacts on the buildings (Luongo *et al.,* 2003).

Although the time gap between the eruption and the occurrence of epiclastic flows is not estimated quantitatively, the Roman villa had been struck by at least four mudflows and two debris flows. The flows of G1-Mf are assumed to have had a higher sediment/water ratio than those of G1-Df because block or boulder-sized coarse particles are heavily included, massive faces are dominant, and sorting is relatively poor (e.g., Lirer *et al.,* 2001). The boundaries of the G1-Mf deposits are almost horizontal without an erosional surface, indicating that the speed of each mudflow was low. Moreover, epiclastic materials engulf architectural structures such as pillars and scattered rubble without causing destruction. This suggests that these flows did not have destructive dynamic pressures. Contrary to G1-Mfs, the flow of G1-Df is considered to have a low sediment/water ratio because the grain-size is relatively small, stratified faces are recognized, and sorting is better. The G1-Df flow did not have enough power to destroy the buildings because we could not find any damaged architectural structures as was the case with G1-Mfs. After a short dormant period suggested by the thin soil layer (G1-So), the next eruption (Group2) occurred.

Deposition of Group2

During the period, four eruptions occurred (G2-Af1, G2-Af2, G2-Af3, and G2-Af4), and each was followed by epiclastic flows (G2-Mf and G2-Dfs). These eruptions are considered to be phreato-magmatic because their deposits are characterized by either or both a consolidated matrix and the presence of accretionary lapilli. Because soil deposits are not embedded by these ash-fall deposits (Fig. 8 (7)), the eruptions should have occurred successively with very short (if any) dormant periods.

Contrary to the relatively nonviolent flow that deposited G1-Df, debris flows during the deposition of Group2 eroded and entrained the underlying deposits to various extents. G2-Df1, especially, had formed a large-scale channel of up to 5 m in depth, which is the deepest channel at the excavation site. Therefore, these fluvial flows could have had enough power to make scours. However, they did not destroy any Roman architecture in spite of their high dynamic pressures. The G2-Df1 flow passed from the South Wall (Appendix 1-1) to the West Wall (Appendix 2-1).

Deposition of Group3A, Group3B, and Group3C

During the period, the products of three eruptions covered the villa (G3A-Af, G3B-Af, and G3C-Af). There are assumed to have been some quiescent periods between eruptions because of the presence of relatively thick interbedding soil deposits. The existence of intercalated epiclastic flow deposits (G3A-Df) among fall deposits also suggests occasional flooding. During this period, destruction of the Roman building did not occur because the villa had been almost buried by deposits of Group1 and Group2 (Fig. 8 (8)). The total thickness of Group3 deposits is about 3 m.

G3A-Af and G3B-Af are thought to be products of the Strombolian eruption. As we discussed in a previous section, G3C-Af is the deposit of the AD 1631 eruption. As in the case of the AD 472 eruption, the AD 1631 eruption is evaluated as one of the most violent and destructive events in the recent history of Mt. Vesuvius. However, its impact on the northern foot of Mt. Vesuvius should be much smaller than the AD 472 eruption (Rosi *et al.,* 1993).

Contrary to the frequent occurrence of epiclastic flows during the periods of Group1 and Group2, only a single epiclastic flow was recognized in Group3 depositions. This might suggest that the consolidated ash deposits had not formed until the deposition of G3C-Af. Because consolidated ash deposits have low permeability to rainwater, it might easily cause a mudflow or a fluvial flow (AD 1631 eruption; Rosi *et al.,* 1993, AD 472 eruption; Mastrolorenzo *et al.,* 2002).

8. Conclusions

Progressive enlargement of the trench at the excavation site of the Roman villa allowed us to investigate the stratigraphy of the volcanic deposits that buried the villa, and to understand the process of transportation and deposition of eruptive materials. The deposits are divided into five groups—Group1, Group2, Group3A, Group3B, and Group3C—by the presence of interbedding soil deposits and lithological differences. Based on spatial distribution and stratigraphy, and considering the relationship between deposit and building, the burial process is as follows. The villa had already been demolished before the AD 472 eruption. When the AD 472 eruption began, ash-fall and surge deposits covered it. After the eruption, several epiclastic flows struck the villa. Finally, flow deposits covered more than half of the villa to a thickness of about 5 m. After a short dormant period, the next eruption began and an air-fall deposit covered Group1. After deposition, epiclastic flows and eruptions occurred alternately. G2-Df1 formed a deep flow-channel up to 5 m without passing over the buildings. During the period of Group3, three eruptions occurred and the deposits covered the villa. Between the eruptions of G3A-Af and G3 B-Af, a fluvial flow occurred without associated phreato-magmatic eruptions. The AD 1631 eruption was the last event to affect the site. Finally, the Roman villa was completely covered by these deposits to a thickness of about 8 m. The lack of damage to the villa resulted from the very low dynamic pressures of the epiclastic flows that formed G1-Mf and G1-Df deposits. The flow of G2-Df1 produced flow channels on pre-existing deposits, however, it did little damage to the villa because it did not pass over the buildings. As a result, the excavated villa was in good condition.

In addition, we did chemical analyses of considerable amounts of juvenile materials discerned at the villa. Petrological characteristics with lithology showed that the last impact on this villa was the sub-plinian eruption in AD 1631. Moreover, detailed chemical analyses revealed that the compositions of juveniles of the AD 472 and AD 1631 deposits had more compositional variations than those of reported data.

Acknowledgements

We thank Satoshi Matsuyama and other excavation team members for their support during our geological survey. We also thank Claudia Angelelli, Tomoo Mukai, Kohe Sugiyama, Katsuhiro Iwaki, and Antonio de Simone for discussions about archaeological objects. We thank Giovanni Longobardi and Akira Matsuda, who satisfied our daily excavation requests. The comments of Fukashi Maeno and an anonymous referee also helped to improve the manuscript. This work was supported by a grant-in-Aid for scientific research from MEXT (No. 16089204).

References

Arrighi, S., Principe, C., and Rossi, M., 2001, Violent strombolian and subplinian eruptions at Vesuvius during post-1631 activity. *Bull. Volcanol.,* **63**, 126–150.

Ayuso, R., Vivo, B. D., Rolandi, G., Seal, R. R. II, and Paone, A., 1998, Geochemical and isotopic (Nd-Pb-Sr-O) variations bearing on the genesis of volcanic rocks from Vesuvius, Italy. *J. Volcanol. Geotherm. Res.,* **82**, 53–78.

Barberi, F., Cioni, R., Rosi, M., Santacroce, R., Sbrana, A., and Vecci, R., 1989, Magmatic and phreato-magmatic phases in explosive eruptions of Vesuvius as deduced by grain-sized and component analysis of the pyroclastic deposits. *J. Volcanol. Geotherm. Res.,* **38**, 287–307.

Cioni, R., Santacroce, R., and Sbrana, A., 1999, Pyroclastic deposits as a guide for reconstructing the multi-stage evolution of the Somma-Vesuvius Caldera. *Bull. Volcanol.,* **60**, 207–222.

Kaneko, T., Nakada, S., Yoshimoto, M., Fujii, T., Yasuda, A., Yoneda, M., and Aoyagi, M., 2005, Determination of burial age of the Augustus' villa (Italy). *Geochem. J.,* **39**, 573–578.

Lirer, L., Vinci, A., Alberico, I., Gifuni, T., Bellucci, F., Petrosino, P., and Tinterri, R., 2001, Occurrence of inter-eruption debris flow and hyperconcentrated flood-flow deposits on Vesuvius volcano, Italy. *Sedimentary Geology,* **139**, 151–167.

Luongo, G., Perrotta, C., and Scarpati, C., 2003, Impact of the AD 79 explosive eruption on Pompeii, Ⅰ. Relations amongst the depositional mechanisms of the pyroclastic products, the framework of the buildings and the associated destructive events. *J. Volcanol. Geotherm. Res.,* **126**. 201–223.

Mastrolorenzo, G., Palladion, D.M., Vecchio, G., and Taddeucci J., 2002, The 472 AD Pollena eruption of Somma-Vesuvius (Italy) and its environmental impact at the end of the Roman Empire. *J. Volcanol. Geotherm. Res.,* **113**, 19–36.

Perrotta, A., Scarpati, C., and Luongo, G., 2006a, Volcaniclastic resedimentation on the northern slope of Vesuvius as a direct response to eruptive activity. *Landslides,* **3**, 295–301.

Perrotta, A., Scarpati, C., Luongo G., and Aoyagi, M., 2006b, Burial of Emperor Augustus' villa at Somma Vesuviana (Italy) by post-79 AD Vesuvius eruptions and reworked (lahars and stream flow) deposits. *J. Volcanol. Geotherm. Res.,* **158**, 445–466.

Principe, C., Tanguy, J.C., Arrighi, S., Paiotti, A., Goff, M.L., and Zoppi, U., 2004, Chronology of Vesuvius' activity from A.D. 79 to 1631 based on archeomagnetism of lavas and historical sources. *Bull. Volcanol.,* **66**, 703–724.

Rolandi, G., Barrella, A.M., and Borrelli, A., 1993, The 1631 eruption of Vesuvius. *J. Voncanol. Geotherm. Res.,* **58**, 183–201.

Rolandi, G., Petrosino, P., and Geehin, J. Mc., 1998, The interplinian activity at Somma-Vesuvius in the last 3500 years. *J. Voncanol. Geotherm. Res.,* **82**, 19–52.

Rolandi, G., Munno, R., and Postinlione, I., 2004, The A.D. 472 eruption of the Somma Volcano. *J. Volcanol. Geotherm. Res.,* **129**, 291–319.

Rosi, M. and Santacroce, R., 1983, The A.D. 472 Pollena eruption: volcanological and petrological data for this poorly-known Plinian type event at Vesuvius. *J. Volcanol. Geotherm. Res.,* **17**, 249–271.

Rosi, M., Principe, C., and Vecci, R., 1993, The 1631 Vesuvius eruption. A reconstruction based on historical and stratigraphical data. *J. Volcanol. Geotherm. Res.,* **58**, 151–182.

Santacroce, R. and Sbrana, A., 2003, Geological map of Vesuvius. *Universita degli studi di PISA*.

Sulpizio, R., Mele, D., Dellino, P., and Volpe, L., 2005, A complex, Subplinian-type eruption from low-viscosity, phonolitic to tephri-phonolitic magma: the AD 472 (Pollena) eruption of Somma-Vesuvius, Italy. *Bull. Volcanol.,* **67**, 743–767.

(Received February 23, 2007)
(Accepted September 28, 2007)

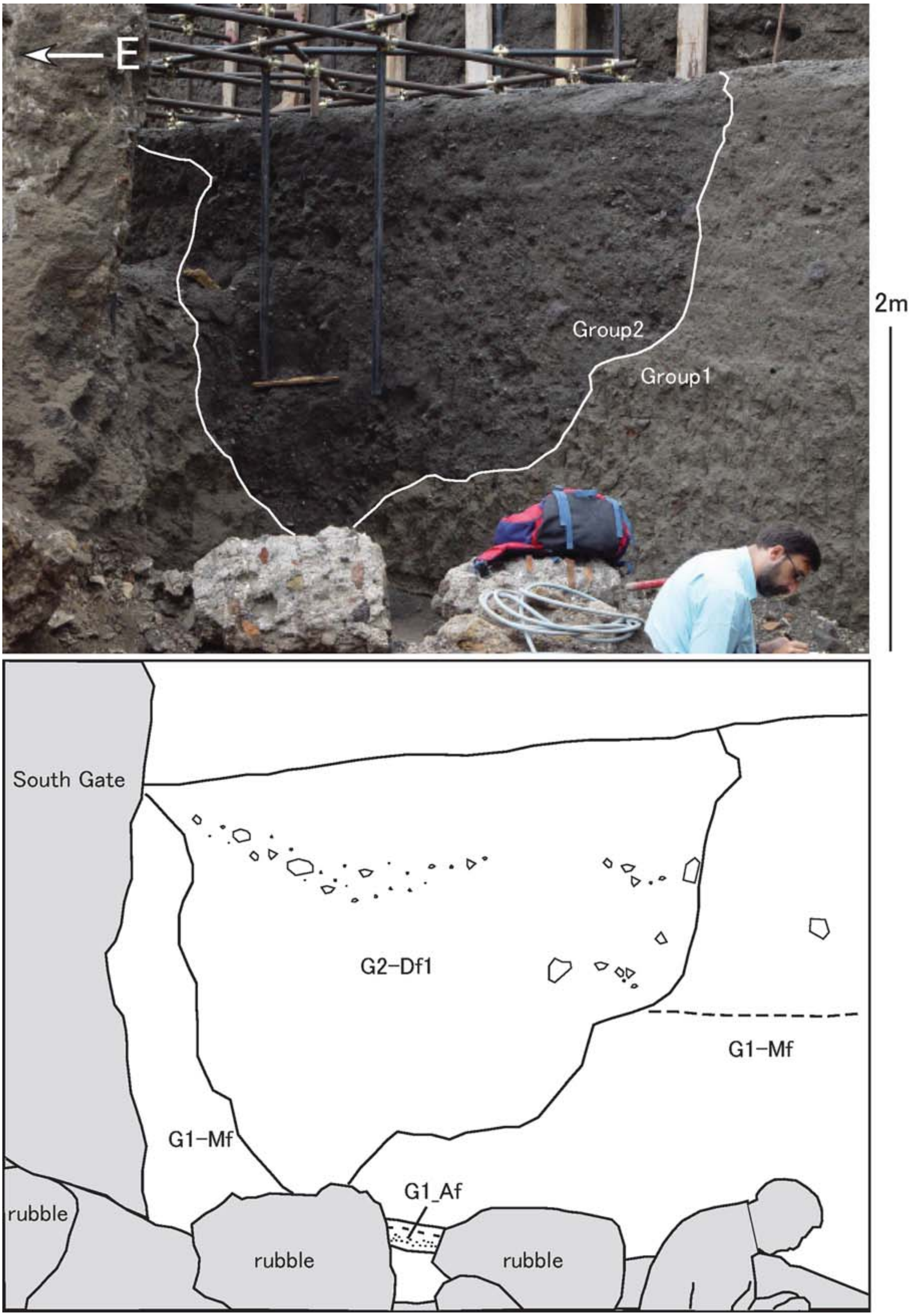

Appendix 1-1. Photograph and sketch showing the relationships among volcanic products and epiclastic flow deposits, and a variety of archaeological structures at the South Wall (Appendix 1-1～Appendix 1-7). G1-Af, which consists of eight layers, covers rubble of the building. G1-Mf is eroded, and G2-Df1 fills the channel-like structure at the lower wall.

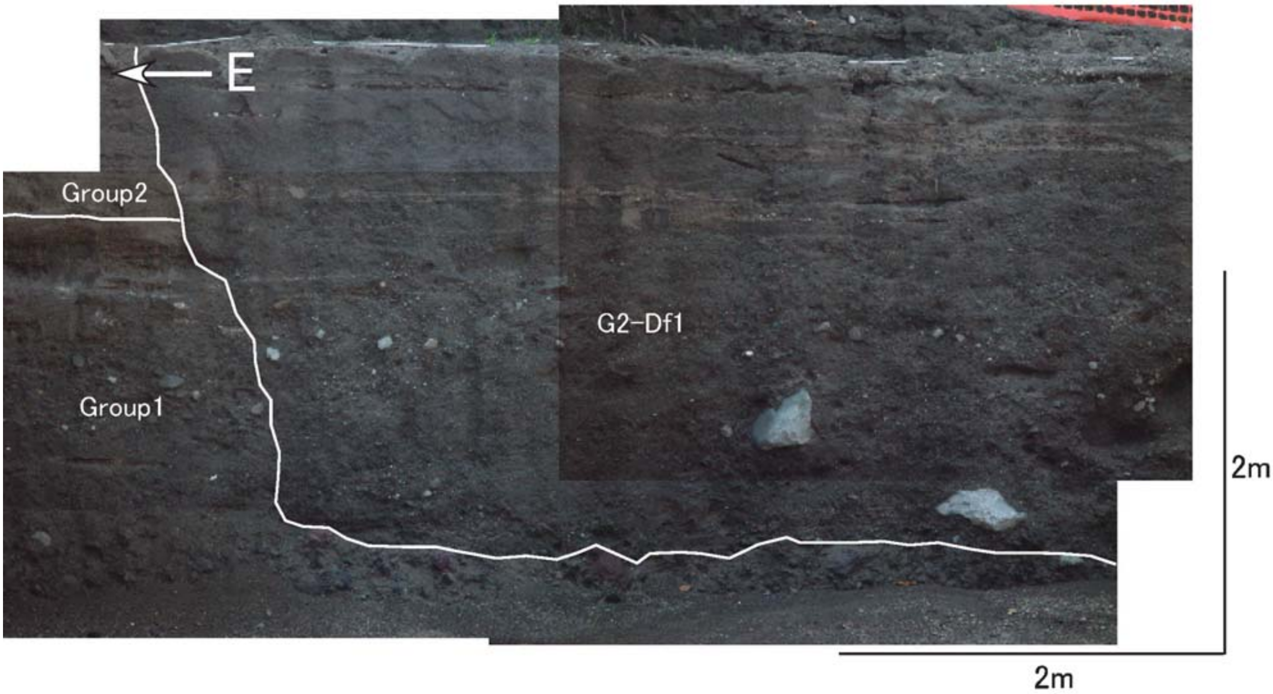

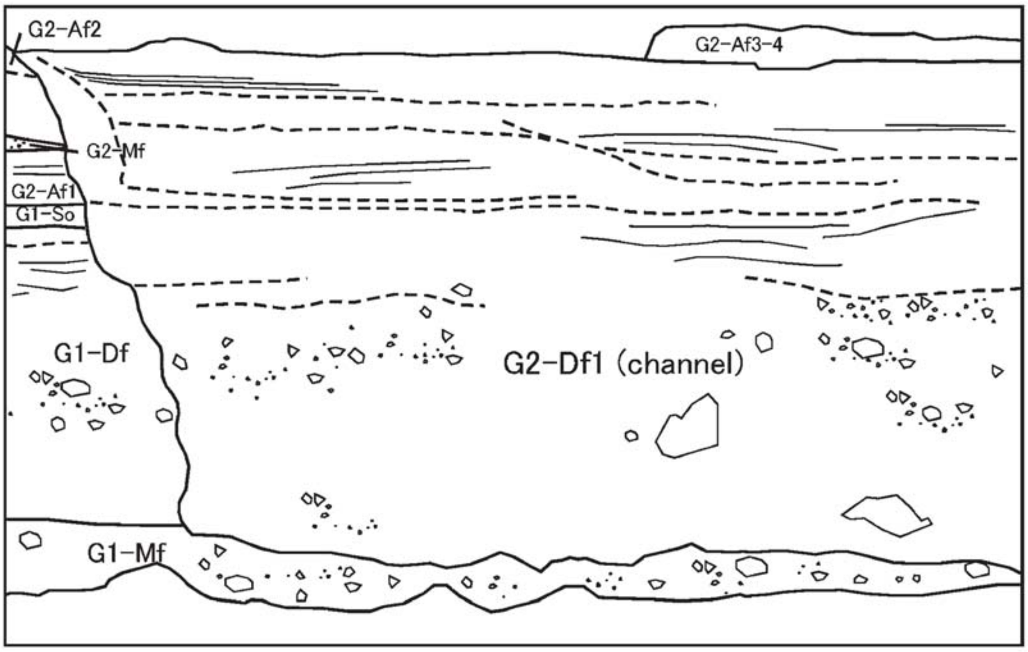

Appendix 1-2. Channel-like structure at the middle wall. G1-Mf, G1-Df, G1-So, G2-Af1, G2-Mf, and G2-Af2 are eroded. G2-Df1 fills the eroded sections, and is covered by G2-Af3-4. The lower boundary between G1-Mf and G2-Df1 forms a horizontal surface.

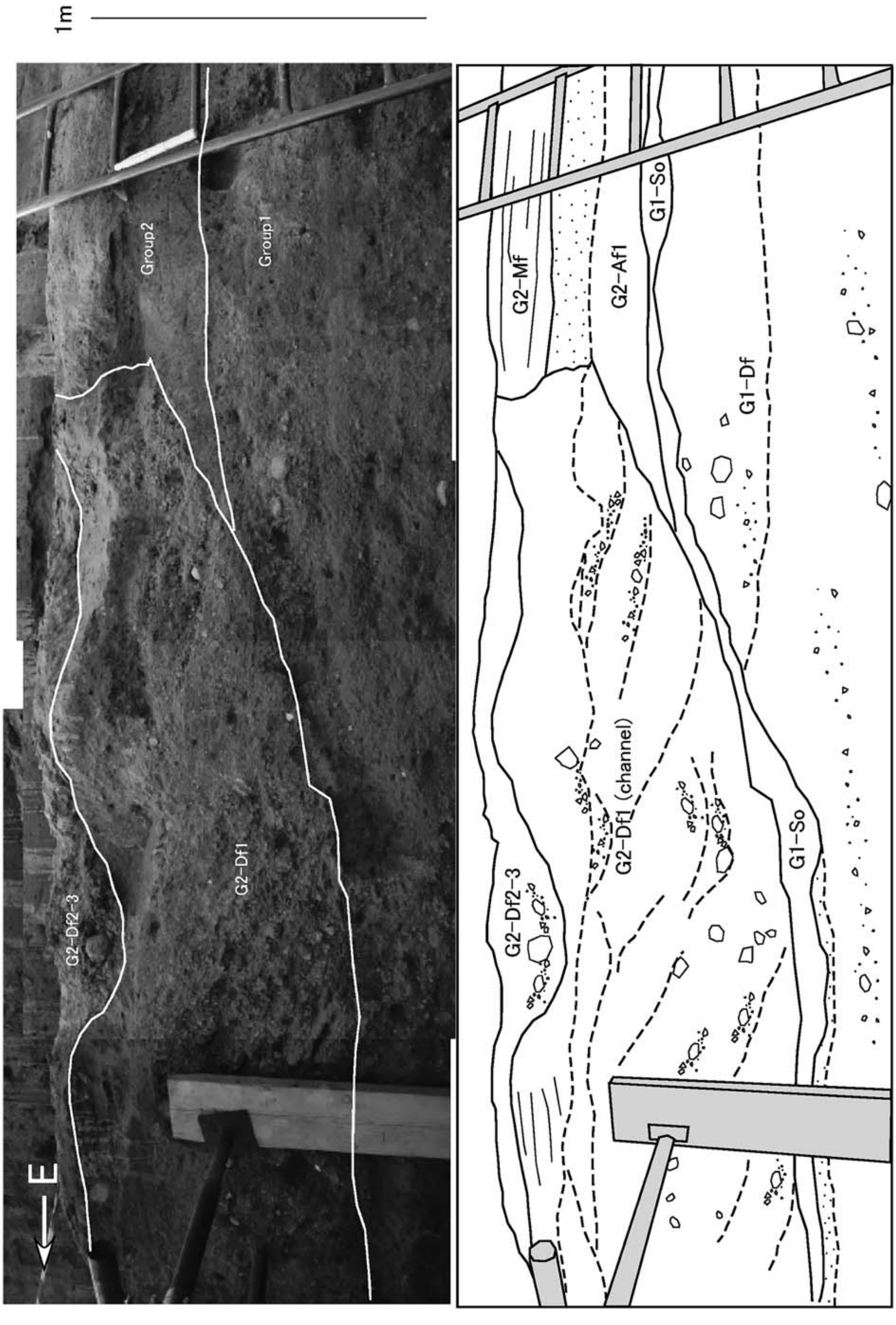

Appendix 1-3. The boundary of G2-Df1's channel at the middle wall at the western-side. Note that G1-So covers a small channel before deposition of G2-Df1.

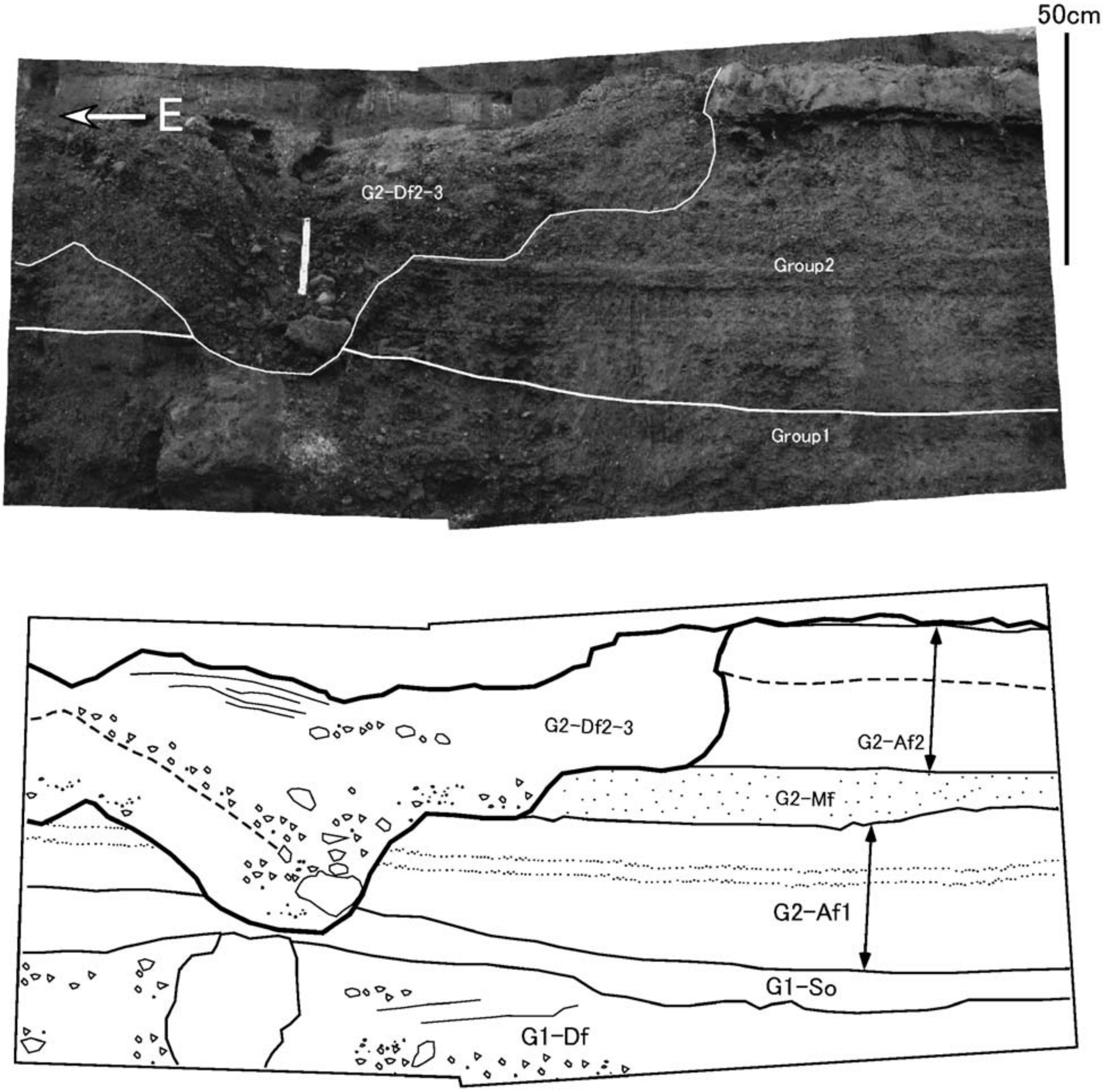

Appendix 1-4. Succession of Group2 deposits at the middle wall. G2-Af1 comprises stratified ash layers covered by alternating ash and scoria layers. G2-Af2 comprises fall deposit including accretionary lapilli interbedding a consolidated ash deposit (about 15 cm). G2-Af2 is eroded by G2-Df2-3.

Appendix 1-5. G2-Mf and G2-Df3 with a channel-like structure at the middle wall. G2-Af1 is eroded by G2-Mf. G2-Mf, G2-Af2, G2-Df2, and G2-Af3 are eroded, and the channel is filled by G2-Df3. G2-Df3 shows stratification.

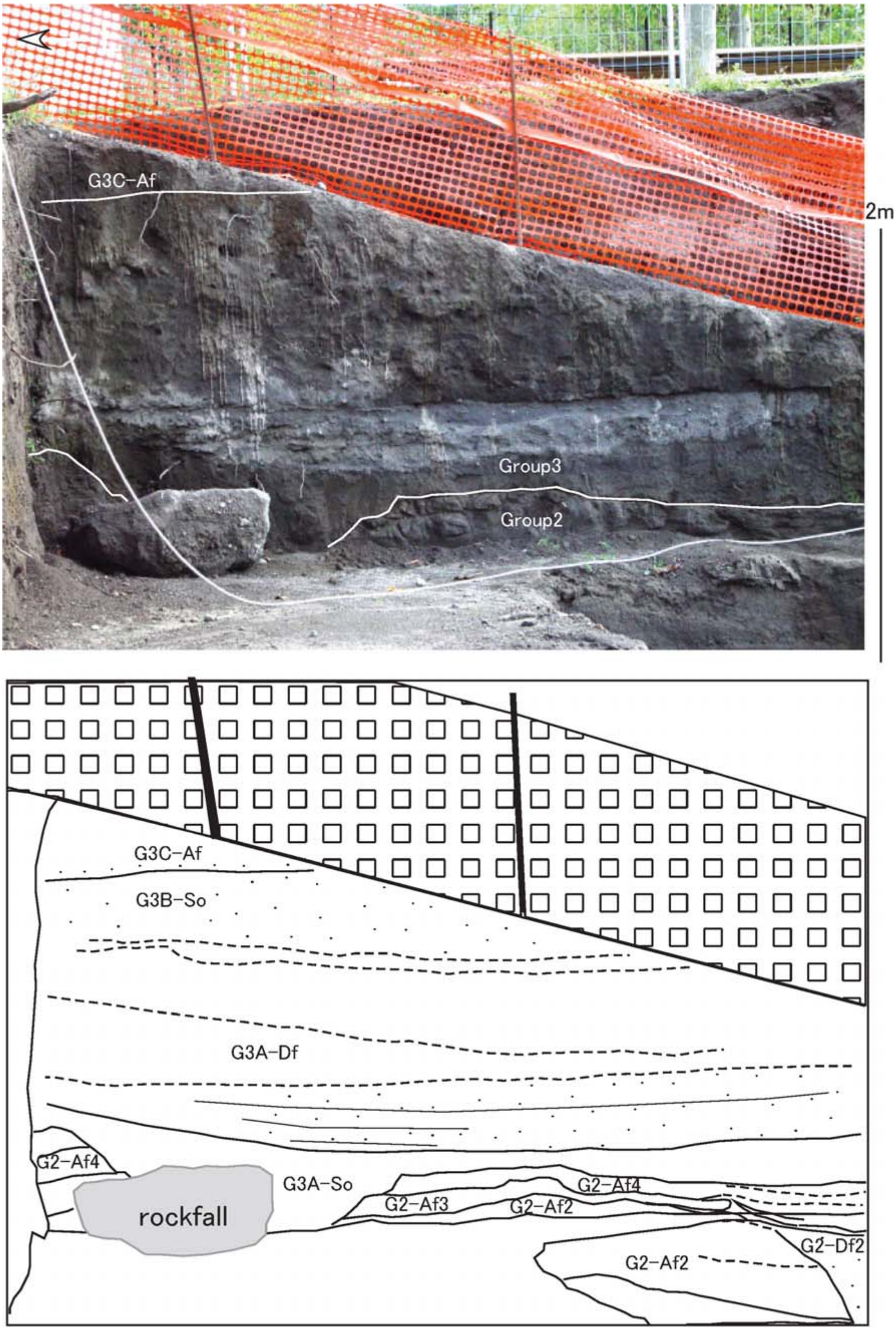

Appendix 1-6. Succession of Group2 deposits composed of ash fall layers (G2-Af2, G2-Af3, and G2-Af4) and Group 3 deposits at the upper wall. G2-Af3 and G2-Af4 are recognized at this site.

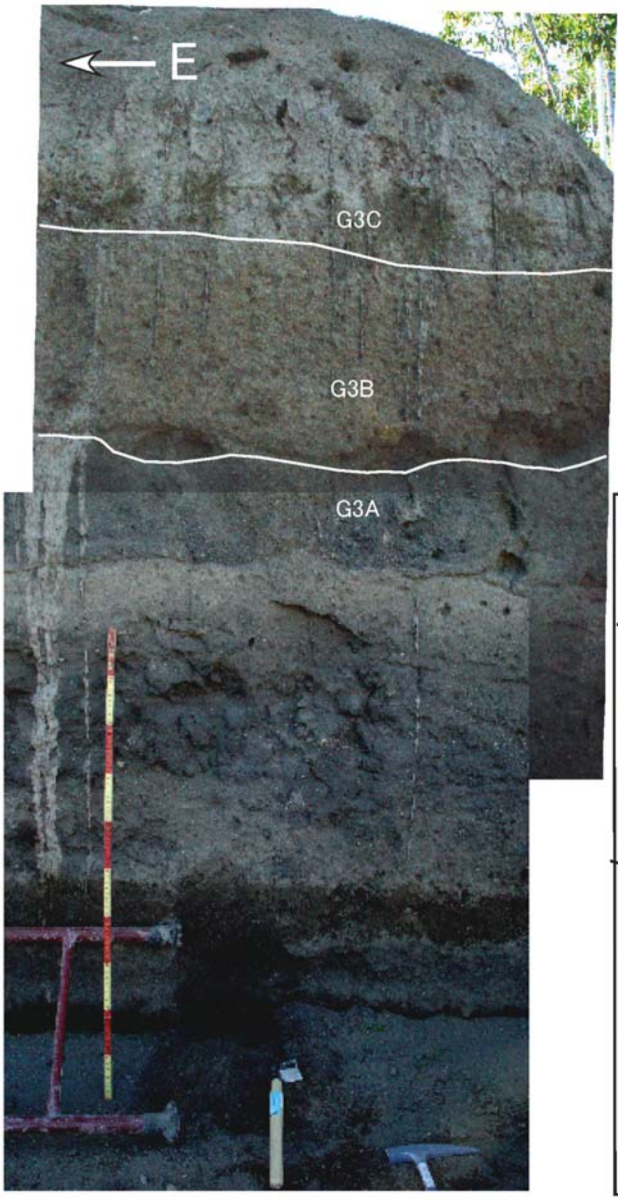

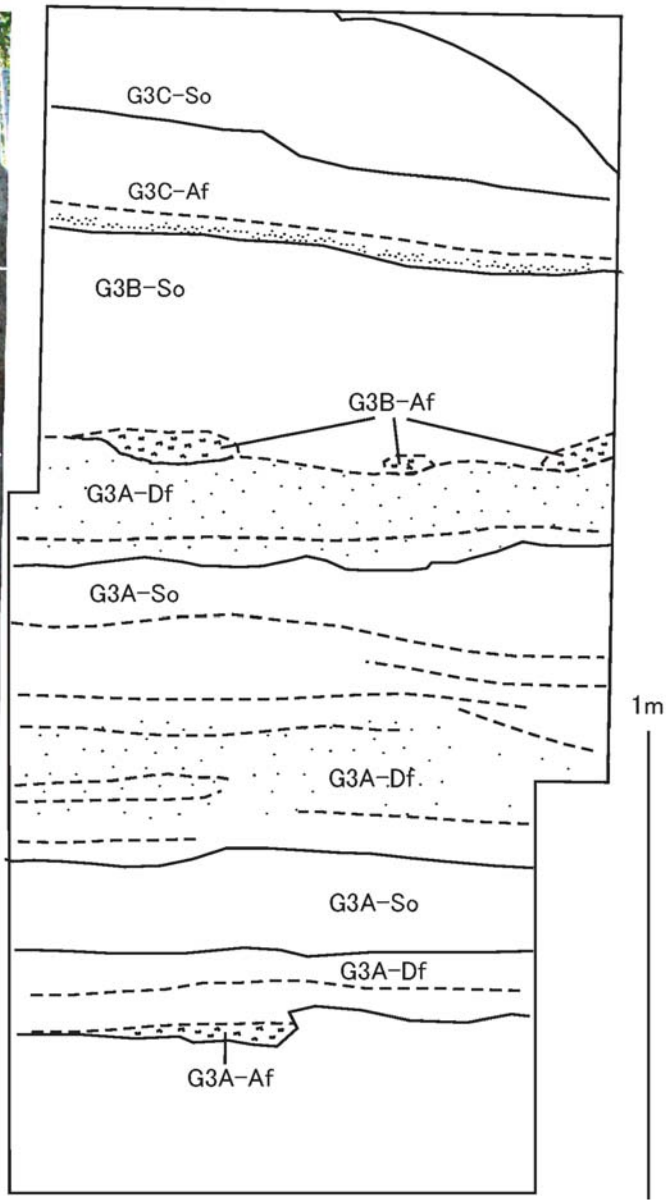

Appendix 1-7. Succession of Group3 deposits at the upper wall. G3A-Df is divided into three parts at this site. Dark grey layer showing stratification corresponding to the middle part is clearly distinguished from the other deposits of Group3. G3A-So (or Df) includes pumice (about 1.5 cm in diameter), but G3B-So includes scoria (about 1.5 cm). G3B-Af is observed as lenticular deposits between G3A-So and G3B-So. G3C-Af is recognized as a massive ash deposit about 40 cm in thickness.

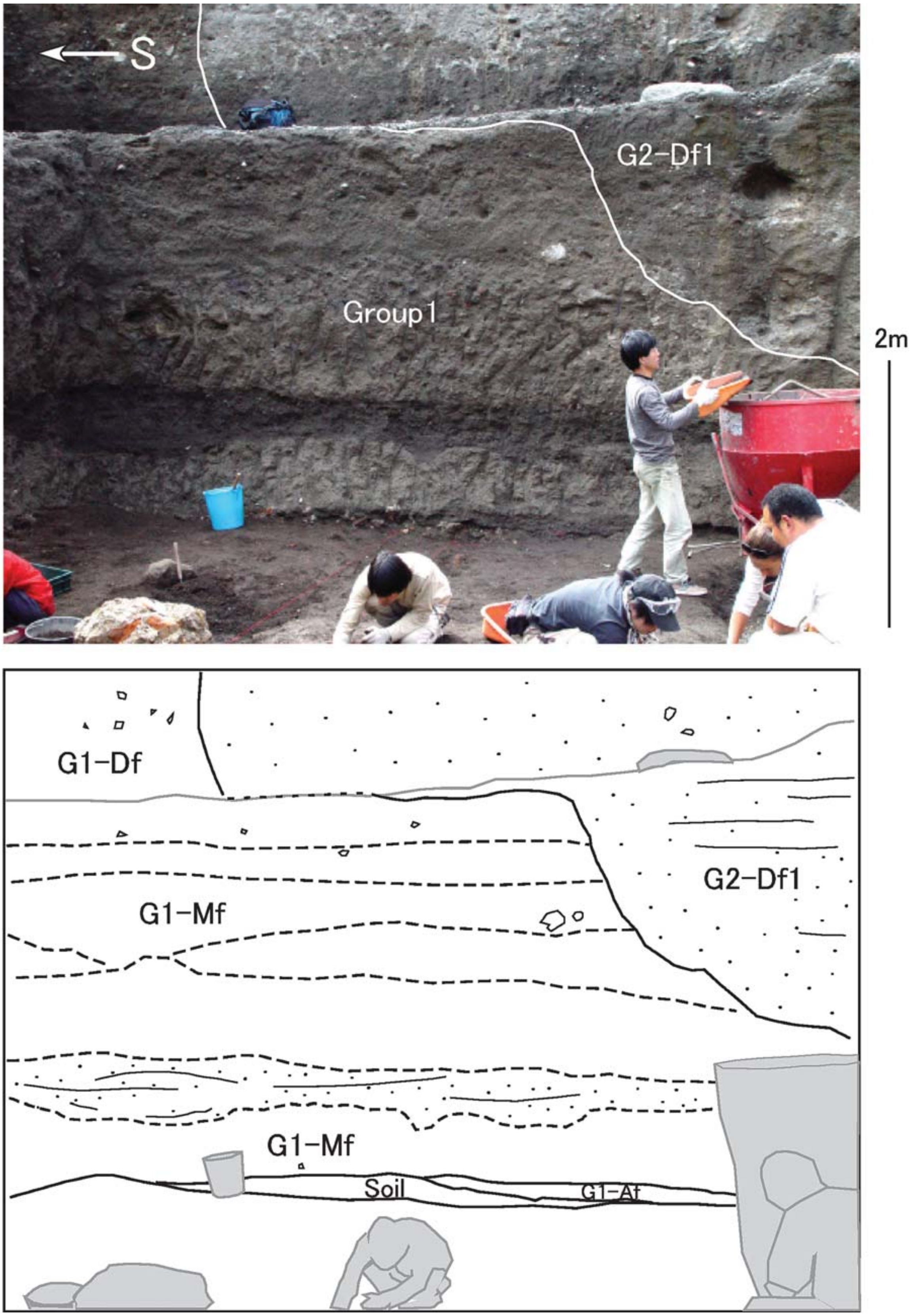

Appendix 2-1. Photograph and sketch showing relationships among volcanic products and associated epiclastic flow deposits and a variety of archaeological structures at the West Wall (Appendix 2-1～Appendix 2-7). The Group1 deposits' succession is eroded, and the channel is filled by G2-Df1. Note that the fluvial layer, interbedded at the boundary between the sub-groups of G1-Mf in this site is the thickest in the villa.

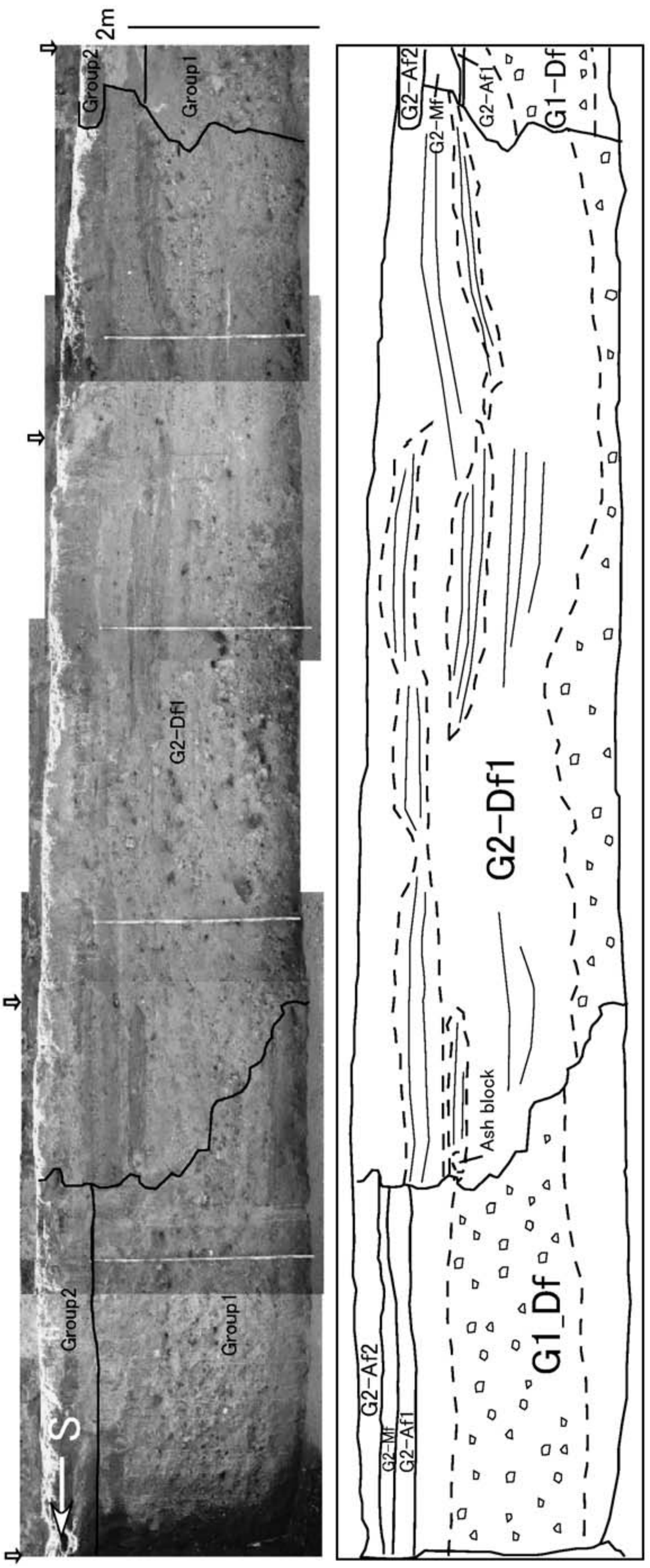

※ Open arrows are marked up at an interval of 5 m.

Appendix 2-2. Deposits of Group1 and Group2 eroded and filled by G2-Df1 at the middle wall. G2-Df1 shows stratification. The G2-Df1 deposit vertically contacts other deposits.

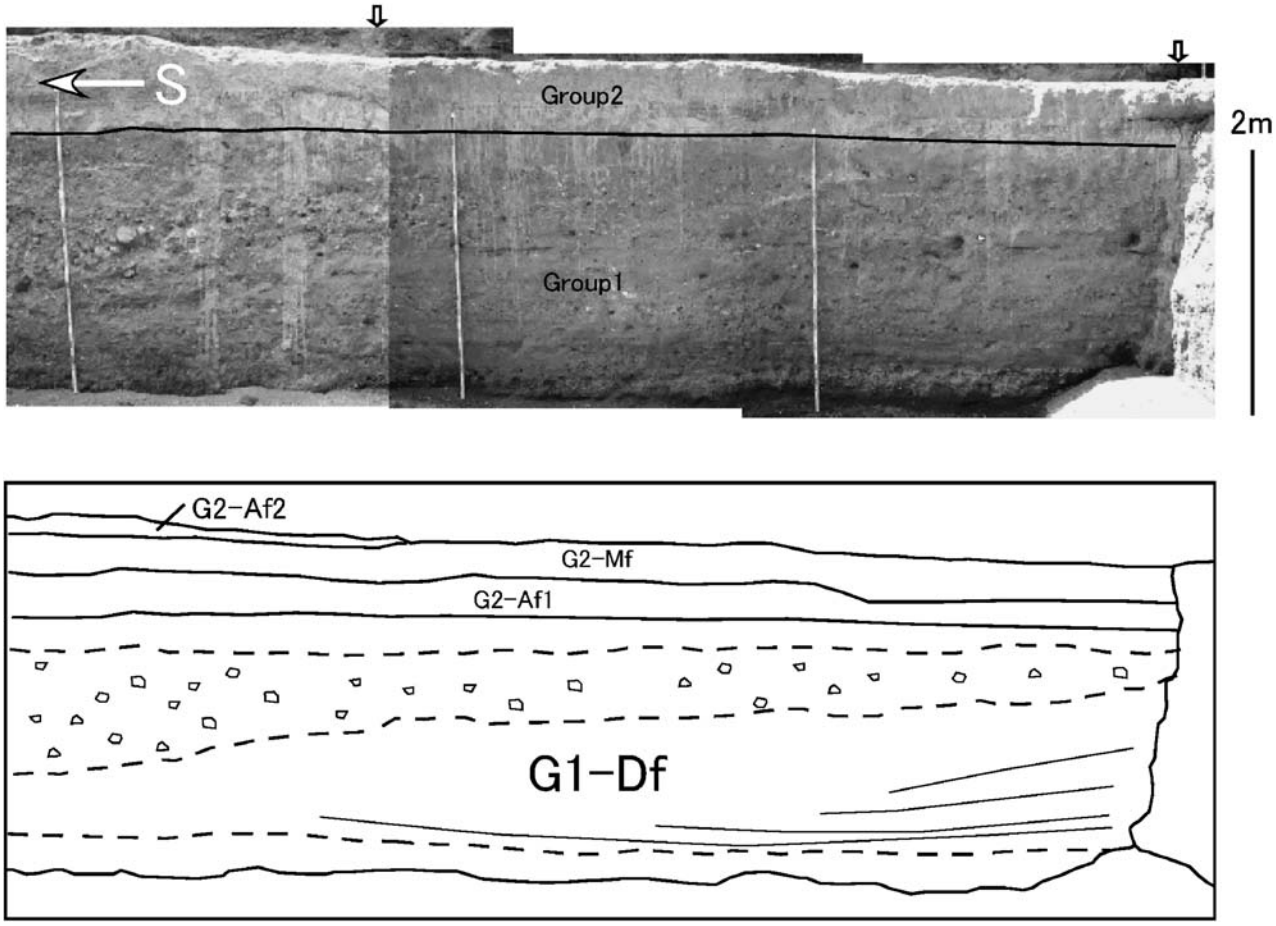

※ Open arrows are marked up at an interval of 5 m.

Appendix 2-3. Succession of Group1 and Group2 continues from Appendix 1-2. The thickness of the upper unit of G1-Df decreases towards the north. The lower unit (G1-Df1) apparently diverges into two parts toward the down current.

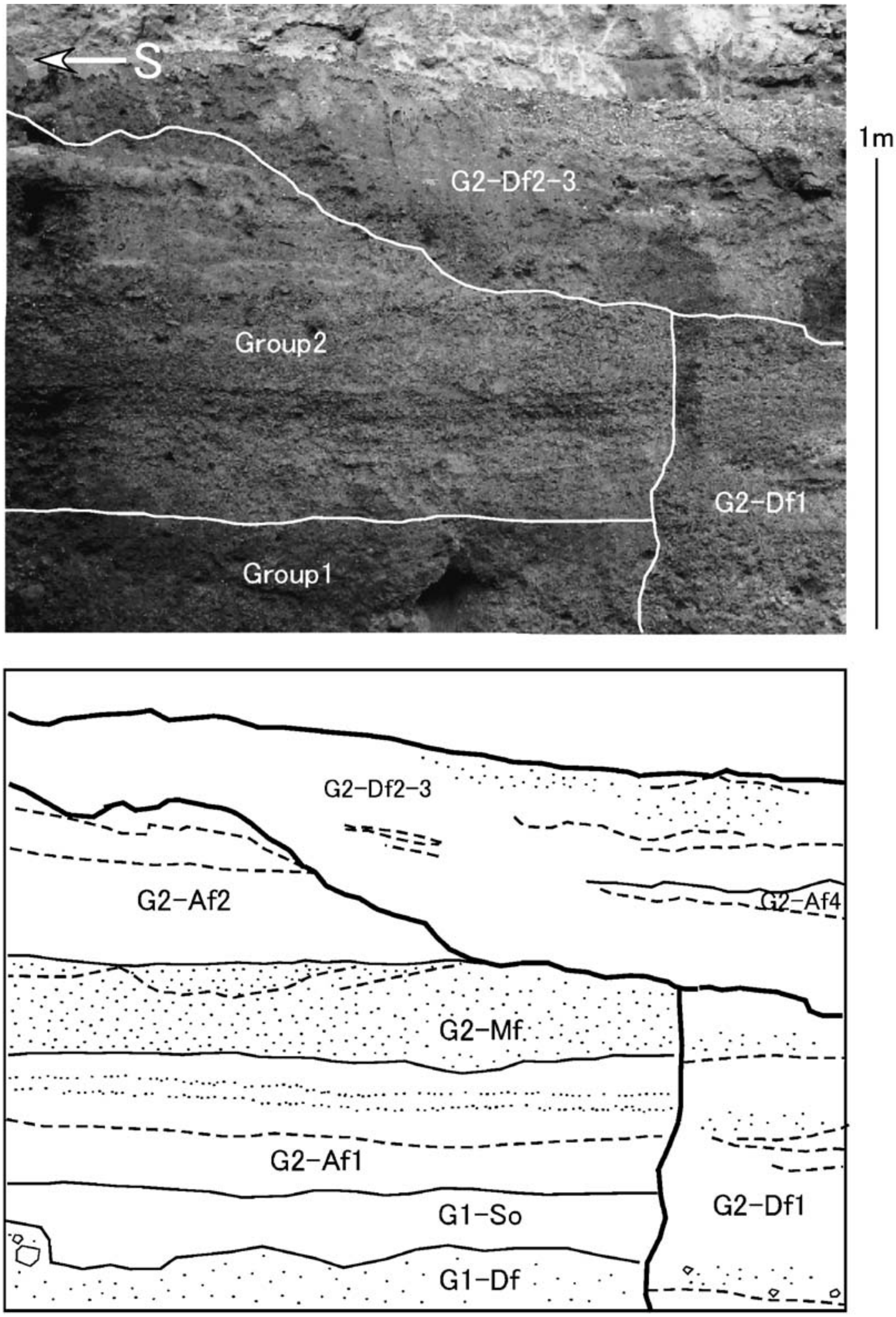

Appendix 2-4. The boundary of G2-Df1 at the middle wall at the southern side. This photograph was taken in 2004. G2-Df1 is eroded, and the channel is filled by G2-Df2-3. G2-Df1 and G2-Df2-3 show stratified structures, but G2-Mf shows massive facies.

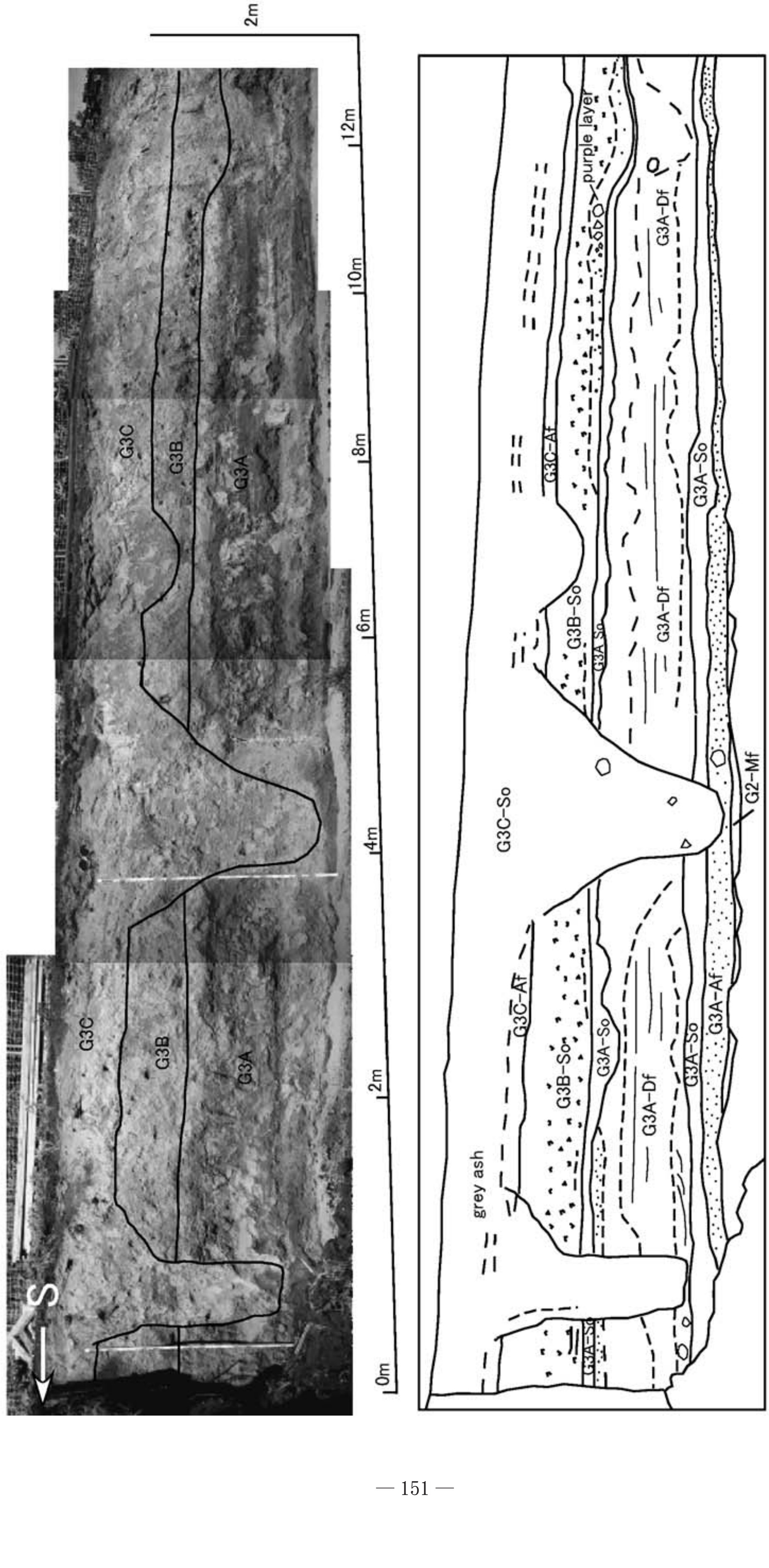

Appendix 2-5. Succession of Group3 deposits at the upper wall. Note that the channels of G3C-So are narrow and deep, indicating artificial furrows or channels formed by stream flows. G3A-Df is recognized as a dark grey stratified deposit.

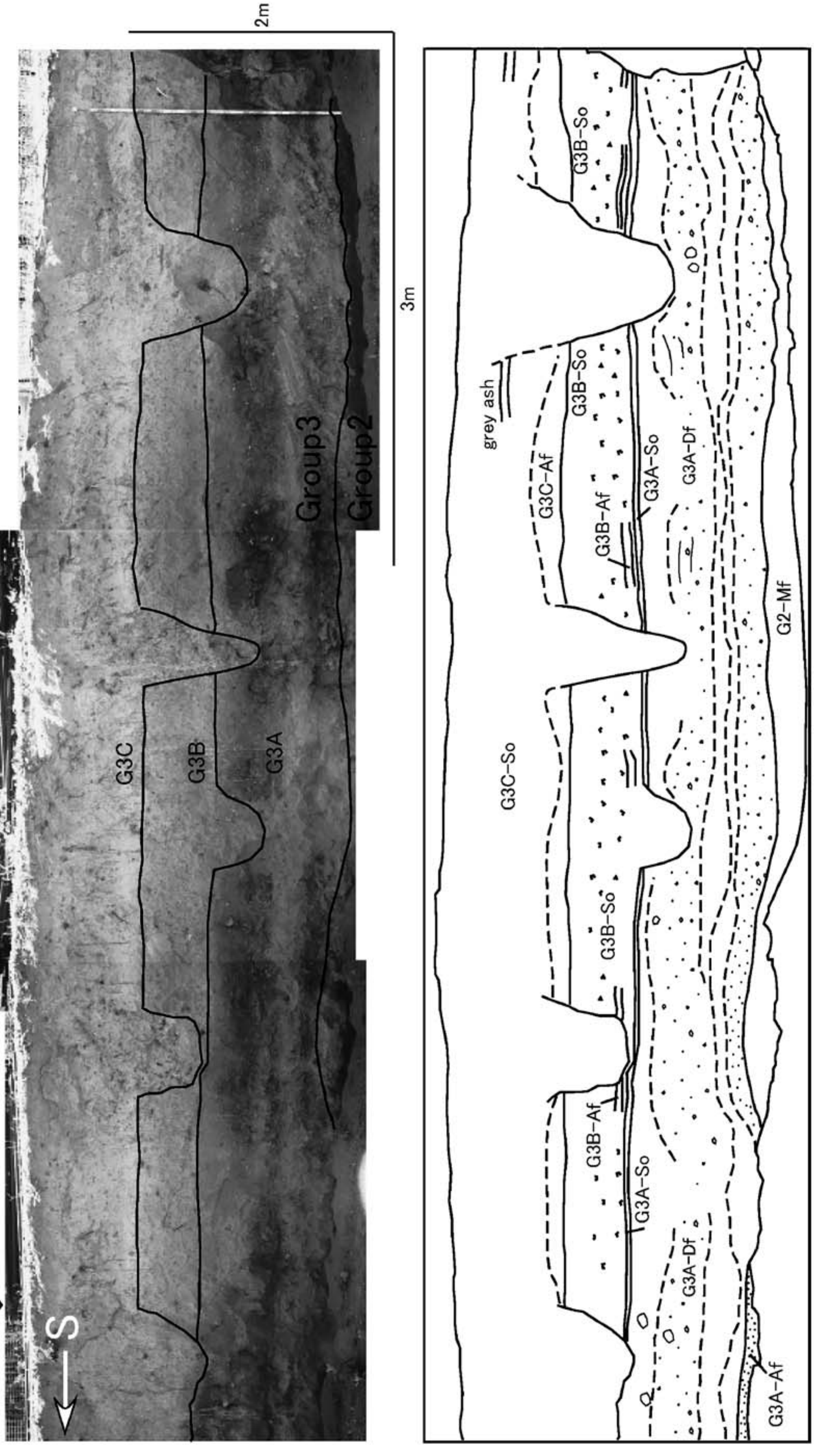

※ Open arrows are marked up at an interval of 5 m.

Appendix 2-6. Succession of Group3 deposits continues from Appendix 2-5.

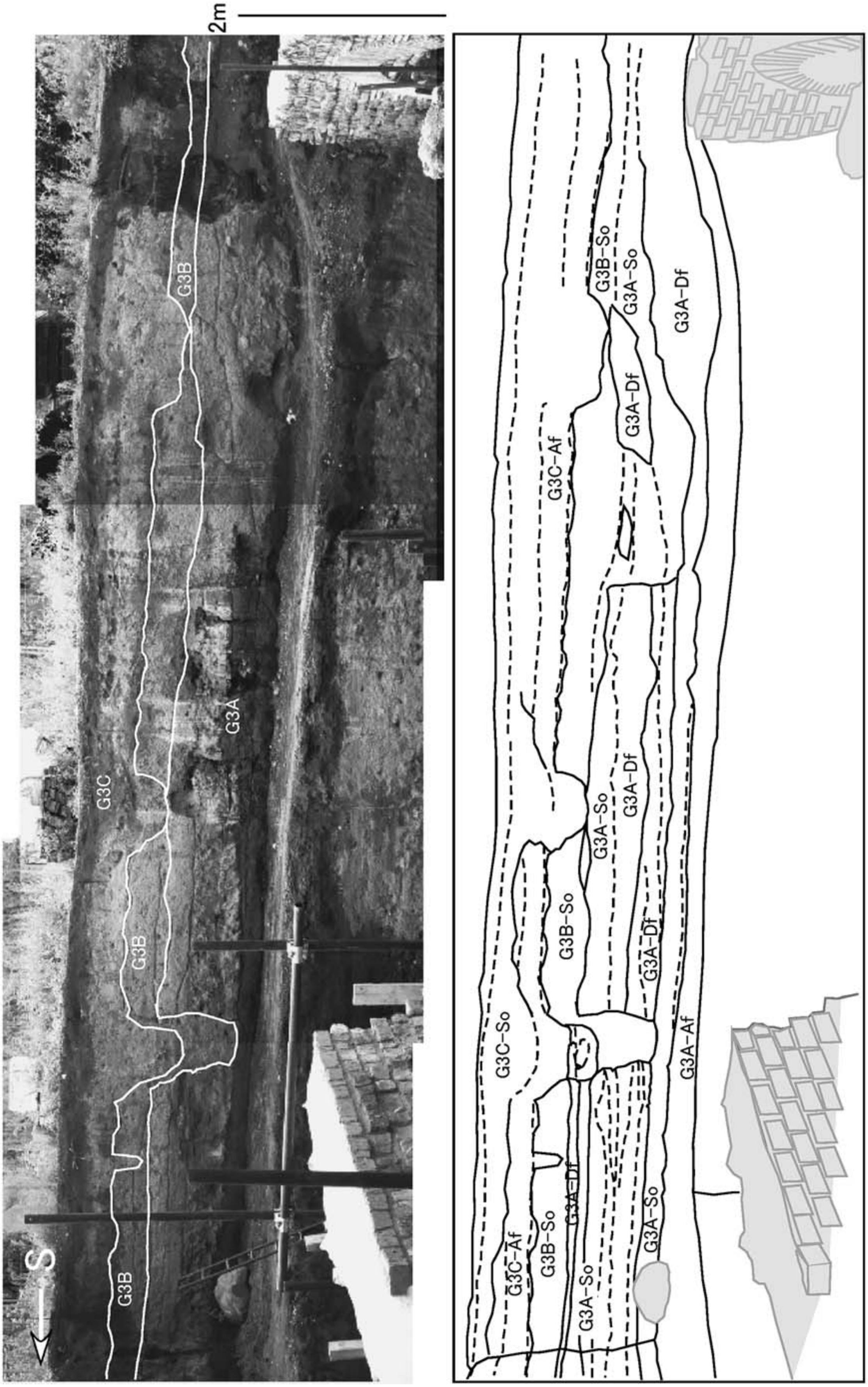

Appendix 2-7. Succession of Group3 deposits at the upper wall showing the relation between deposit and Roman building. Photograph was taken in 2004. Note that very complicated erosional surfaces of G3A-Df, G3B-So, and G3C-So are observed.

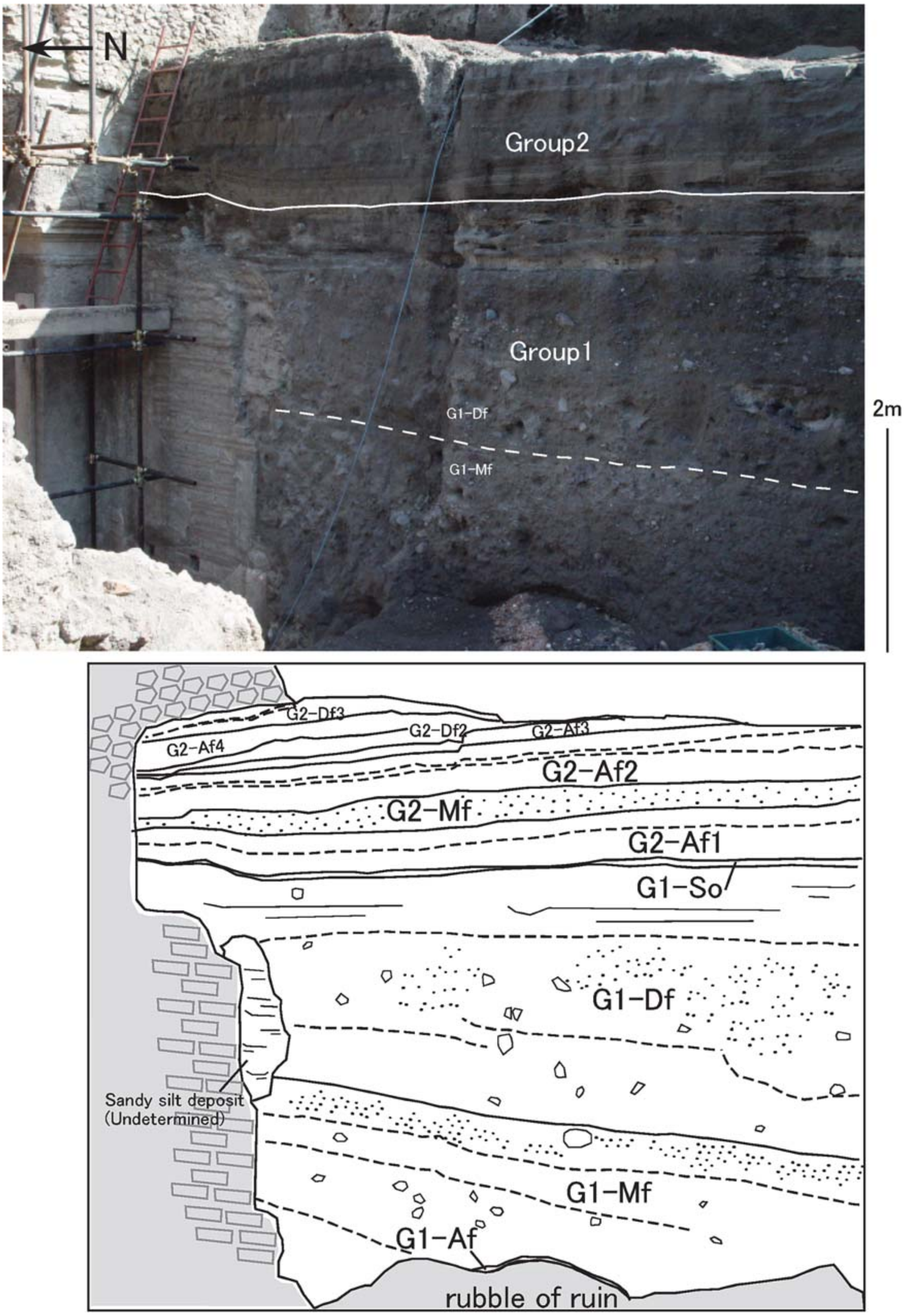

Appendix 3-1. Photograph and sketch showing the relationships among volcanic products and associated epiclastic flow deposits and a variety of archaeological structures at the East Wall (Appendix 3-1～Appendix 3-5). Successions of Group1 and Group2 deposits at the East Wall partially cover the wall of the building to a height of about 8 m. G1-Af covers rubble of the building. We can recognize the whole series of Group2 deposits in this site.

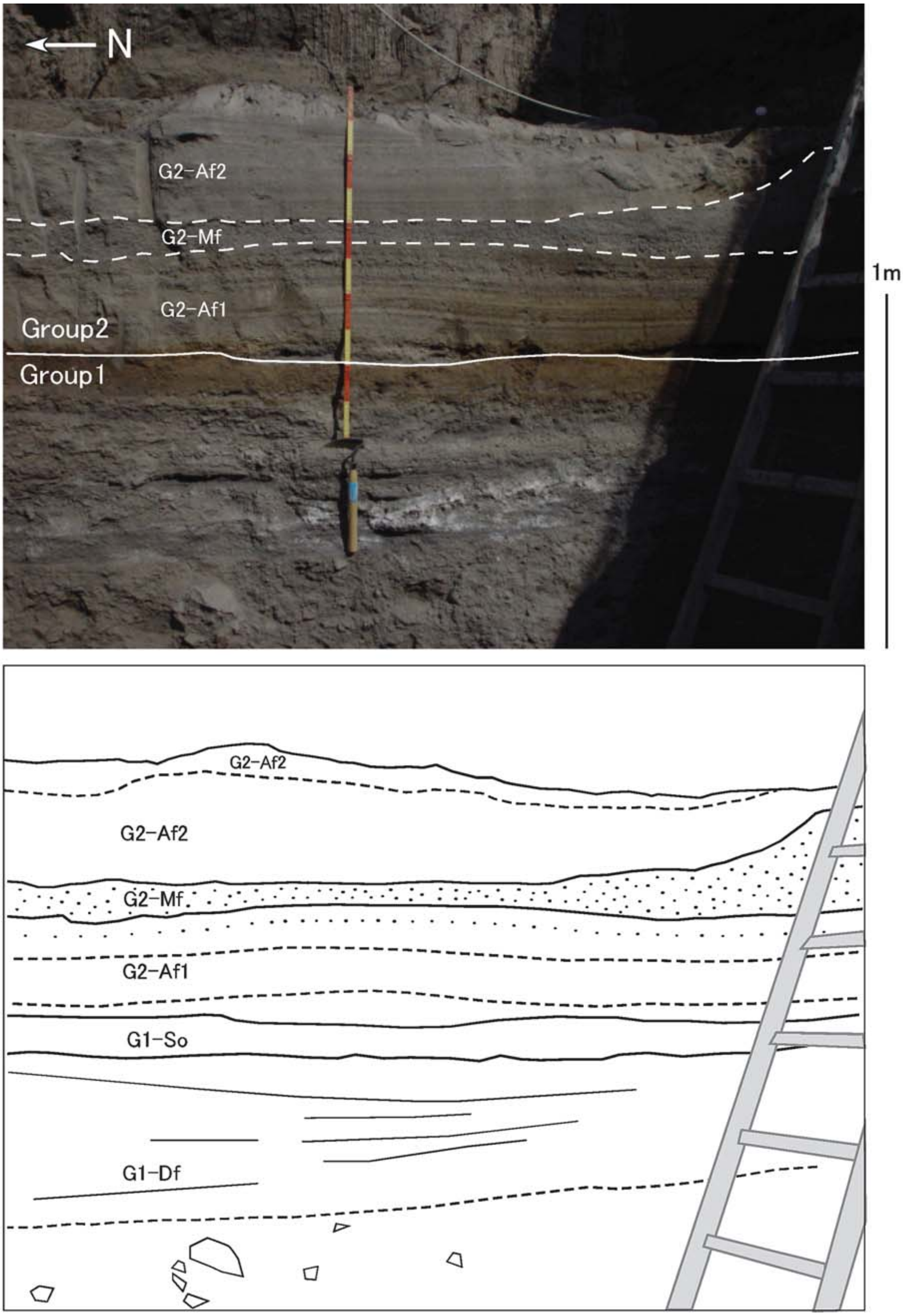

Appendix 3-2. Succession from G1-Df to G2-Af2 at the middle wall. The structures of G2-Af1 and G2-Af2 are well observed. G2-Af1 consists of ash dominant part and overlying scoria-rich part. G2-Af2 consists of accretionary lapilli layer and interbedding consolidated ash layer.

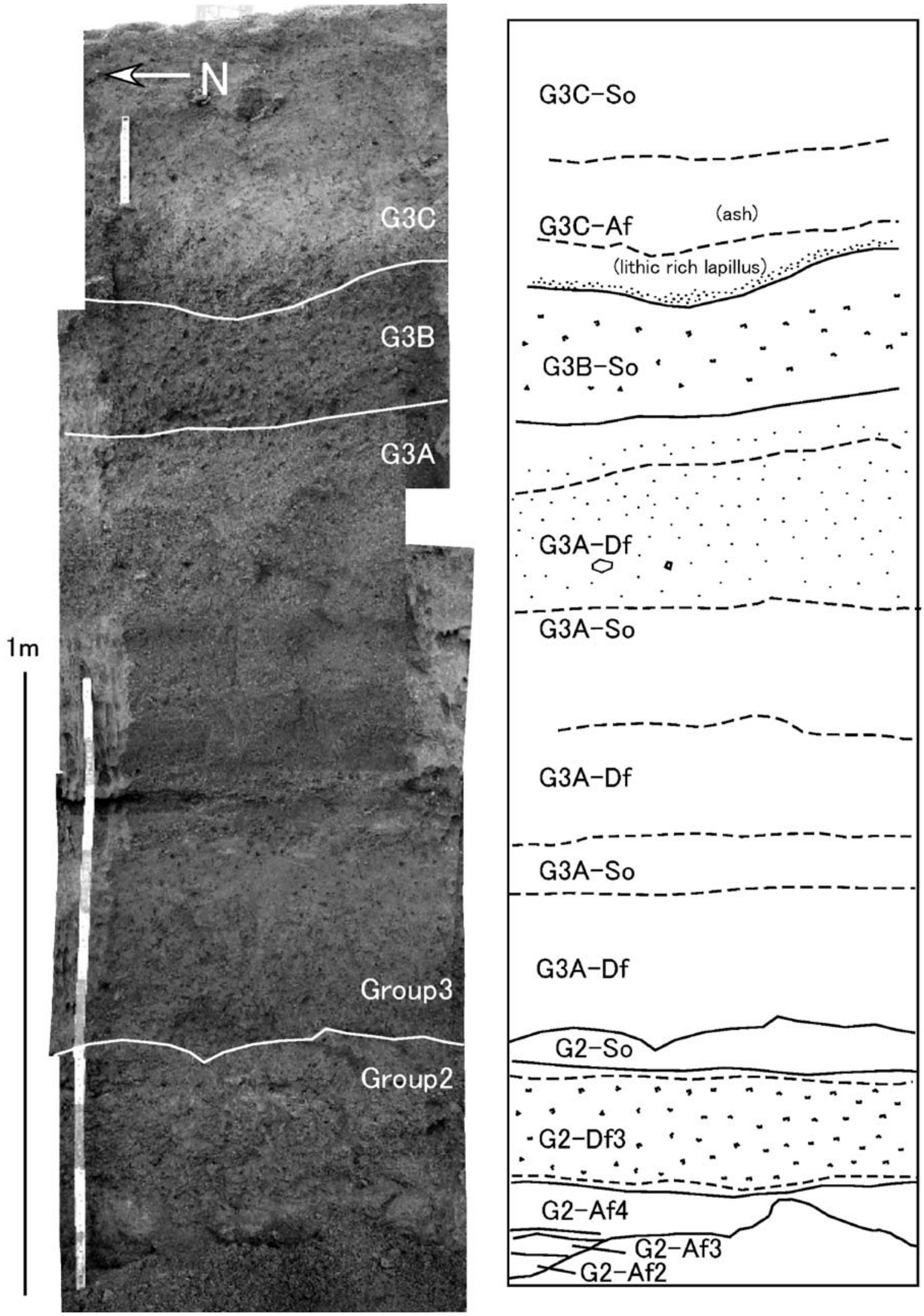

Appendix 3-3. Succession of Group3 deposits at the upper wall. Note that G3A-Af and G3B-Af deposits are not recognized at this site. G3C-Af consists of two parts: the alternating scoria and ash layers and the overlying massive ash layer with accretionary lapilli.

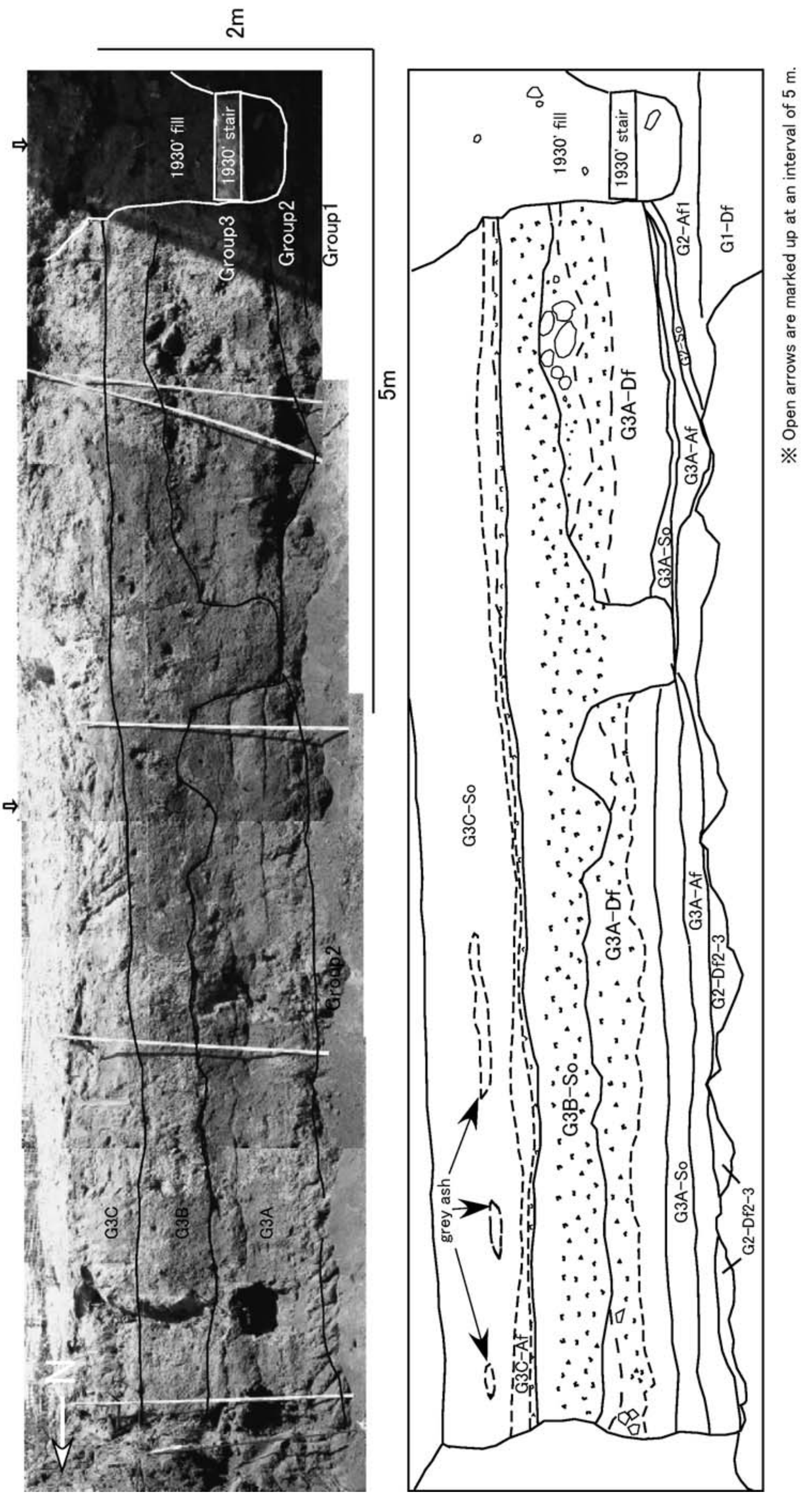

Appendix 3-4. Succession of Group3 deposits at the upper wall. 1930 stair was built during the AD 1930 excavation. 1930 fill was re-filled after the AD 1930 excavation.

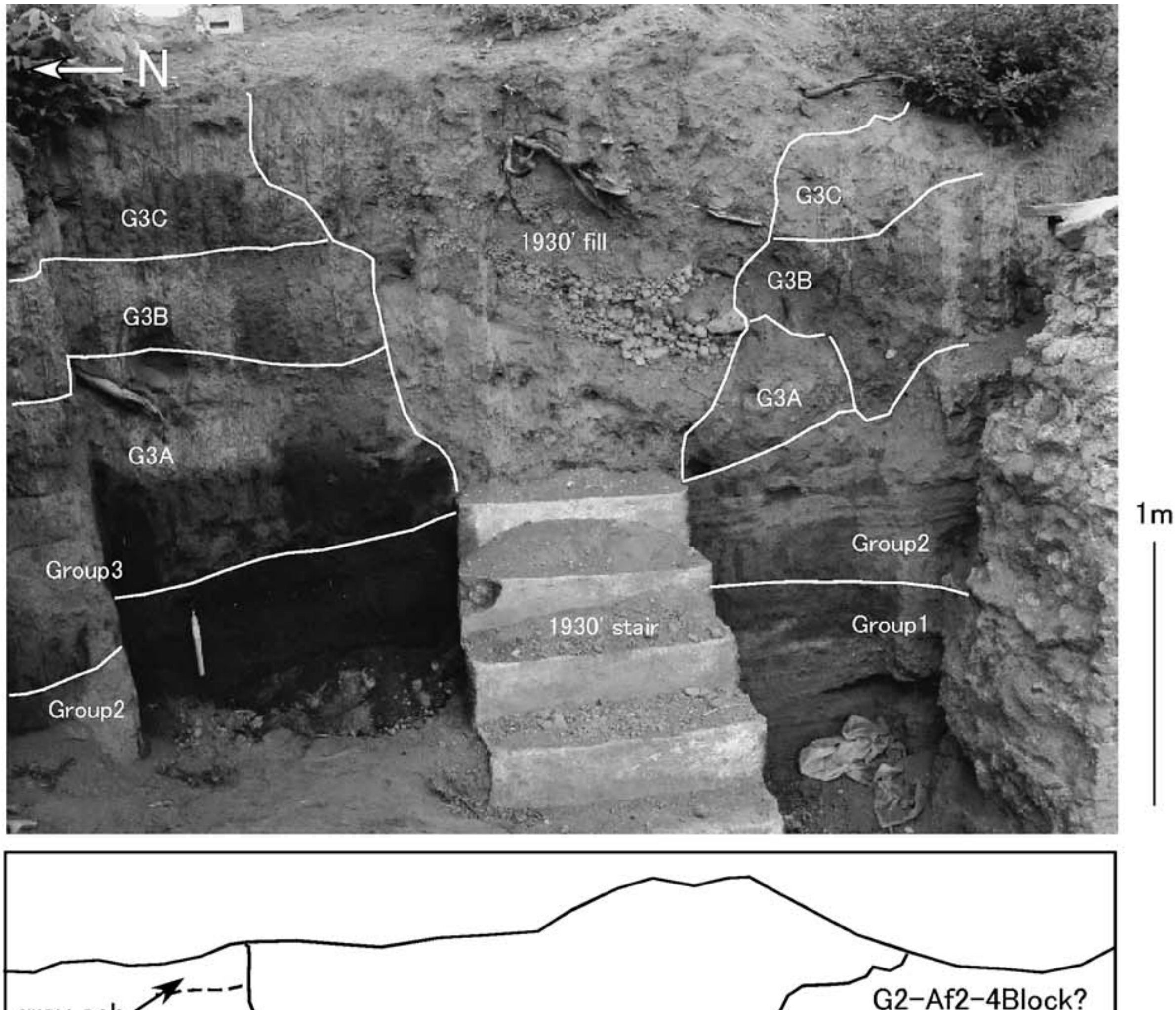

Appendix 3-5. The stair built during the AD 1930 excavation at the upper wall. This photograph was taken in 2004. Note that G2-Af2 is not recognized near the wall of this villa.

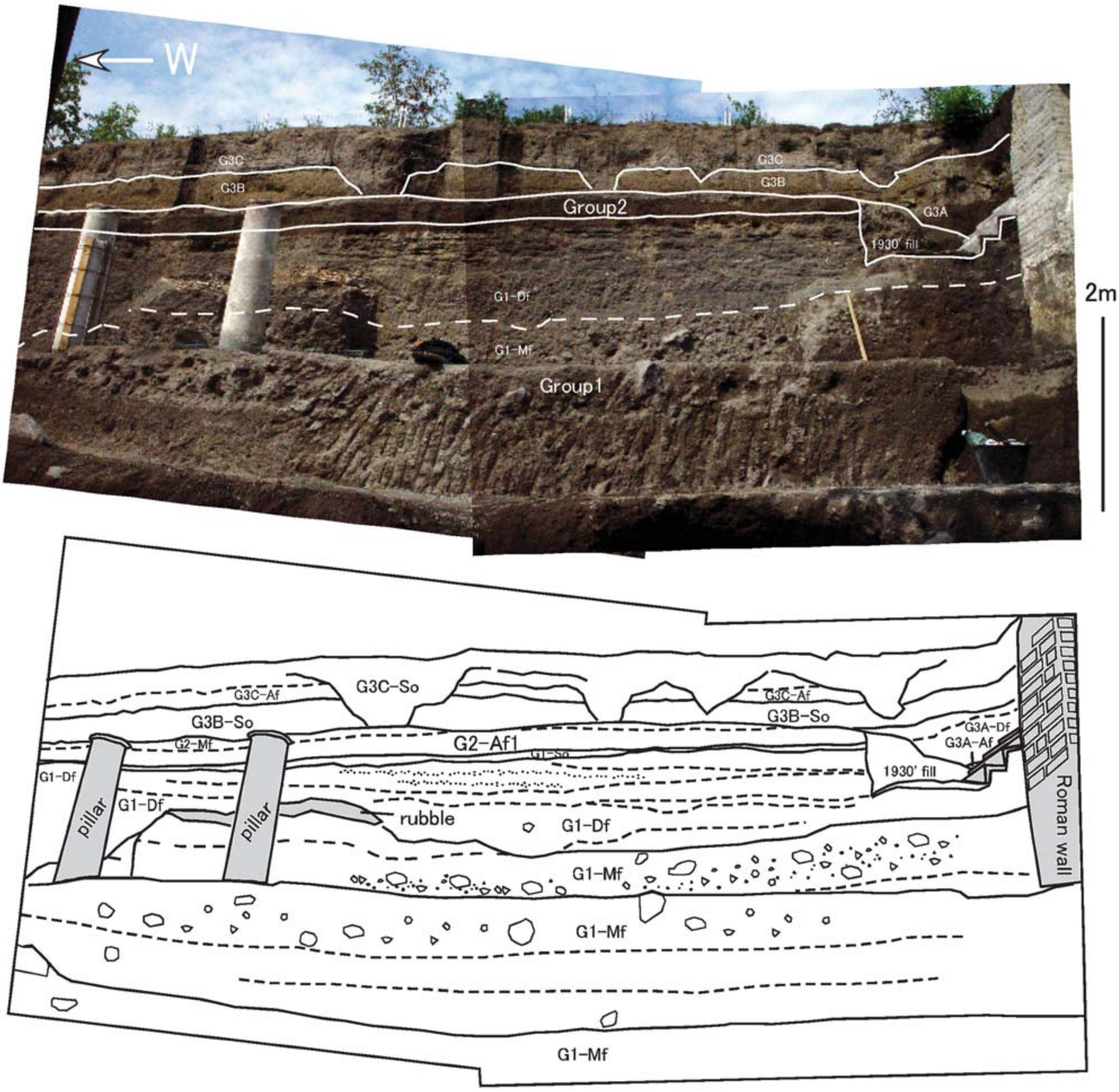

Appendix 4-1. Photograph and sketch showing the relationships among volcanic products, epiclastic flow deposits, and variety of archaeological structures at the North Wall (Appendix 4-1〜Appendix 4-9). This is an overview of the North Wall. The archaeological structures such as pillars, Roman wall, and demolished monolithic wall of the villa are covered by volcanic products and epiclastic flow deposits.

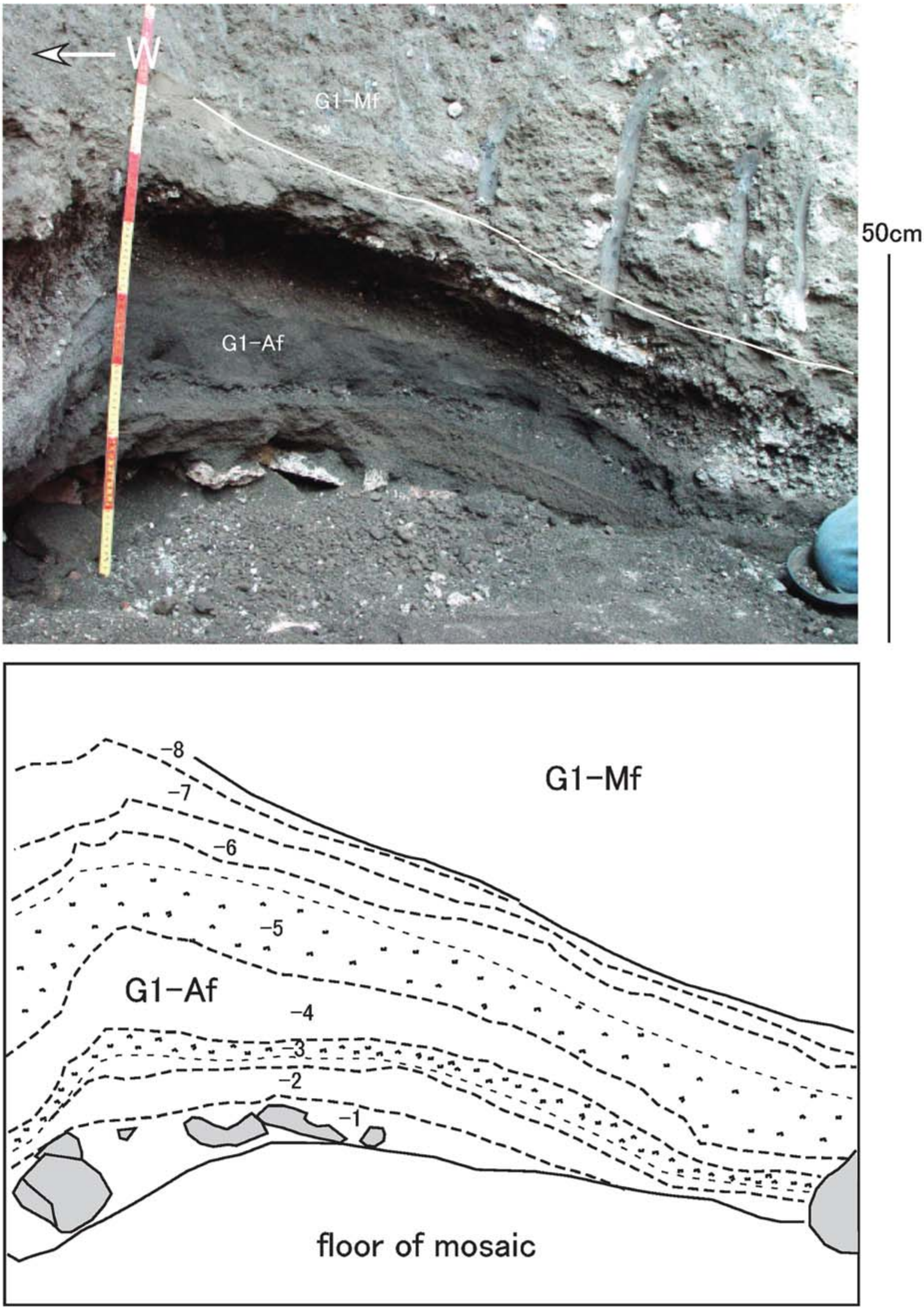

Appendix 4-2. Occurrence of G1-Af near the wall of Vano2. Total thickness of G1-Af increases towards the wall facing east, and the thickest part is about 65 cm.

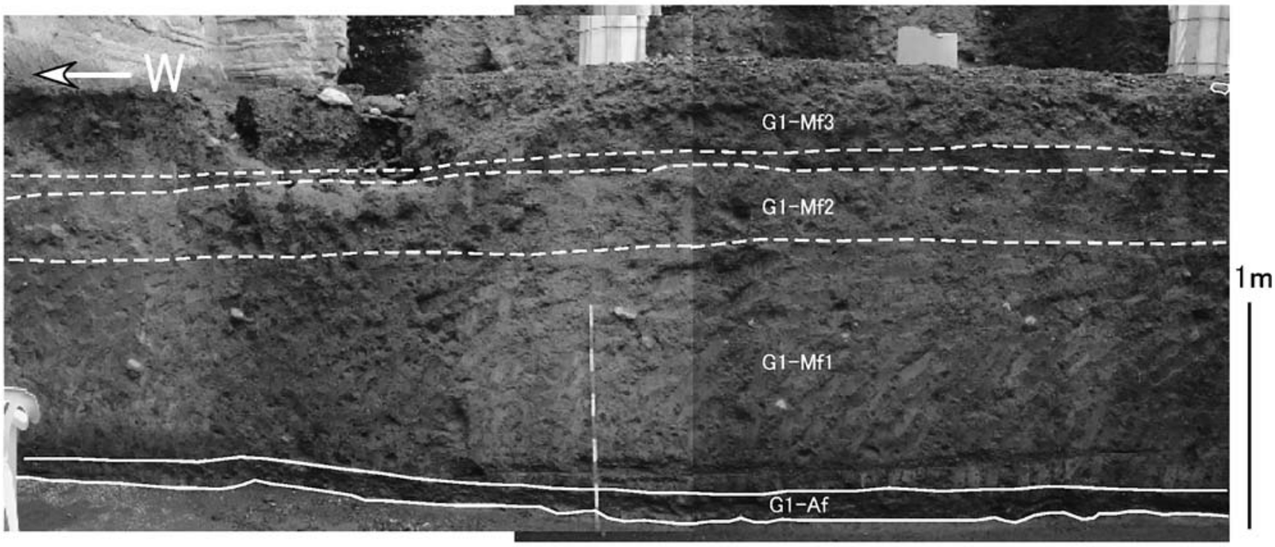

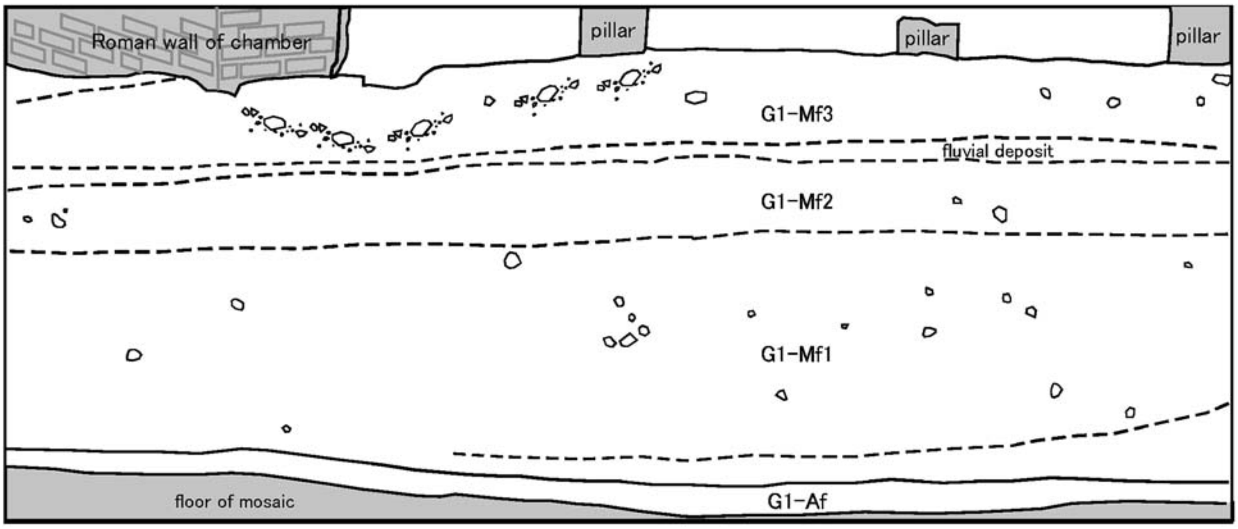

Appendix 4-3. G1-Af and G1-Mf deposits at the lower wall. Each flow-unit of G1-Mf has different amounts and maximum sizes of lithic. The thin fluvial deposits are interbedded between each flow-unit. These fluvial deposits show weakly stratified layers with dune.

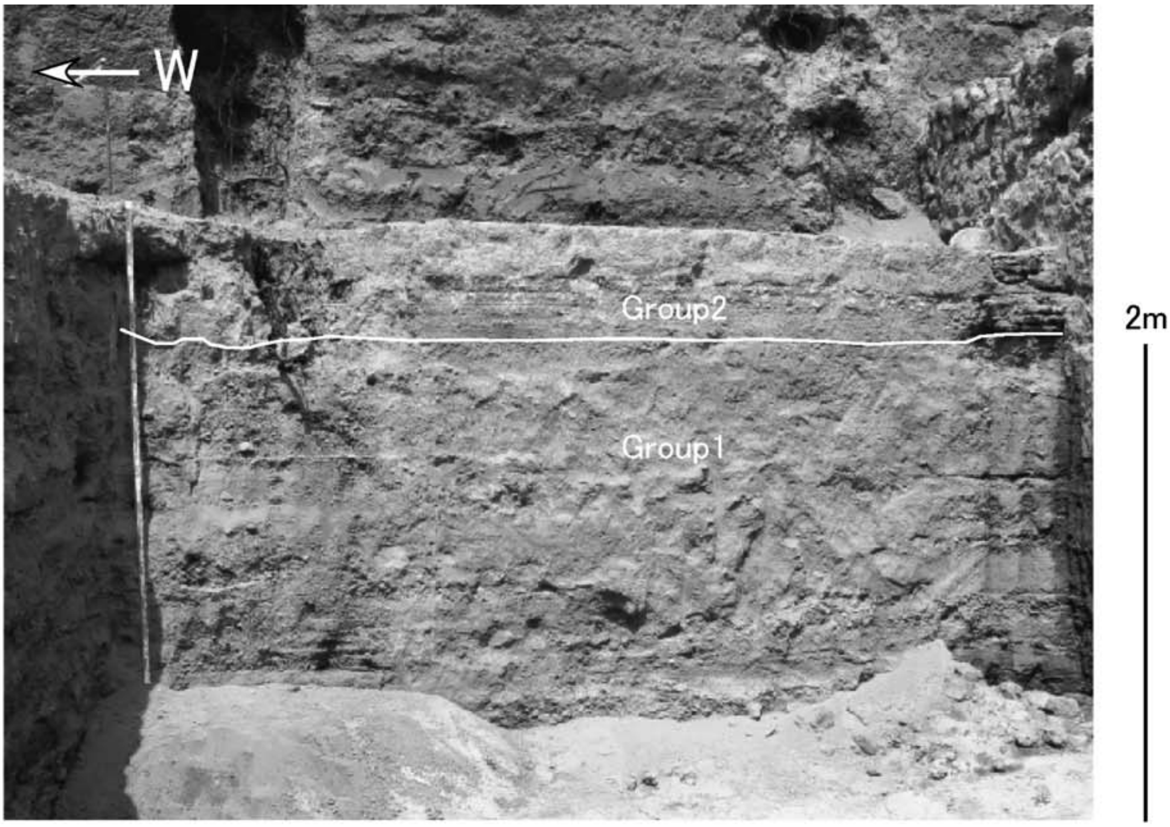

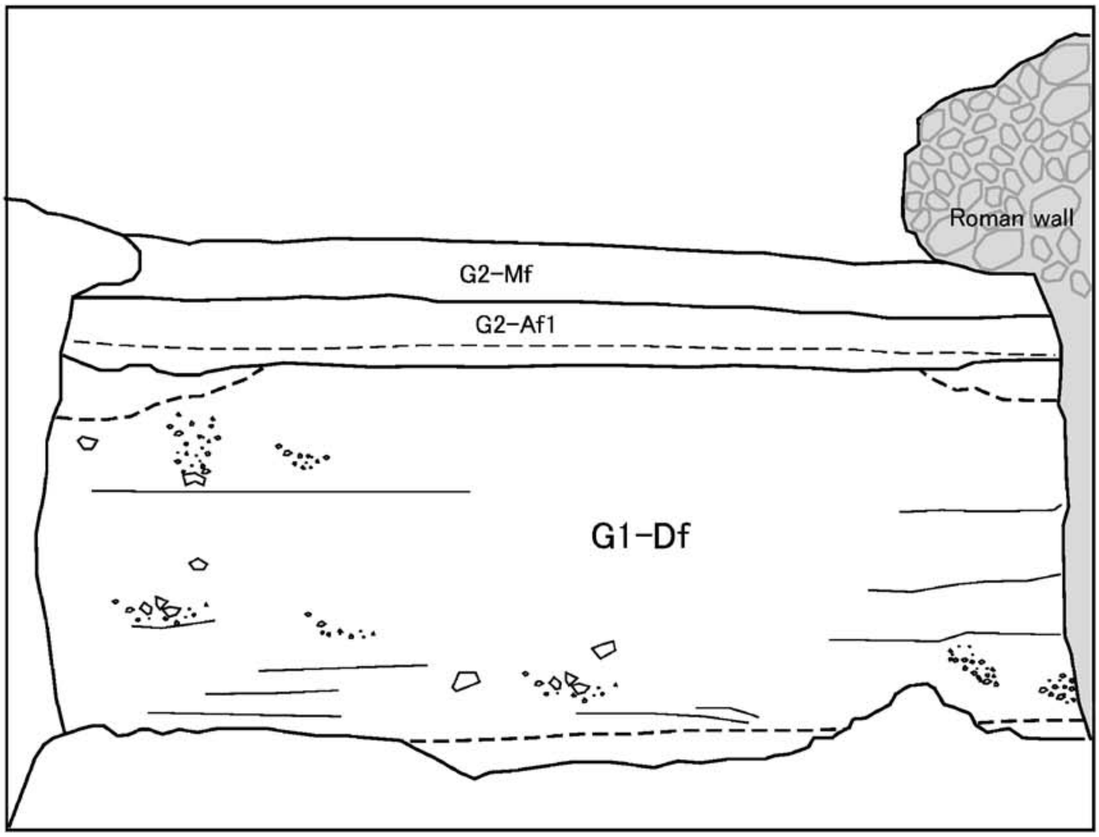

Appendix 4-4. G1-Df, G2-Af1, and G2-Mf deposits near the western wall of Vano2 at the middle wall. Note that the thickness of G2-Af1 does not change in contrast to the eastern wall of Vano2 (see Appendix 4-5).

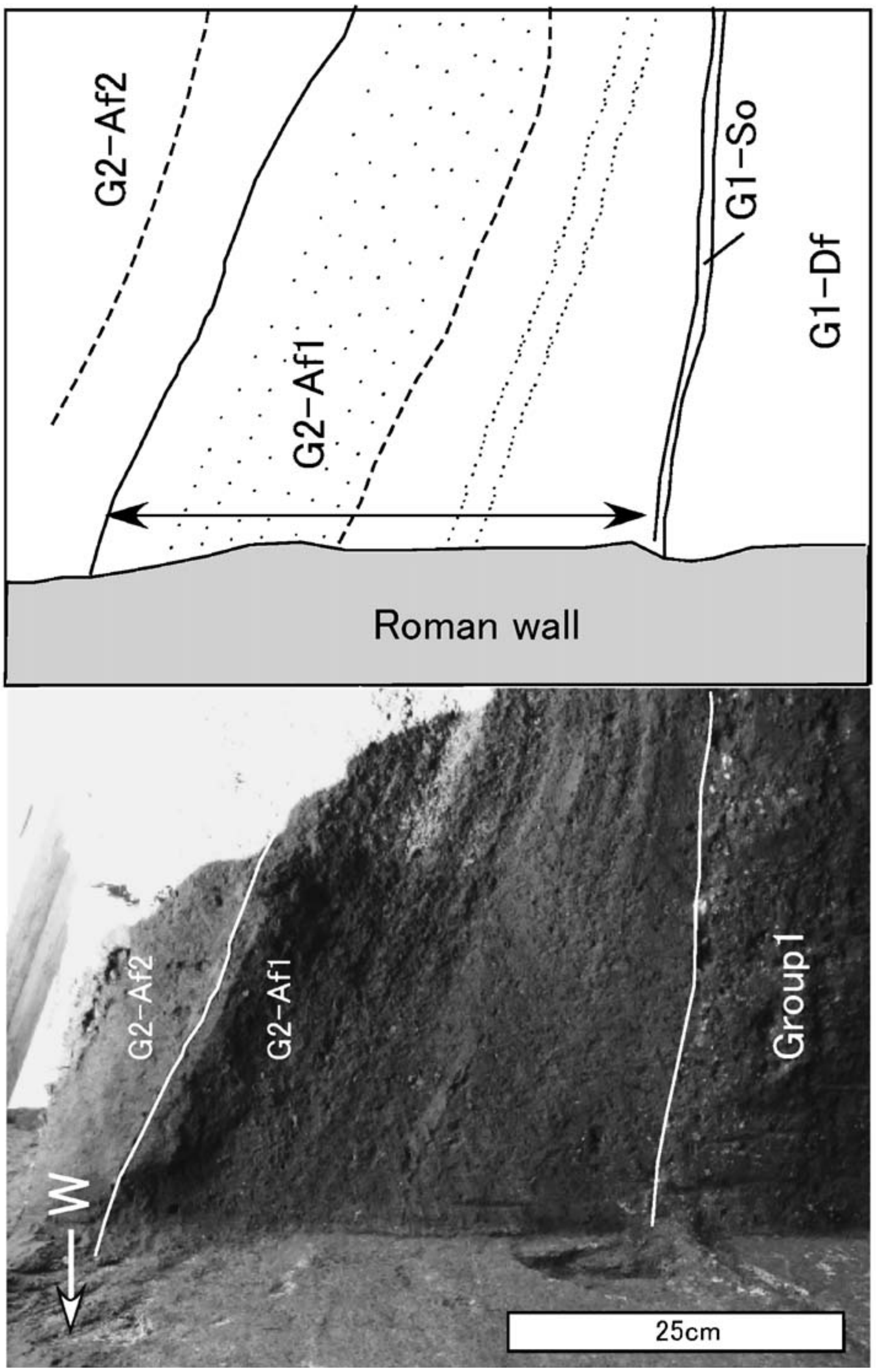

Appendix 4-5. G2-Af1 deposit near the eastern wall of Vano2 showing an increase of total thickness towards the wall.

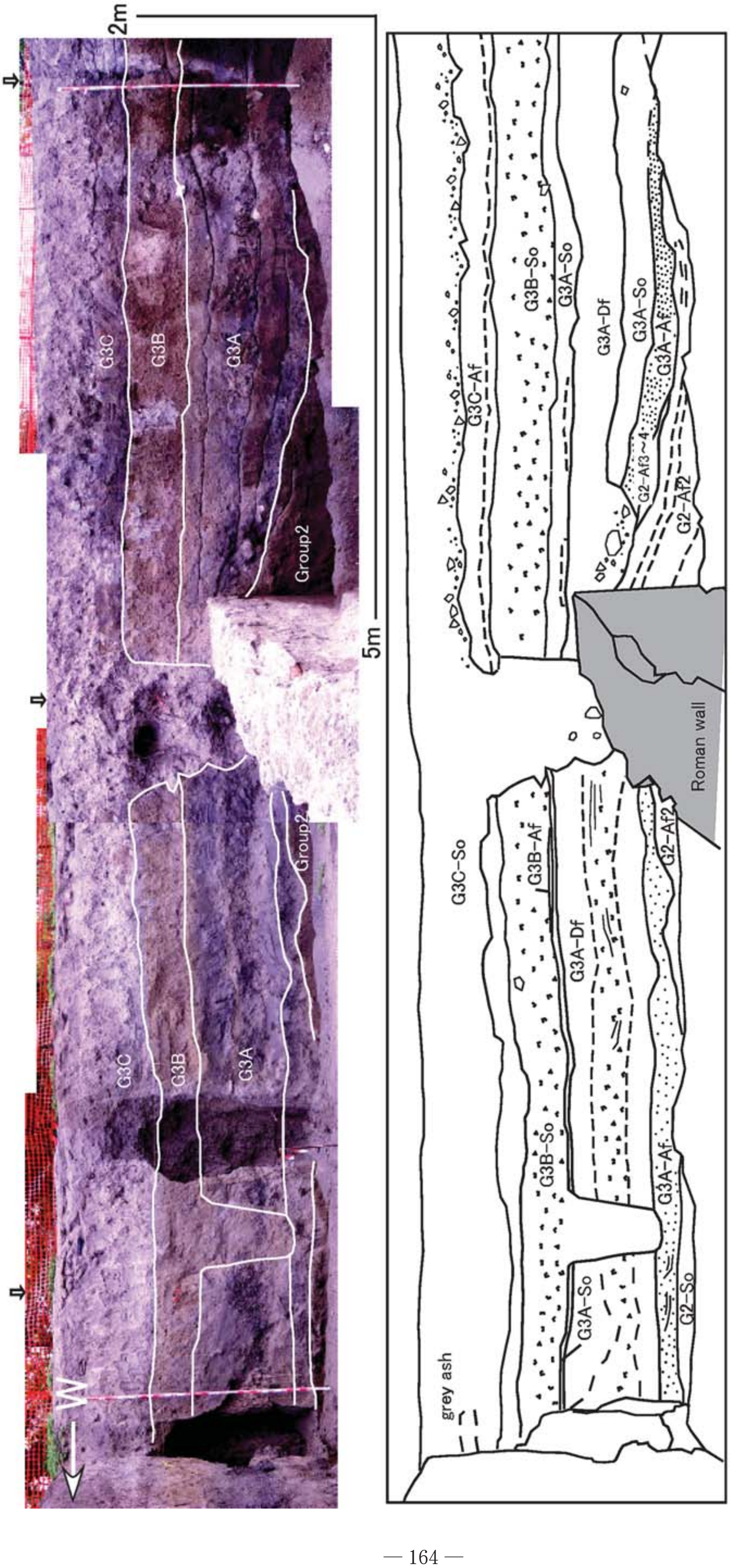

※ Open arrows are marked up at an interval of 5 m.

Appendix 4-6. Overview of upper wall. Relationships of deposits and building are well observed. Thickness of G2-Af2 increases toward the eastern wall of the Roman wall, but at the opposite side, such does not occur.

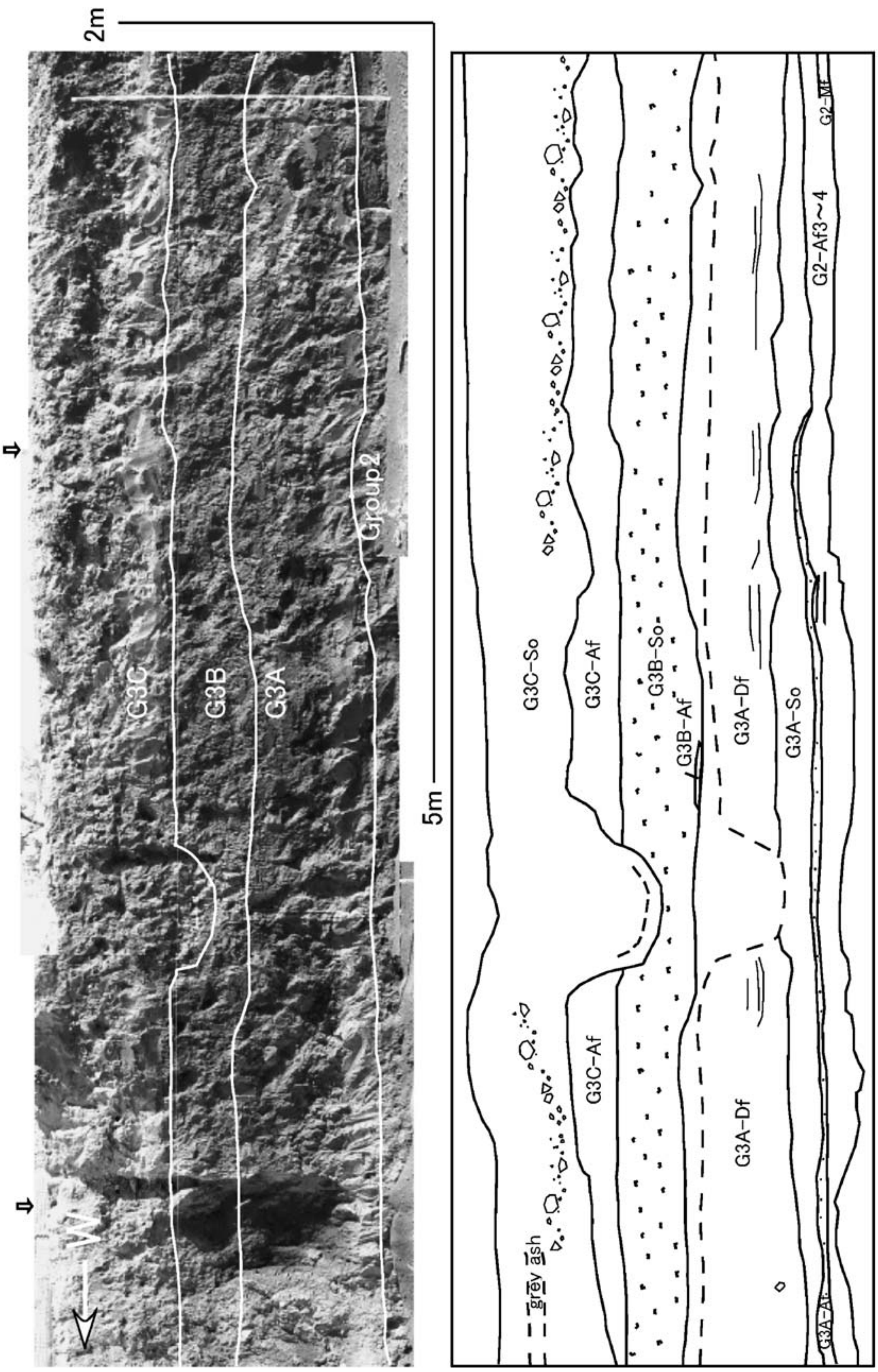

※ Open arrows are marked up at an interval of 5m.

Appendix 4-7. Succession of Group3 deposits continues from Appendix 4-5.

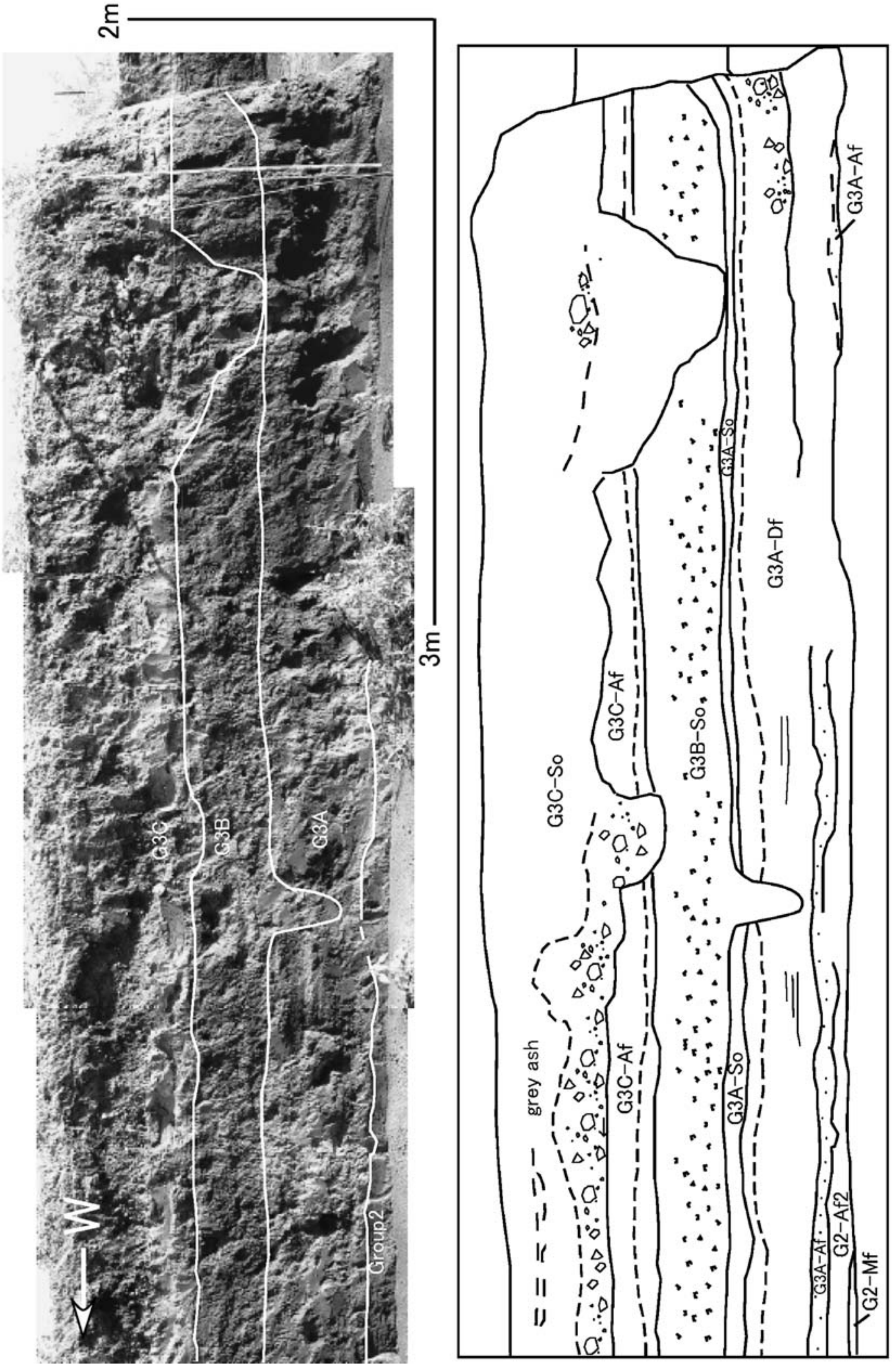

Appendix 4-8. Succession of Group3 deposits continues from Appendix 4-7. G3C-Af is eroded, and channels are formed. The channels are buried by lithic-rich epiclastic flow deposits.

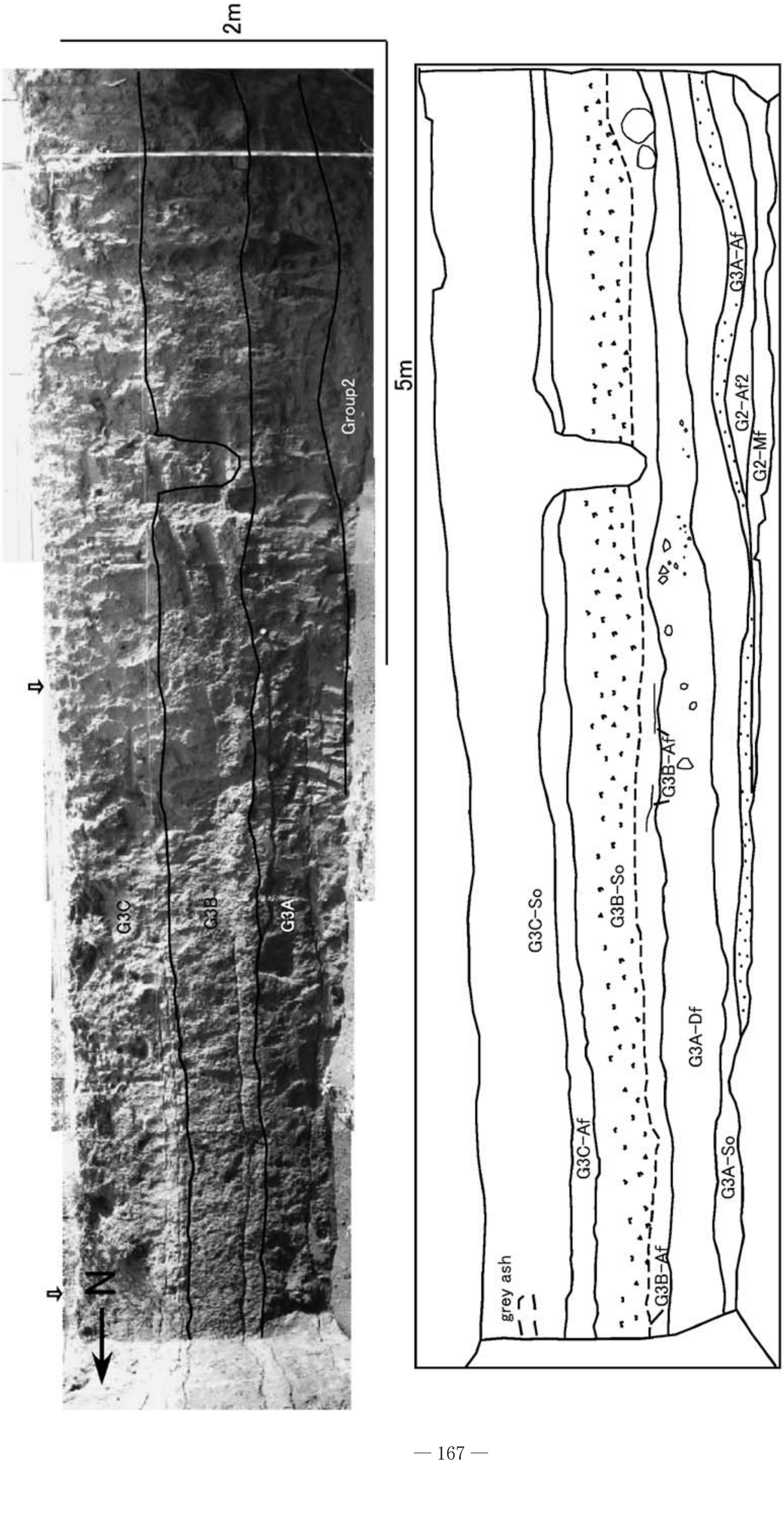

※ Open arrows are marked up at an interval of 5 m.

Appendix 4-9. Succession of Group3 deposits continues from Appendix 4-8. This is the eastern end of the upper wall.

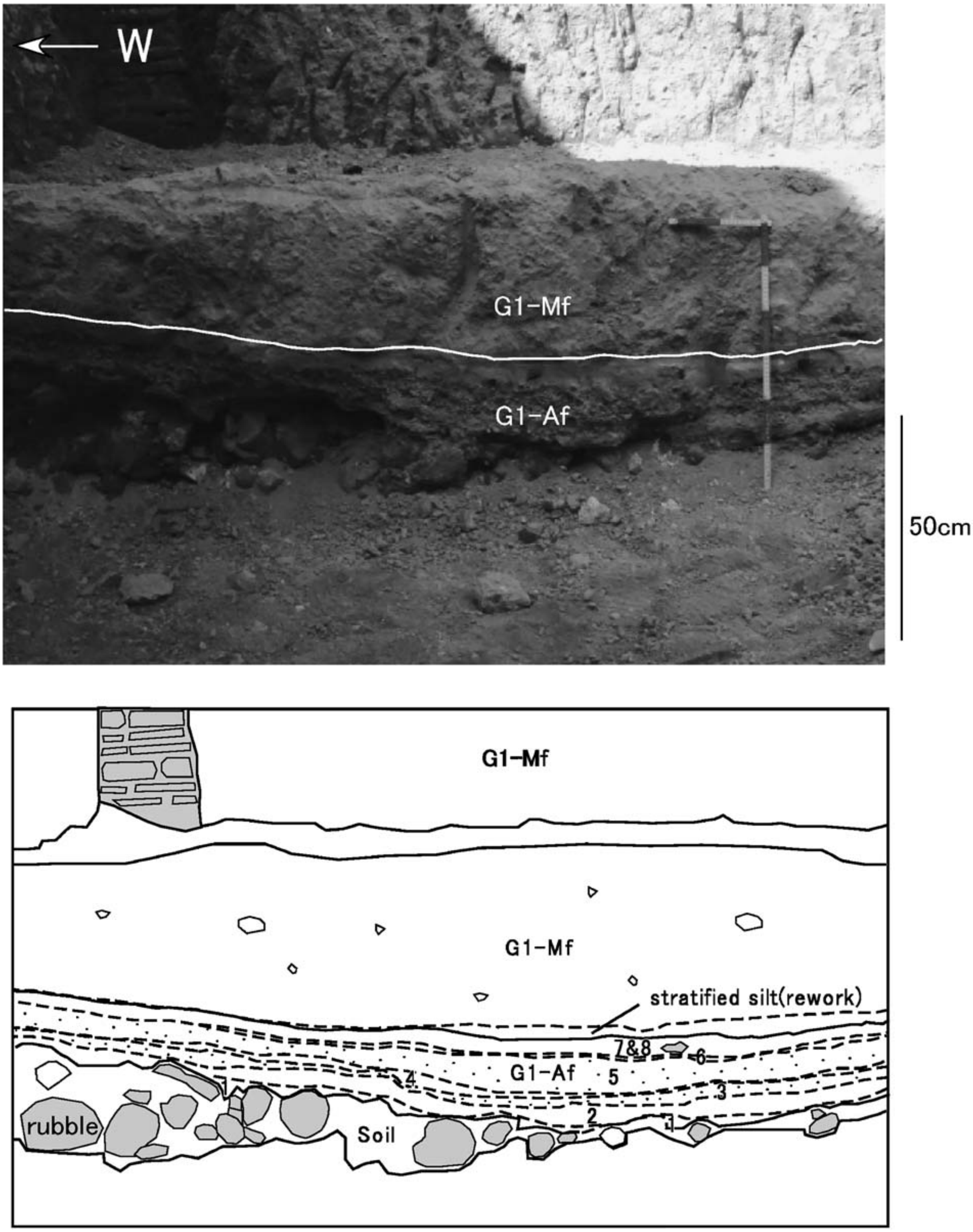

Appendix 5-1. Photograph and sketch showing the relationships among volcanic products and epiclastic flow deposits and a variety of archaeological structures inside Vano2. G1-Af deposit covers the scattered rubble and plaster of the Roman villa. The maximum size of these artificial objects is about 20 cm. Note that small pieces are also included among the deposits of G1-Af7 and G1-Af8.

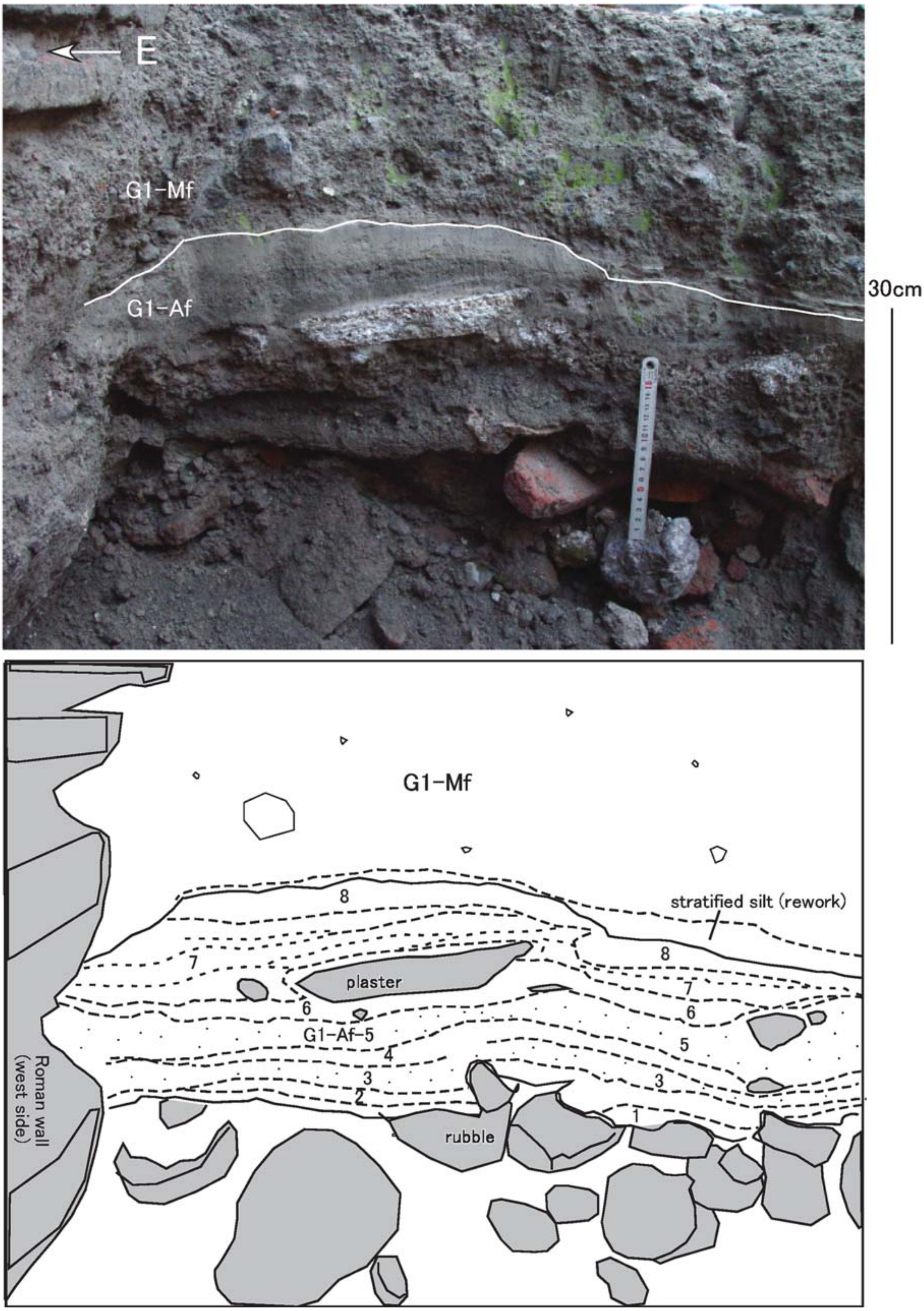

Appendix 5-2. Occurrence of G1-Af deposit inside Vano2. G1-Af deposit covers scattered rubble and plaster. Thickness of G1-Af does not increase towards the inside wall of Vano2 in contrast to the outside wall (see Appendix 4-2). Note that small pieces of rubble and plaster are included among the deposits of G1-Af5, G1-Af6, G1-Af7, and G1-Af8. The amounts of rubble increase towards the wall (see and compare with Appendix 5-1).

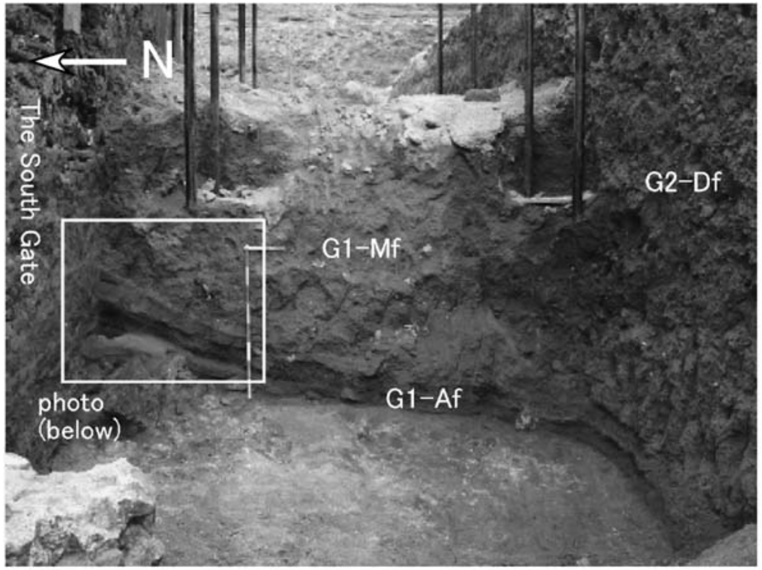

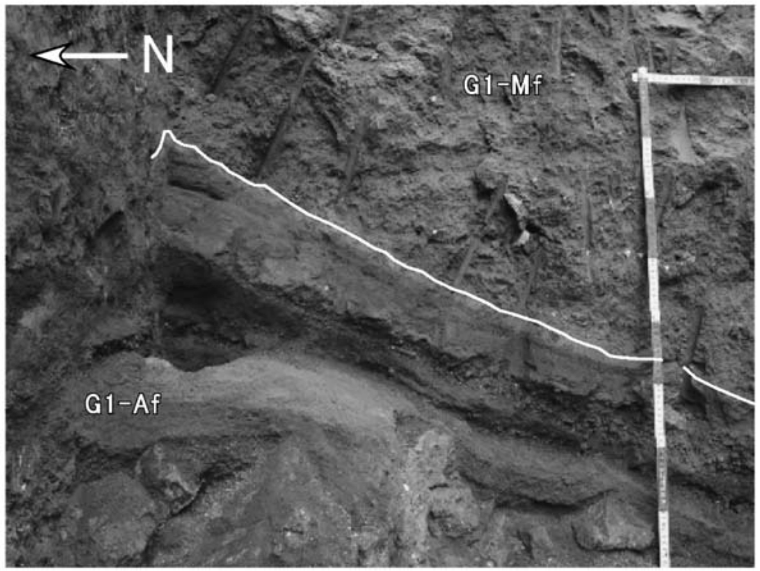

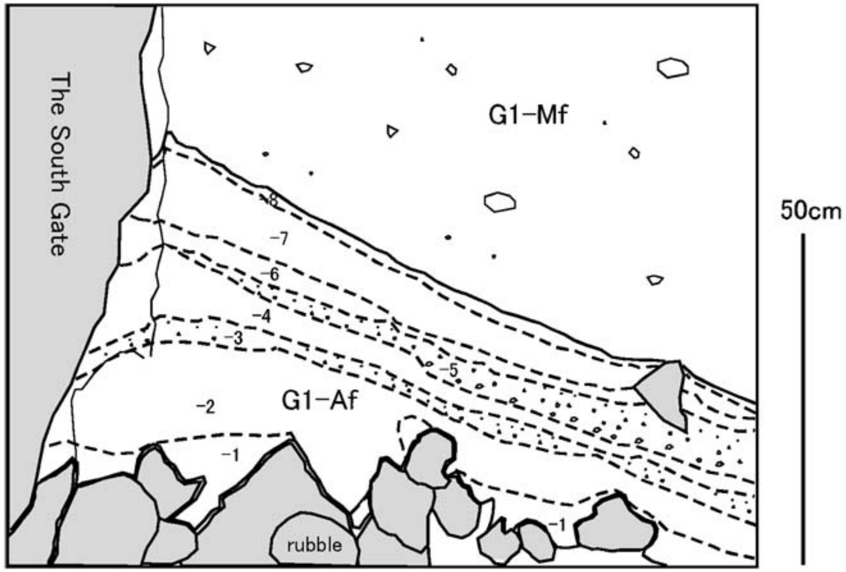

Appendix 6-1. Photograph and sketch showing relationships among architectures, volcanic products, and epiclastic flow deposits around the South Gate. The occurrence of G1-Af near the South Gate facing Mt Somma-Vesuvius is shown. The thickness of G1-Af, especially G1-Af7, increases toward the South Gate.

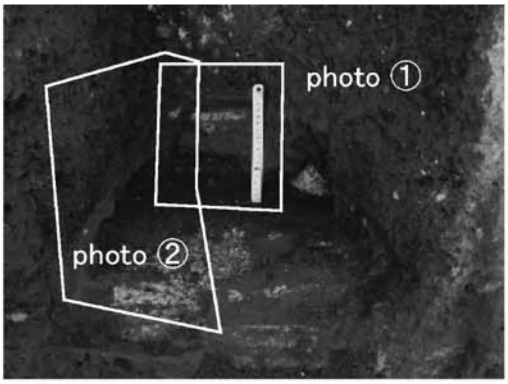

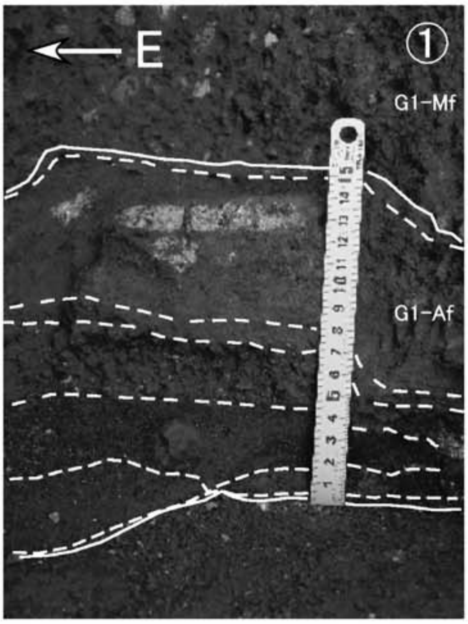

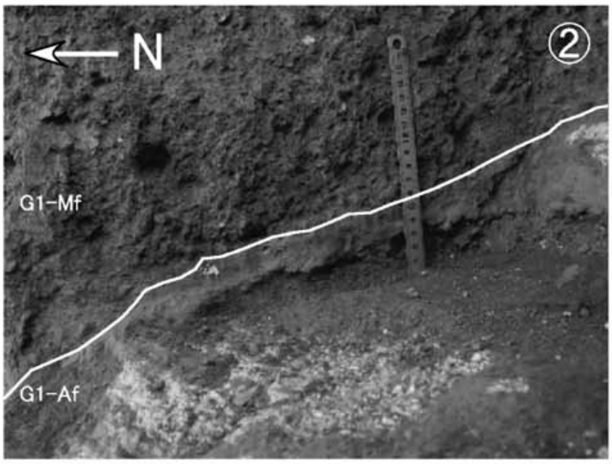

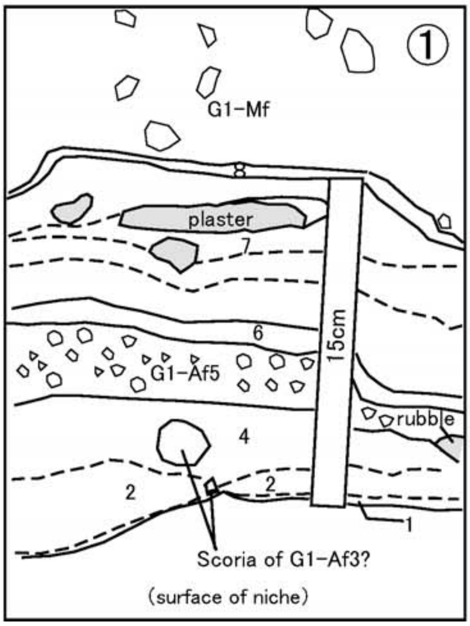

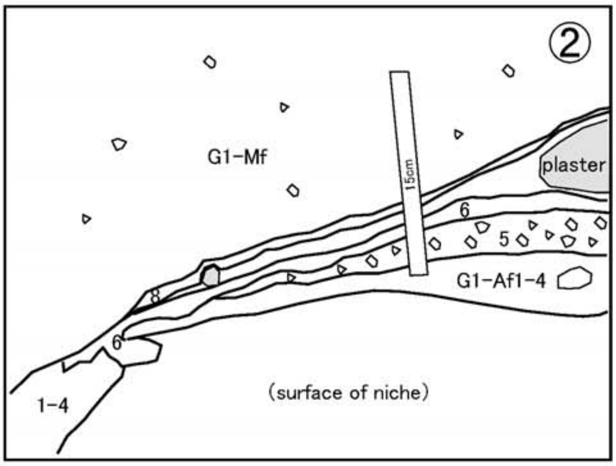

Appendix 6-2. Occurrence of G1-Af in the niche attached to the South Gate. This niche faces north. Note that rubble and plaster are interbedded in G1-Af5 and G1-Af7. The thickness of G1-Af7 increases towards the inside of the niche.

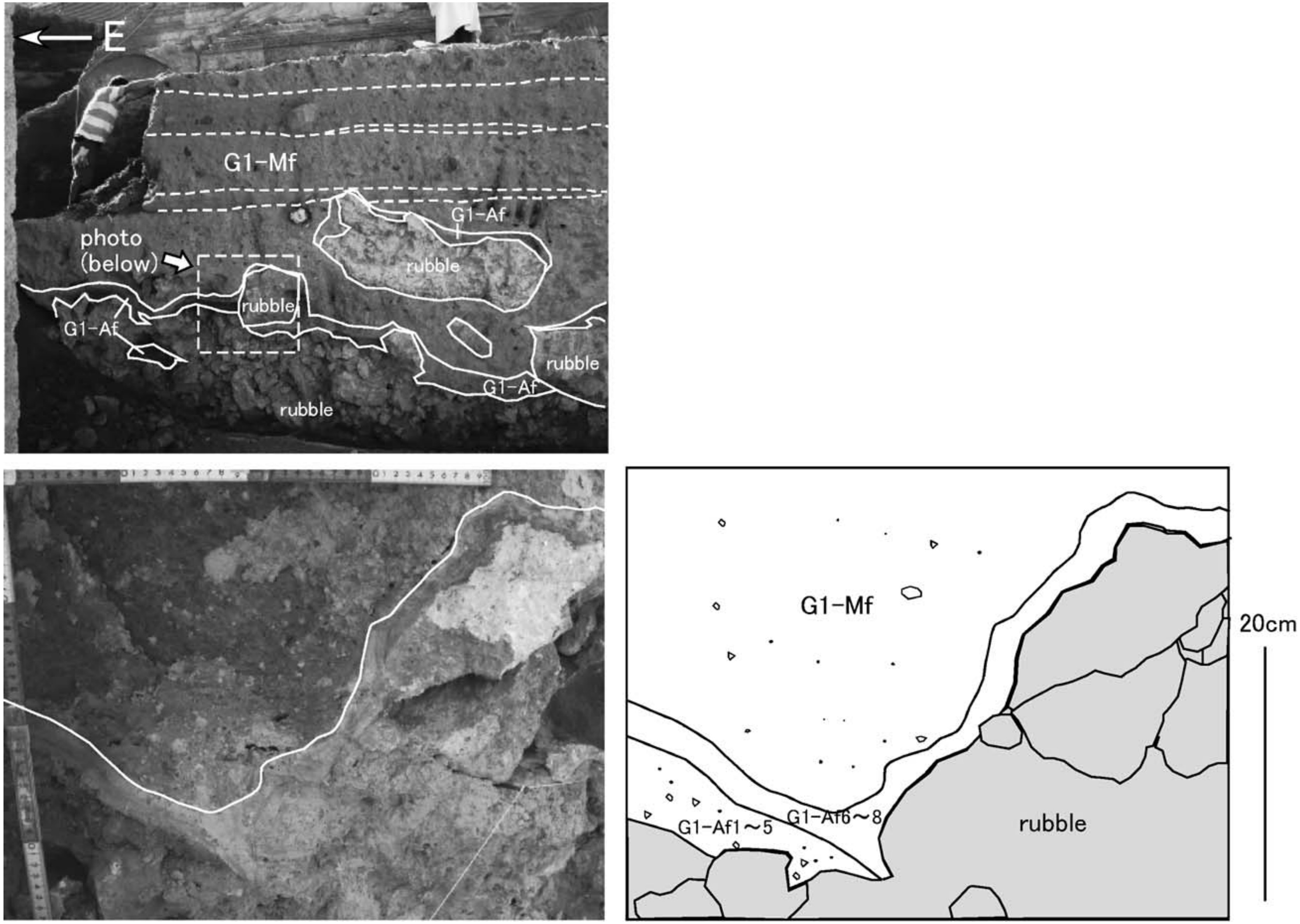

Appendix 6-3. Occurrence of G1-Af and G1-Mf deposits around the South Gate. Note that G1-Mf engulfs the rubble covered by G1-Af. This indicates that the rubble had already been created and scattered on the floor before the AD 472 eruption, and G1-Mf had engulfed them without moving them after emplacement of G1-Af deposit.

Appendix 7. Whole-rock chemistry of juvenile materials of Mt. Somma-Vesuvius.

Sample	Stratification	Flux*	SiO_2	TiO_2	Al_2O_3	FeO*	MnO	MgO	CaO	Na_2O	K_2O	P_2O_5	Total	Na_2O + K_2O	Ba	Cr	V	Ni	Rb	Zr	Sr
			wt.%	wt.%	wt.%	wt.%	wt.%	wt.%	wt.%	wt.%	wt.%	wt.%	wt.%	wt.%	ppm	ppm	ppm	ppm	ppm	ppm	ppm
	Tephra collected from excavation site																				
VS20030929-01a	G1_Af	1:20	50.1	0.8	18.2	5.7	0.2	3.5	9.4	3.3	8.2	0.5	100.0	11.5	2266	25.3	16.8	84	276	268	1215
VS20030929-01b	G1_Af	1:20	50.0	0.8	18.6	5.6	0.2	3.1	9.0	3.9	8.3	0.5	100.0	12.2	2401	19.8	17.8	87	269	289	1349
VS20030929-01c	G1_Af	1:20	50.1	0.8	18.5	5.7	0.2	3.3	9.3	3.3	8.4	0.5	100.0	11.7	2233	24.8	15.8	80	281	272	1233
VS20030929-01d	G1_Af	1:20	50.2	0.8	17.8	5.5	0.2	4.1	9.8	3.3	7.9	0.5	100.0	11.2	2246	24.7	17.6	82	252	275	1279
SV05101302-1-	G1_Af	1:5	51.4	0.5	21.8	4.4	0.2	0.7	5.5	6.1	9.2	0.1	100.0	15.3	2038	9.4	0.9	113	245	297	1663
SV05082402-3-	G1_Af	1:5	50.6	0.8	19.7	5.7	0.1	2.0	7.8	4.0	8.8	0.4	100.0	12.8	3782	16.3	9.1	88	297	271	1950
SV05082402-5-	G1_Af	1:5	49.5	0.9	18.3	6.5	0.2	3.2	9.5	3.4	8.0	0.6	100.0	11.4	2492	23.0	19.3	82	313	263	1371
SV05082601-	G1_Af	1:5	49.6	0.9	18.3	6.3	0.2	3.4	9.4	3.5	8.0	0.6	100.0	11.4	2499	21.9	25.2	90	301	263	1395
SV05100702-	G1_Af	1:5	50.3	0.8	19.9	5.7	0.2	2.0	7.7	4.1	9.1	0.4	100.0	13.1	2396	16.1	9.8	90	317	279	1481
SV05051204-2	G2_Af1	1:5	49.7	0.9	18.1	6.5	0.2	3.5	9.5	3.2	7.8	0.5	100.0	11.0	2318	20.7	27.9	83	313	262	1296
SV05051204-3	G2_Af1	1:5	50.0	0.9	17.9	6.5	0.2	3.7	9.6	3.1	7.6	0.5	100.0	10.7	2452	23.0	29.9	81	302	258	1292
SV05081002-	G2_Af1	1:5	50.9	0.7	20.8	6.1	0.2	1.5	6.7	4.4	8.5	0.3	100.0	12.9	1887	16.4	3.8	89	350	266	1448
SV040909-04	G2_Af1	1:20	50.6	0.6	20.7	6.1	0.2	1.7	6.8	4.4	8.5	0.3	100.0	12.9	2008	14.8	tr.	90	320	281	1384
SV040930-06-1	G2_Af1	1:20	50.3	0.7	19.6	6.5	0.2	2.6	7.9	3.9	7.9	0.5	100.0	11.8	1904	18.8	6.0	86	299	263	1255
SV041002-02-1	G2_Af1	1:20	50.0	0.8	19.5	6.5	0.2	2.8	8.0	3.9	7.9	0.5	100.0	11.8	2002	18.8	8.9	85	303	261	1279
SV040909-04 A	G2_Af1	1:20	51.2	0.6	21.1	5.6	0.2	1.7	6.6	4.3	8.5	0.3	100.0	12.8	1797	18.0	3.5	93	315	272	1360
SV040909-04 B	G2_Af1	1:20	50.2	0.8	19.8	5.8	0.2	2.9	7.9	3.9	8.1	0.5	100.0	12.1	1756	26.3	13.6	83	304	261	1268
SV05081002 sc-	G2_Af1	1:5	50.2	0.8	19.4	6.6	0.2	2.8	8.3	3.6	7.7	0.5	100.0	11.3	1878	19.7	15.1	84	330	256	1313
SV040909-04 C	G2_Af1	1:20	51.0	0.6	21.0	5.6	0.2	1.6	6.6	4.5	8.6	0.3	100.0	13.0	1745	18.7	2.4	92	311	276	1360
SV05081001 bb-	G3A_Af	1:5	49.8	1.0	17.5	7.4	0.2	3.5	9.4	2.9	7.8	0.6	100.0	10.7	1907	24.5	20.8	79	378	279	1139
SV040913-	G3A_Af	1:20	49.5	0.9	17.9	7.3	0.2	3.4	8.9	3.2	8.1	0.6	100.0	11.3	1989	22.6	18.9	85	359	281	1064
SV05081001 bt-	G3A_Af	1:5	49.5	1.0	17.7	7.4	0.2	3.3	9.0	3.3	8.1	0.6	100.0	11.3	1933	25.4	20.0	83	380	281	1157
SV040910-02-3	G3B_Af	1:20	49.6	0.9	16.8	7.5	0.1	4.7	9.5	2.7	7.4	0.8	100.0	10.1	2290	25.9	33.3	75	267	227	1047
SV040908-04-1-1	G3C_Af	1:20	49.5	0.8	16.1	5.8	0.1	5.6	12.2	2.8	6.4	0.6	100.0	9.2	1171	17.4	30.1	58	360	228	901
SV040908-04-1-8	G3C_Af	1:20	49.5	0.9	15.6	6.0	0.1	6.0	12.8	2.8	5.5	0.7	100.0	8.3	1178	21.5	43.6	64	179	218	802
SV040908-04-2-1	G3C_Af	1:20	48.8	0.9	14.7	6.3	0.1	7.1	13.8	2.3	5.0	0.9	100.0	7.3	1412	19.7	53.1	60	172	205	839
SV040908-04-2-8	G3C_Af	1:20	49.7	1.0	17.0	7.6	0.1	5.3	10.6	2.9	5.1	0.9	100.0	7.9	2499	28.2	38.0	55	184	194	979

Appendix 7. (Continue)

Sample	Stratification	Flux*	SiO_2	TiO_2	Al_2O_3	FeO*	MnO	MgO	CaO	Na_2O	K_2O	P_2O_5	Total	$Na_2O + K_2O$	Ba	Cr	V	Ni	Rb	Zr	Sr
			wt.%	wt.%	wt.%	wt.%	wt.%	wt.%	wt.%	wt.%	wt.%	wt.%	wt.%	wt.%	ppm	ppm	ppm	ppm	ppm	ppm	ppm
SV040908-04-2-18	G3C_Af	1:20	51.1	0.7	18.9	5.7	0.1	3.0	8.8	4.0	7.2	0.5	100.0	11.2	1761	12.7	10.4	77	228	273	1148
SV040910-01-2	G3C_Af	1:20	49.4	1.0	17.4	7.7	0.1	4.6	9.6	2.1	7.2	0.9	100.0	9.3	2250	26.9	32.6	74	293	192	937
SV040910-01-4	G3C_Af	1:20	49.5	0.9	16.1	5.9	0.1	6.2	11.7	3.0	6.0	0.7	100.0	8.9	1398	20.1	56.3	61	194	214	832
SV040910-01-5	G3C_Af	1:20	49.5	0.9	15.6	6.0	0.1	6.2	12.4	2.9	5.7	0.7	100.0	8.6	1209	20.7	28.1	67	187	216	763
	Tephra collected from the flank of Mt. Somma Vesuvius																				
021003-01-03 AD472 b	AD 472	1:5	49.9	0.8	18.3	5.8	0.2	3.4	9.7	3.4	7.9	0.5	100.0	11.3	2441	43.0	350.6	26	79	312	264
021003-01-03 AD472 c	AD 472	1:5	51.1	0.6	21.0	4.6	0.2	1.3	6.7	5.0	9.3	0.2	100.0	14.3	2346	6.4	266.3	7	98	297	292
SV040908-30 A	AD 472	1:5	50.1	0.9	18.5	5.7	0.2	3.4	9.3	3.5	8.1	0.5	100.0	11.5	2335	36.3	202.4	23	79	321	253
SV040908-30 B	AD 472	1:5	49.7	0.9	18.4	5.9	0.2	3.2	9.8	3.4	7.9	0.5	100.0	11.4	2414	38.3	212.9	19	80	312	261
SV040908-30 C	AD 472	1:5	50.5	0.9	18.7	5.5	0.2	3.1	9.3	3.5	8.0	0.5	100.0	11.5	2346	38.6	192.8	18	83	292	268
SV040908-31 A	AD 472	1:5	51.3	0.6	21.3	4.3	0.2	1.2	6.2	5.1	9.5	0.2	100.0	14.6	2050	5.5	134.6	4	98	306	274
SV040908-31 B	AD 472	1:5	51.5	0.6	21.2	4.3	0.1	1.2	6.2	4.8	9.8	0.2	100.0	14.6	2083	3.2	137.3	4	92	330	268
SV040908-31 C	AD 472	1:5	51.3	0.7	20.7	4.7	0.2	1.5	6.9	4.6	9.3	0.3	100.0	13.9	2383	6.3	156.3	5	93	321	283
SV040907-03-1	AD 472	1:5	51.7	0.5	21.9	4.1	0.1	0.7	5.3	5.7	9.8	0.1	100.0	15.5	2372	2.9	107.0	3	101	292	269
SV040907-03-2	AD 472	1:5	50.7	0.7	20.1	5.5	0.2	1.8	7.4	4.3	9.0	0.3	100.0	13.3	2340	9.4	166.7	8	92	304	284
SV040907-03-3	AD 472	1:5	49.9	0.9	18.1	6.3	0.2	3.5	9.6	3.1	8.0	0.5	100.0	11.1	2445	46.4	206.4	26	79	315	255
SV040907-03-4	AD 472	1:5	49.3	0.9	17.8	6.7	0.2	3.5	10.1	3.3	7.6	0.5	100.0	10.9	2367	56.6	216.3	24	80	299	268
SV040907-03-5	AD 472	1:5	49.5	0.9	18.0	6.7	0.2	3.3	9.8	3.2	7.8	0.5	100.0	11.0	2429	39.9	220.5	19	82	307	265
SV05051308①-	AD 472	1:5	50.0	0.8	18.3	6.1	0.2	3.2	9.6	3.8	7.7	0.5	100.0	11.4	2261	36.2	195.6	30	82	320	270
SV05051308②-1	AD 472	1:5	50.1	0.8	18.3	6.0	0.2	3.2	9.4	3.4	8.2	0.4	100.0	11.6	2081	40.0	195.5	20	80	328	271
SV05051308 MN-1	AD 472	1:5	49.9	0.8	18.2	6.0	0.2	3.3	9.5	3.5	8.0	0.5	100.0	11.5	2449	43.5	198.4	24	83	309	264
SV05051308 MN-3	AD 472	1:5	50.1	0.8	18.8	5.9	0.1	2.9	8.9	3.5	8.4	0.5	100.0	11.9	2528	34.0	190.0	20	84	321	258
SV05051308 MN-7	AD 472	1:5	49.9	0.8	18.6	6.1	0.2	3.1	9.2	3.6	8.0	0.5	100.0	11.6	2265	38.0	195.3	21	84	299	268
SV05051401-472①-5	AD 472	1:5	51.4	0.6	21.6	4.4	0.1	0.8	5.8	5.5	9.8	0.1	100.0	15.3	2232	3.1	123.9	3	100	316	279
SV05051401-472①-gray	AD 472	1:5	52.0	0.5	22.1	3.8	0.1	0.6	5.0	6.1	9.8	0.1	100.0	15.9	2259	0.8	97.9	4	104	293	275
SV05051401-472①-white	AD 472	1:5	52.5	0.3	22.9	3.3	0.2	0.2	4.1	7.5	9.0	0.1	100.0	16.5	1578	tr.	60.2	1	120	202	310

Appendix 7. (Continue)

Sample	Stratification	Flux*	SiO_2	TiO_2	Al_2O_3	FeO*	MnO	MgO	CaO	Na_2O	K_2O	P_2O_5	Total	$Na_2O + K_2O$	Ba	Cr	V	Ni	Rb	Zr	Sr
			wt.%	wt.%	wt.%	wt.%	wt.%	wt.%	wt.%	wt.%	wt.%	wt.%	wt.%	wt.%	ppm	ppm	ppm	ppm	ppm	ppm	ppm
SV05051401-472②-	AD 472	1:5	51.3	0.5	21.6	4.4	0.1	0.9	5.7	5.8	9.4	0.2	100.0	15.2	1956	1.7	118.6	4	103	287	284
SV05051401-472③-	AD 472	1:5	51.2	0.6	20.8	4.9	0.1	1.3	6.5	4.8	9.5	0.2	100.0	14.4	2505	3.1	150.3	6	93	323	271
SV05051401-472④-	AD 472	1:5	49.8	0.9	19.0	6.3	0.2	2.5	9.1	3.8	8.2	0.4	100.0	12.0	2321	17.7	207.4	15	87	302	294
SV05051401-472⑤-	AD 472	1:5	49.6	0.9	18.3	6.3	0.2	3.3	9.6	3.6	7.8	0.5	100.0	11.4	2316	34.2	212.0	22	84	303	269
SV05051401-472⑥-	AD 472	1:5	49.7	0.9	18.0	6.5	0.2	3.4	9.8	3.2	7.8	0.5	100.0	11.0	2389	36.5	215.9	23	81	313	267
SV05051401-472⑦-	AD 472	1:5	49.6	0.9	18.1	6.6	0.2	3.3	9.8	3.2	7.8	0.5	100.0	11.0	2438	35.0	219.6	23	83	315	267
SV05051401-472⑧-	AD 472	1:5	49.9	0.9	18.0	6.5	0.2	3.4	9.7	3.1	7.7	0.5	100.0	10.9	2363	40.1	216.9	23	79	325	261
SV05051405 ①-1	AD 472	1:5	49.7	0.9	17.6	6.7	0.2	3.8	10.4	3.1	7.2	0.5	100.0	10.3	2288	51.5	217.3	24	83	295	264
SV05051403-	AD 472	1:5	49.5	0.9	17.9	6.6	0.2	3.5	10.1	3.2	7.7	0.5	100.0	10.9	2359	38.9	222.6	24	80	292	266
SV05051405 ①-5	AD 472	1:5	51.1	0.6	21.5	4.6	0.1	1.0	6.0	5.5	9.4	0.2	100.0	14.9	2281	1.7	130.3	6	105	284	283
SV05051405 ①-7	AD 472	1:5	51.1	0.6	21.0	4.9	0.1	1.3	6.4	5.1	9.3	0.2	100.0	14.4	2179	4.5	144.1	6	97	302	280
SV05051405 ②-	AD 472	1:5	50.1	0.8	18.6	5.9	0.2	3.1	9.1	3.6	8.3	0.5	100.0	11.9	2293	37.9	189.4	25	82	323	259
SV05092803-1①-	AD 472	1:20	51.0	0.5	21.4	4.6	0.1	1.1	5.9	5.3	9.9	0.2	100.0	15.2	1930	13.1	120.9	tr.	106	300	313
SV05092803-1④-	AD 472	1:20	50.5	0.6	20.8	6.1	0.2	1.6	6.7	4.4	8.8	0.3	100.0	13.2	1532	29.2	169.2	tr.	94	332	291
SV05092901 ②-	AD 472	1:20	49.5	0.8	18.2	6.1	0.2	3.7	9.7	3.6	7.9	0.5	100.0	11.5	2015	72.9	191.5	20	85	263	280
SV05092901 ②-	AD 472	1:20	49.4	0.8	18.6	6.1	0.2	3.2	9.3	3.6	8.4	0.5	100.0	12.0	2057	64.9	195.9	14	84	295	290
SV05092902 ②-	AD 472	1:20	49.8	0.8	17.9	6.0	0.1	3.8	9.8	3.3	8.0	0.5	100.0	11.3	1804	115.4	197.0	20	79	282	265
SV05092902 ②-	AD 472	1:20	49.8	0.8	18.6	6.0	0.1	3.3	9.1	3.6	8.3	0.5	100.0	11.9	1941	88.2	186.2	18	87	299	278
SV05092702-	AD 472-1631	1:5	49.6	0.9	18.0	6.4	0.2	3.4	9.8	3.3	8.0	0.5	100.0	11.2	2322	40.7	211.2	20	79	319	261
SV040907-04-4	AD 472-1631	1:5	48.4	0.9	12.4	6.6	0.1	9.3	14.8	2.0	4.5	0.8	100.0	6.5	1361	256.6	206.0	111	58	203	200
SV040907-05-1	AD 472-1631	1:5	49.8	0.9	18.7	6.9	0.2	3.6	8.9	3.5	7.1	0.6	100.0	10.6	1829	37.1	202.9	25	79	300	250
SV040907-05-2	AD 472-1631	1:5	49.7	0.9	18.3	6.9	0.2	3.9	9.3	3.3	6.9	0.6	100.0	10.2	1789	48.7	202.6	29	76	297	246
SV040907-05-3	AD 472-1631	1:5	49.6	0.9	17.8	6.9	0.2	4.3	9.7	3.2	6.6	0.7	100.0	9.9	1782	63.0	207.0	35	75	290	240
SV040907-05-4	AD 472-1631	1:5	49.1	1.0	16.8	7.0	0.2	5.2	10.8	3.0	6.2	0.8	100.0	9.2	1713	96.5	214.4	48	70	280	228
SV040907-05-1 A	AD 472-1631	1:20	50.1	0.8	19.1	6.1	0.2	3.6	8.6	3.7	7.4	0.6	100.0	11.0	1721	50.4	194.0	20	83	276	264
SV040907-05-1 B	AD 472-1631	1:20	50.0	0.8	19.3	6.0	0.2	3.5	8.4	3.7	7.5	0.6	100.0	11.2	1732	46.5	196.9	22	82	289	257

Appendix 7. (Continue)

Sample	Stratification	Flux*	SiO_2	TiO_2	Al_2O_3	FeO*	MnO	MgO	CaO	Na_2O	K_2O	P_2O_5	Total	Na_2O + K_2O	Ba	Cr	V	Ni	Rb	Zr	Sr
			wt.%	wt.%	wt.%	wt.%	wt.%	wt.%	wt.%	wt.%	wt.%	wt.%	wt.%	wt.%	ppm	ppm	ppm	ppm	ppm	ppm	ppm
SV040907-05-1 C	AD 472-1631	1:20	49.9	0.8	19.0	6.1	0.2	3.7	8.6	3.6	7.4	0.6	100.0	11.0	1767	49.8	208.2	18	80	276	262
SV040907-05-2 A	AD 472-1631	1:20	50.3	0.8	18.7	6.1	0.2	3.9	8.8	3.5	7.1	0.7	100.0	10.5	1717	70.1	200.0	22	80	271	255
SV040907-05-2 B	AD 472-1631	1:20	51.9	0.8	19.5	6.2	0.2	3.7	7.1	3.1	7.0	0.6	100.0	10.1	1729	67.4	185.7	25	84	264	260
SV040907-05-2 C	AD 472-1631	1:20	50.1	0.8	19.1	6.1	0.2	3.7	8.4	3.5	7.4	0.7	100.0	11.0	1804	43.0	192.9	25	84	284	257
SV040907-05-3 A	AD 472-1631	1:20	50.0	0.9	17.3	6.0	0.1	5.2	10.2	3.1	6.5	0.7	100.0	9.7	1537	n.d.	202.9	37	74	253	238
SV040907-05-3 B	AD 472-1631	1:20	49.8	0.9	18.3	6.1	0.2	4.3	9.6	3.2	7.0	0.7	100.0	10.2	1672	75.2	208.1	25	77	271	253
SV05051402 ①-	AD 472-1631	1:5	49.1	1.1	17.5	7.9	0.2	4.1	9.0	2.7	7.6	0.9	100.0	10.3	2146	11.8	250.4	34	77	322	225
SV05051402 ②-	AD 472-1631	1:5	49.7	0.9	16.1	6.0	0.1	5.6	11.7	2.5	6.7	0.7	100.0	9.2	1563	69.8	202.2	47	60	285	204
SV05051402 MN-	AD 472-1631	1:5	49.9	0.8	19.3	6.7	0.2	2.9	8.4	3.8	7.5	0.5	100.0	11.3	1870	17.8	204.0	18	83	316	262
SV05090305 ③-	AD 472-1631	1:20	50.5	0.7	19.7	6.6	0.2	2.5	7.7	3.3	8.4	0.4	100.0	11.7	1803	67.3	177.1	9	86	308	242
SV05090305 ②-	AD 472-1631	1:20	49.0	1.0	17.0	7.5	0.2	5.1	10.3	2.3	6.9	0.8	100.0	9.2	1830	101.2	237.6	38	73	252	197
SV05090305 ①-1-	AD 472-1631	1:20	49.4	0.9	16.8	7.5	0.2	4.8	9.4	2.7	7.5	0.8	100.0	10.2	1840	116.9	228.5	38	78	263	234
SV05090305 ①-2-	AD 472-1631	1:20	48.6	1.0	17.8	7.8	0.2	4.2	9.1	2.6	7.8	1.0	100.0	10.4	1792	30.7	251.3	32	79	284	214
SV05090305 ①-3-	AD 472-1631	1:20	48.6	1.0	17.7	7.8	0.2	4.3	9.3	2.6	7.7	0.9	100.0	10.2	1753	31.6	254.4	31	76	284	217
021003-01-01 1631 a	AD 1631	1:5	50.4	0.8	17.3	5.5	0.1	4.6	10.9	3.1	6.5	0.6	100.0	9.6	1648	57.9	270.3	37	68	247	228
021003-01-01 1631 b	AD 1631	1:5	52.5	0.6	20.4	4.6	0.1	1.6	7.0	4.5	8.2	0.3	100.0	12.7	1846	11.9	227.8	11	81	272	268
021003-01-01 1631 c	AD 1631	1:5	51.9	0.7	19.6	4.7	0.1	2.5	8.0	3.8	8.4	0.4	100.0	12.1	1754	26.6	250.4	17	70	330	239
SV040907-06-1 A	AD 1631	1:5	52.1	0.7	19.9	4.7	0.1	2.2	7.6	3.8	8.7	0.4	100.0	12.4	1699	20.5	154.1	13	71	340	236
SV040907-06-1 B	AD 1631	1:5	51.4	0.8	19.0	5.1	0.1	2.9	8.9	3.7	7.7	0.5	100.0	11.4	1692	24.9	168.2	18	73	283	245
SV040907-06-1 C	AD 1631	1:5	52.1	0.7	19.4	4.7	0.1	2.4	8.1	3.8	8.3	0.4	100.0	12.0	1730	17.2	154.2	13	71	314	242
SV040907-06-2 A	AD 1631	1:5	51.6	0.7	19.4	5.0	0.1	2.5	8.5	4.0	7.5	0.5	100.0	11.5	1695	23.3	166.5	15	76	262	256
SV040907-06-2 B	AD 1631	1:5	51.9	0.7	19.6	4.9	0.1	2.4	8.1	4.0	7.8	0.4	100.0	11.9	1643	19.0	160.3	15	75	284	252
SV040907-06-2 C	AD 1631	1:5	51.8	0.7	19.6	5.0	0.1	2.3	8.3	4.1	7.5	0.4	100.0	11.6	1835	13.4	165.8	14	77	254	261
SV040907-06-3 A	AD 1631	1:5	49.5	0.9	15.9	5.9	0.1	5.8	12.8	2.8	5.4	0.8	100.0	8.2	1367	74.6	207.5	43	64	208	223
SV040907-06-3 B	AD 1631	1:5	49.8	0.9	16.7	5.8	0.1	5.2	11.7	2.9	6.0	0.8	100.0	9.0	1463	67.2	206.4	39	66	235	226

Appendix 7. (Continue)

Sample	Stratification	Flux*	SiO_2	TiO_2	Al_2O_3	FeO*	MnO	MgO	CaO	Na_2O	K_2O	P_2O_5	Total	Na_2O + K_2O	Ba	Cr	V	Ni	Rb	Zr	Sr
			wt.%	wt.%	wt.%	wt.%	wt.%	wt.%	wt.%	wt.%	wt.%	wt.%	wt.%	wt.%	ppm	ppm	ppm	ppm	ppm	ppm	ppm
SV040907-06-3 C	AD 1631	1:5	50.0	0.9	17.3	5.6	0.1	4.7	11.0	3.0	6.5	0.7	100.0	9.5	1680	63.2	200.8	39	68	251	225
SV040907-06-1	AD 1631	1:5	50.7	0.8	18.4	5.9	0.1	3.2	9.6	3.8	6.9	0.5	100.0	10.7	1599	28.0	182.7	22	74	241	256
SV040907-06-2	AD 1631	1:5	51.8	0.7	19.5	5.3	0.1	2.3	7.9	4.0	8.1	0.4	100.0	12.0	1766	20.9	158.4	14	74	302	251
SV040907-06-3	AD 1631	1:5	49.7	0.9	16.4	6.0	0.1	5.3	11.5	2.7	6.7	0.7	100.0	9.4	1309	70.2	201.1	39	59	278	209
SV05051501 ①-1	AD 1631	1:5	52.6	0.6	20.6	5.0	0.1	1.2	6.7	4.6	8.2	0.2	100.0	12.8	1885	4.7	140.2	6	83	265	279
SV05051501 ①-2	AD 1631	1:5	51.6	0.7	19.3	5.5	0.1	2.4	8.2	4.0	7.8	0.4	100.0	11.8	1659	20.6	167.2	15	77	289	259
SV05051501 ②-	AD 1631	1:5	51.6	0.7	19.1	5.3	0.1	2.7	8.3	3.7	8.0	0.4	100.0	11.7	1659	27.1	167.1	21	70	328	239
SV05051501 ③-	AD 1631	1:5	48.8	0.9	15.6	6.3	0.1	6.4	13.2	2.5	5.4	0.8	100.0	7.9	1460	78.1	212.8	56	59	228	208
SV05051501 MN-	AD 1631	1:5	52.8	0.6	20.5	5.0	0.1	1.3	6.7	4.6	8.2	0.2	100.0	12.8	2019	4.5	143.9	6	83	260	281

tr.: trace, n.d.: not detected, * :see text.

Appendix 8. Stratigraphic comparison between this study and Perrotta *et al.* (2006a, b).

Unit name	
This study	Perotta
G1-Df2	A13
G1-Df1	A12
G1-Mf4	A11
(fluvial deposit)	A10
G1-Mf3	A9
(fluvial deposit)	A8
G1-Mf2	A7
G1-Mf1	A7
G1-Af8	A6
G1-Af7	A6
G1-Af6	A6
G1-Af5	A5
G1-Af4	A4
G1-Af3	A3
G1-Af2	A2
G1-Af1	A1

Unit name	
This study	Perotta
G2-Df3	E1
G2-Af4	B2
G2-Df2	B2
G2-Af3	B2
G2-Df1	C
G2-Af2	B2
G2-Mf	B2
G2-Af1	B1

Unit name	
This study	Perotta
G3C-So	G
G3C-Af	F2
G3C-Af	F1
G3B-So	E2, E3
G3B-Af	E2, E3
G3A-So	E2, E3
G3A-Df	E2, E3
G3A-Af	D